LA-UR-98-2026

Title: **LEVITATION ZONE REFINING AND DISTILLATION OF PLUTONIUM METAL**

Author(s): Michael S. Blau

Submitted to:

Http://lib-www.lanl.gov/la-pubs/00418618.pdf

Los Alamos
NATIONAL LABORATORY

Los Alamos National Laboratory, an affirmative action/equal opportunity employer, is operated by the University of California for the U.S. Department of Energy under contract W-7405-ENG-36. By acceptance of this article, the publisher recognizes that the U.S. Government retains a nonexclusive, royalty-free license to publish or reproduce the published form of this contribution, or to allow others to do so, for U.S. Government purposes. The Los Alamos National Laboratory requests that the publisher identify this article as work performed under the auspices of the U.S. Department of Energy. Los Alamos National Laboratory strongly supports academic freedom and a researcher's right to publish; therefore, the Laboratory as an institution does not endorse the viewpoint of a publication or guarantee its technical correctness.

Form No. 836 R5
ST 2629 10/91

LEVITATION ZONE REFINING AND DISTILLATION OF PLUTONIUM METAL

LAUR-98-2026

A Dissertation

Presented in Partial Fulfillment of the Requirements for the

Degree of Doctor of Philosophy

with a

Major in Mining Engineering/Metallurgy

in the

College of Graduate Studies

University of Idaho

by

Michael S. Blau

April 1998

Major Professor: T. Alan Place, Ph.D.

AUTHORIZATION TO SUBMIT

DISSERTATION

This thesis of Michael Steven Blau, submitted for the degree of Doctor of Philosophy with a major in Mining Engineering/Metallurgy and titled "Levitation Zone Refining and Distillation of Plutonium Metal" has been reviewed in final form and approved, as indicated by the signatures and dates given below. Permission is now granted to submit final copies to the college of Graduate Studies for approval.

Major Professor_____Date_____
T. Alan Place

Committee Members_____Date_____
Keith Prisbrey

_____Date_____
Dale Everson

_____Date_____
J. David Olivas

Department
Administrator _____Date_____
Patrick R. Taylor

College Dean _____Date_____
Earl H. Bennett

Final Approval and Acceptance by the College of Graduate Studies

_____Date_____
Jean'ne M. Shreeve

ABSTRACT

Magnetic levitation of plutonium metal at elevated temperatures was demonstrated to be valuable in separating impurities by both zone refining and vacuum distillation. The levitation force kept molten plutonium from touching crucible walls, enabling handling molten plutonium for extended periods without mutual dissolution.

Plutonium was heated by radio-frequency power in Crystalox® gold-plated, conducting crucibles. The RF power induced electric currents flowing in opposite directions in the crucible and plutonium. Magnetic fields in crucible and plutonium opposed, causing repulsion and levitation of the plutonium a small distance from crucible walls. Separate systems were used to study zone refining and vacuum distillation of plutonium. Differing plutonium metal alloys containing known amounts of impurities were studied for the two systems.

Zone refining was done using plutonium rods. The presence of oxygen had a large negative effect on zone refining effectiveness. Decreasing travel speed of the molten zone improved separation as did increasing the number of passes on a given rod. In all cases, all plutonium impurity elements tracked, moved in accord with anticipated element movement based on the distribution coefficient determined from the binary phase diagram of each element, with plutonium.

Vacuum distillation used molten plutonium in a relatively spherical bolus. Concentrations of americium in plutonium dropped by approximately 50% after 2 h experiments.

In each system, room temperature plutonium separated readily from the crucible without evidence of corrosion or deposits on either crucible or plutonium.

ACKNOWLEDGMENTS

I would like to take this opportunity to express my deep appreciation to T. Alan Place and Gene Bobeck for serving as my advisors. I would like to thank J. David Olivas, Dale Everson, and Keith Prisbrey for serving on my committee.

The technical expertise, generous support, and the valuable time of Larry Vaughan on the induction heating used in this experiment made the completion of this paper possible. I would also like to thank Robert Madeira of Fluxtrol Manufacturing who designed and built the induction coil. Others who contributed significantly to this work were Floyd Rodriquez and Gerald Lucero for some of the hands-on work for this experiment; George Havrilla for all the plutonium metal analysis work, Carol Noons for editing of this thesis, George Biggs for reviewing this document for classification and Gary Tietjen for help with statistics.

I want to give a very special thanks to my group leaders, Larry R. Avens and Michael F. Stevens, who made it possible for me to attend graduate school at University of Idaho.

I want to thank the Los Alamos Neutron Science Center at the Los Alamos National Laboratory for funding this project for the last two years.

TABLE OF CONTENTS

AUTHORIZATION TO SUBMIT DISSERTATION ii

ABSTRACT iii

ACKNOWLEDGMENTS iv

CHAPTER 1. INTRODUCTION 1

CHAPTER 2. THE THEORY OF ZONE REFINING 21

2.1. Theory of Solidification 21
2.1.1. Equilibrium Solidification (Case 1) 21
2.1.2. Solidification with No Diffusion in Solid and Perfect Mixing in Liquid (Case 2) 23
2.1.3. Solidification with No Diffusion in Solid and Partial Mixing in Liquid (Case 3) 24
2.1.4. Solidification with No Diffusion in Solid, Diffusion in Liquid and No Stirring (Case 4) 25
2.1.5. Segregation During Normal Freezing 25

2.2. Theory of Single-Pass Zone Refining 26

2.3. Multiple-Pass Zone Refining 36

2.4. Molten Zone Speed and Width 41

2.5. Molten Zone Heating 42
2.5.1. Molten Zone Heating Techniques 42

2.6. Containers 43

CHAPTER 3. THE THEORY OF VACUUM METALLURGY (DISTILLATION) 44

3.1. Introduction 44

3.2. Vapor Pressure of Metals 45

3.3. Partial Pressures of Metals 46

3.4. Rate of Evaporation 47

3.5. Selective Distillation 52

3.6. Engineering Problems of Distillation 53

CHAPTER 4. REVIEW OF THE LITERATURE 56

4.1. Zone Refining of Plutonium 56
4.1.1. First Investigation 56
4.1.2. Latest Investigation 57

4.2. Zone Refining of Similar Metals 57

4.3. Special Issues With Plutonium 58
4.3.1. Glovebox 58
4.3.2. Reactivity 59

4.4. Distillation of Plutonium Impurities 60
4.4.1. Impurity Distillation 60
4.4.2. Vacuum Distillation of Americium Metal. 63
4.4.3. Separation of Zinc from Plutonium by Vacuum Melting. 66

4.5. Induction Heating 69

4.6. Levitation Cold Crucible 70
4.6.1. Important Results from Sterling and Warren 71
4.6.2. Important Results from Sterling 73
4.6.3. Crystalox® Cold Crucibles 76

4.7. Coil Design 79

4.8. Molten Zone Speed 82

4.9. Statistically Designed Experiments 82
4.9.1. Experimental Factorial Designs 83
4.9.2. Analysis of Variance for Experimental Factorial Designs 83

CHAPTER 5. EXPERIMENTAL PROCEDURES 88

5.1. Material Preparation 89

5.1.1. Low Impurity Alloy 91
5.1.2. High Impurity Alloy 91

5.2. Zone Refining Apparatus 92
5.2.1. Zone Refining Apparatus 92
5.2.2. Distillation Apparatus 98
5.2.3. Experimental Glovebox 103

5.3. Distillations Runs 107
5.3.1. Low-Impurity Alloy 108
5.3.2. High-Impurity Alloy 111

5.4. Zone Refining Runs 111
5.4.1. Low-Impurity Alloy 111
5.4.2. High-Impurity Alloy 115

5.5. Chemical Analysis 115

CHAPTER 6. RESULTS AND DISCUSSIONS 116

6.1. Analyses of As-Cast Alloys 116

6.2. Zone Refining Observations 117

6.3. Results of Chemical Analysis on Zone Refined Rods 119

6.4. Determination of Variables for Zone Refining 123

6.5. Analysis of Variance of Zone Refining Data 138

6.6. Impurity Distillation Observations 147

6.7. Results of Chemical Analysis on Impurity Distillation Samples 156

6.8. Computer Modeling 158
6.8.1. Zone Refining Induction Coil 158
6.8.2. Zone Refining Induction Crucible 162

6.9. Zone Refining Parameters to Produce First Pure Plutonium 165

CHAPTER 7. SUMMARY AND CONCLUDING REMARKS 166

REFERENCES 169

APPENDIX 171

LIST OF FIGURES

Figure 1. Production of plutonium from neutron irradiation of natural uranium 2

Figure 2. Idealized expansion behavior of plutonium..... 4

Figure 3. Thermal conductivity (experimental and calculated) for plutonium..... 5

Figure 4. Plutonium-gallium binary phase diagram..... 6

Figure 5. Electrorefined plutonium ring 9

Figure 6. Top-half of standard plutonium metal vacuum casting furnace..... 10

Figure 7a. Top-half of Vycor® tube used for vacuum containment of standard Plutonium casting furnace after a single casting of an above average electrorefined ring into rods..... 11

Figure 7b. Top-half of Vycor® tube used for vacuum containment of standard plutonium casting furnace after a single casting of a poor electrorefined ring into rods..... 12

Figure 8. Vapor pressures of elements often found as impurities in metallic plutonium 18

Figure 9. Hypothetical solid-liquid region of a eutectic-type phase diagram..... 23

Figure 10. Hypothetical solid-liquid region of a eutectic-type phase diagram..... 24

Figure 11. Molten zone traversing a rod..... 27

Figure 12. Variation of composition along a rod produced by zone melting after one pass (K<1) 27

Figure 13. Curves for single-phase zone refining showing solute concentrations in the solid versus distance in zone lengths from beginning of charge, for various values of K 35

Figure 14a. Relative solute concentration C/C_o versus distance in zone lengths X/l from the rod head-end for various numbers of passes n. 37

Figure 14b. Relative solute concentration C/C_o versus distance in zone lengths X/l from the rod head-end for various numbers of passes n. 38

Figure 14c. Relative solute concentration C/C_o versus distance x with number of passes n as a parameter for K = 0.9524, l = 1 and L = 100 39

Figure 15. Americium content of the americium-plutonium vapor phase and liquid phase as a function of the total pressure at 1200 C..... 64

Figure 16. Americium distillation apparatus used for the Rocky Flats study..... 65

Figure 17. Distillation rate (theoretical and experimental) of zinc from a zinc-plutonium alloy at 800 C..... 68

Figure 18. Section through a horizontal silver boat..... 72

Figure 19. Section through a horizontal silver boat..... 74

Figure 20a. Crystalox® HCB-150 horizontal cold boat 77

Figure 20b. Crystalox® HCC-50 vertical cold boat 77

Figure 20c. Water manifold for both Crystalox® cold boats..... 78

Figure 21a. Flux lines of a proposed three-turn pancake coil without Fluxtrol® flux field concentrator..... 80

Figure 21b. Flux lines of proposed three-turn pancake coil with Fluxtrol® flux field concentrator..... 81

Figure 22a. Experimental procedure flow diagram for low-impurity alloy..... 89

Figure 22b. Experimental procedure flow diagram for high-impurity alloy 90

Figure 23a. Side-view drawing of the zone refining apparatus 94

Figure 23b: Front-view drawing of the zone refining apparatus 95

Figure 23c: Plan-view drawing of the zone refining apparatus 96

Figure 23d. Zone refining apparatus with stainless steel rod in the Crystalox® cold boat at a power setting of 10 kW. 97

Figure 24a. Front-view drawing of the distillation apparatus.....100

Figure 24b. Distillation apparatus with vacuum chamber lid raised.....101

Figure 24c. Distillation apparatus with crucible raised.....102

Figure 25a: Front-side of zone refining glovebox 105

Figure 25b: Back-side of zone refining glovebox.....106

Figure 26: Six cuts used to obtain a chemical analysis sample from the distilled sample 110

Figure 27a: Oxide removal system 113

Figure 27b: Oxide removal system wire brush mechanism.....114

Figure 28: Sampling of zone refined rods for chemical analyses.....115

Figure 29: As-cast _-in diameter rod of high-impurity alloy.....117

Figure 30: Rod 1 (high-impurity alloy) after completion of zone refining run 119

Figure 31a: Zone refining parameters.....126

Figure 31b: Zone refining parameters.....127

Figure 32a Change in concentration from nominal (520 ppm) for chromium (K= 0.2) after zone refining (high-impurity rods 1 and 2, After six passes at a speed of 0.75 in/h).....129

Figure 32b Change in concentration from nominal (1,095 ppm) for cobalt(K= 0.2) after zone refining (high-impurity rods 1 and 2, After six passes at a speed

of 0.75 in/h).
.....130

Figure 32c Change in concentration from nominal (1,105 ppm) for copper (K= 0.3) after zone refining (high-impurity rods 1 and 2, After six passes at a speed of 0.75 in/h).....131

Figure 32d Change in concentration from nominal (1,100 ppm) for iron (K= 0.2) after zone refining (high-impurity rods 1 and 2, After six passes at a speed of 0.75 in/h).....132

Figure 32e Change in concentration from nominal (1,120 ppm) for nickel (K= 0.3) after zone refining (high-impurity rods 1 and 2, After six passes at a speed of 0.75 in/h).....133

Figure 32f Change in concentration from nominal (962 ppm) for neptunium (K= 0.8) after zone refining (high-impurity rods 1 and 2, After six passes at a speed of 0.75 in/h).....134

Figure 32g. Change in concentration from nominal (1,120 ppm) for aluminum (K= 1.4) after zone refining (high-impurity rods 1 and 2, After six passes at a speed of 0.75 in/h).....135

Figure 32h. Change in concentration from nominal (1,120 ppm) for americium (K= 19) after zone refining (high-impurity rods 1 and 2, After six passes at a speed of 0.75 in/h).....136

Figure 32i. Change in concentration from nominal (9,850 ppm) for gallium (K= 1.4) after zone refining (high-impurity rods 1 and 2, After six passes at a speed of 0.75 in/h).....137

Figure 33a. Percent change (head to tail) for chromium, with the vertices denoting the levels of each factor and the numbers being the mean yield at the vertices 141

Figure 33b. Percent change (head to tail) for iron, with the vertices denoting the levels of each factor and the numbers being the mean yield at the vertices.....142

Figure 33c. Percent change (head to tail) for cobalt, with the vertices denoting the levels of each factor and the numbers being the mean yield at the vertices.....143

Figure 33d. Percent change (head to tail) for nickel, with the vertices denoting the levels of each factor and the numbers being the mean yield at the vertices.....144

Figure 33e. Percent change (head to tail) for copper, with the vertices denoting the levels of each factor and the numbers being the mean yield at the vertices.....145

Figure 34. Plutonium metal (high-impurity alloy) in levitation distillation apparatus after 1 h at 1200 C (power supply at 40 kW) 148

Figure 35. Standard magnesium oxide crucible after melting plutonium metal.....150

Figure 36a. Plutonium metal (high-impurity alloy) half-sphere formed from distillation run (top).....152

Figure 36b. Plutonium metal (high-impurity alloy) half-sphere formed from distillation run (bottom). 153

Figure 37a. Plutonium metal (high-impurity alloy) half-sphere formed from distillation run (top) with fast cooling.....155

Figure 37b. Blowup of top surface of plutonium metal (high-impurity alloy) half-sphere formed from distillation run.....156

Figure 38. Modeling results of new Fluxtrol® induction coil done at The Center for Induction Technology 159

Figure 39a. New zone refining apparatus (side-view) 160

Figure 39b. New zone refining apparatus (top-view) 161

Figure 40a. Cross section of the magnetic flux density (Tesla) produced in the horizontal crucible and molten plutonium contained in the crucible.....163

Figure 40b. Cross section of the electromagnetic forces (Newtons) produced in the horizontal crucible and molten plutonium contained in the crucible.....164

LIST OF TABLES

Table 1. Crystal Structure, Densities, and Range of Stability for Plutonium Allotropes 3

Table 2. Chemical Analyses of As-Cast Alloys.....116

Table 3. Results of Chemical Analyses of Zone Refined Rods.....121

Table 4. Results of Chemical Analyses of Zone Refined Rods.....124

Table 5. Statistical Analyses Results (Pr>F) Using a Completely Random Split Plot Design with a 2^4 Factorial Arrangement of Treatments 139

Table 6. Statistical Analyses Results (Pr>F) Using a 2^3 Factorial Model 140

Table 7. Statistical Analyses Results (Regression) Using a 2^3 Factorial Model.....145

Table 8. Chemical Analyses of Distillation Samples.....157

CHAPTER 1

INTRODUCTION

Plutonium, element 94, was the second transuranium element of the actinide series to be discovered. The first synthesized plutonium (the Pu^{238} isotope) was produced on February 23, 1941 by A. C. Wahl, J. W. Kennedy, and G. T. Seaborg by deuteron bombardment of uranium (16,000,000 electron volt deuterons) in the 60-in cyclotron at Berkeley, California. Plutonium-239 was produced shortly thereafter by the capture in U^{238} of neutrons produced by deuteron, neutron reactions using the same cyclotron. Plutonium does occur in nature in uranium ores as a result of the capture in U^{238} of neutrons from spontaneous fission and alpha-neutron reactions. The concentrations of plutonium are minute, on the order of 1 in 10^{11} (one part in one hundred billion) of the uranium present. Since the discovery of plutonium and its dramatic emergence at Nagasaki, plutonium has altered the course of history, changed the concepts and consequences of war, and paradoxically has become a powerful instrument for peace (1).

In fact, since plutonium brought an end to World War II in 1945, it has prevented another world war for fifty years (87,000,000 deaths due to war 1900 to 1948 compared to 17,000,000 deaths due to war 1948 to 1996). The discovery of plutonium has brought many side effects, the most important being nuclear energy. Another important device brought about by the discovery of plutonium is the common smoke detector. Each smoke detector

has a small amount of plutonium (Russia) or the plutonium daughter, americium (most countries), which ionizes the smoke particles and causes the alarm to work.

Almost all plutonium has been produced in natural-uranium-fueled, thermal, heterogeneous nuclear reactors. Plutonium is produced as the result of neutron capture in U^{238} and subsequent beta decays to Pu^{239} as shown in Figure 1. Plutonium Isotopes 240, 241, 242, and 243 are formed from successive neutron captures as shown; the short half-life of Pu^{243} essentially terminates the plutonium isotope production at Pu^{242}. Plutonium-238 is also formed in small quantities from neutron reactions in Pu^{239} and U^{238} (1).

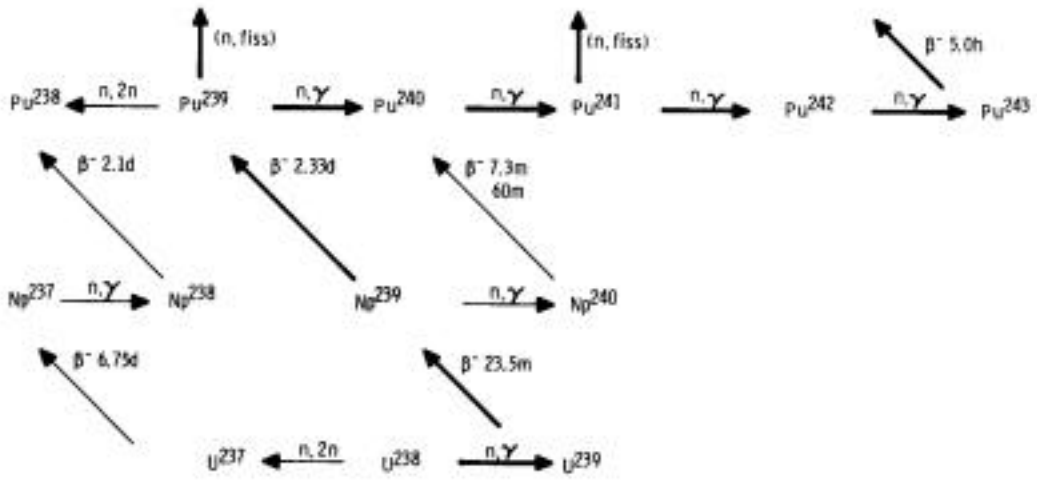

Figure 1. Production of plutonium from neutron irradiation of natural uranium (1).

Plutonium is an unique metal because there are at least six equilibrium allotropes (the phases: alpha, beta, gamma, delta, delta-prime, and epsilon), which range in crystallographic

structure from simple monoclinic at low temperatures to a body-centered cubic structure just below the melting point. Five allotropes were identified early in studies of the physical metallurgy of plutonium and were designated conventionally as alpha through epsilon. A few years later, in 1954, dilatometric work of relatively high-purity metal revealed clear evidence for the existence of a sixth phase in the temperature range between delta and epsilon. This phase, which is strongly influenced by relatively small amounts of certain impurities, was designated as delta-prime by Schonfeld. The crystal structure, densities, and range of stability for plutonium allotropes are shown in Table 1 (1).

TABLE 1: CRYSTAL STRUCTURE, DENSITIES, AND RANGE OF STABILITY FOR PLUTONIUM ALLOTROPES (1).

Phase	Crystal Lattice	Atoms/Unit Cell	Stability Range (C)	Density (g/cm^3)
Alpha	Simple monoclinic	16	below 112	19.82
Beta	Body-centered monoclinic	34	112-185	17.80
Gamma	Face-centered orthorhombic	8	185-310	17.14
Delta	Face-centered cubic	4	310-452	15.92
Delta-prime	Body-centered tetragonal	2	452-480	16.00
Epsilon	Body-centered cubic	2	480-640	16.51

The complexity of plutonium is further illustrated by the fact that many of its properties (e.g., thermal expansion, electrical resistivity, thermal conductivity, temperature

range of molten plutonium) do not vary with temperature in usual ways. The idealized expansion behavior of plutonium is shown in Figure 2. The thermal conductivity (experimental and calculated) for plutonium is shown in Figure 3. Plutonium metal has a low melting point of 640 C, but a high boiling point of approximately 3240 C (1).

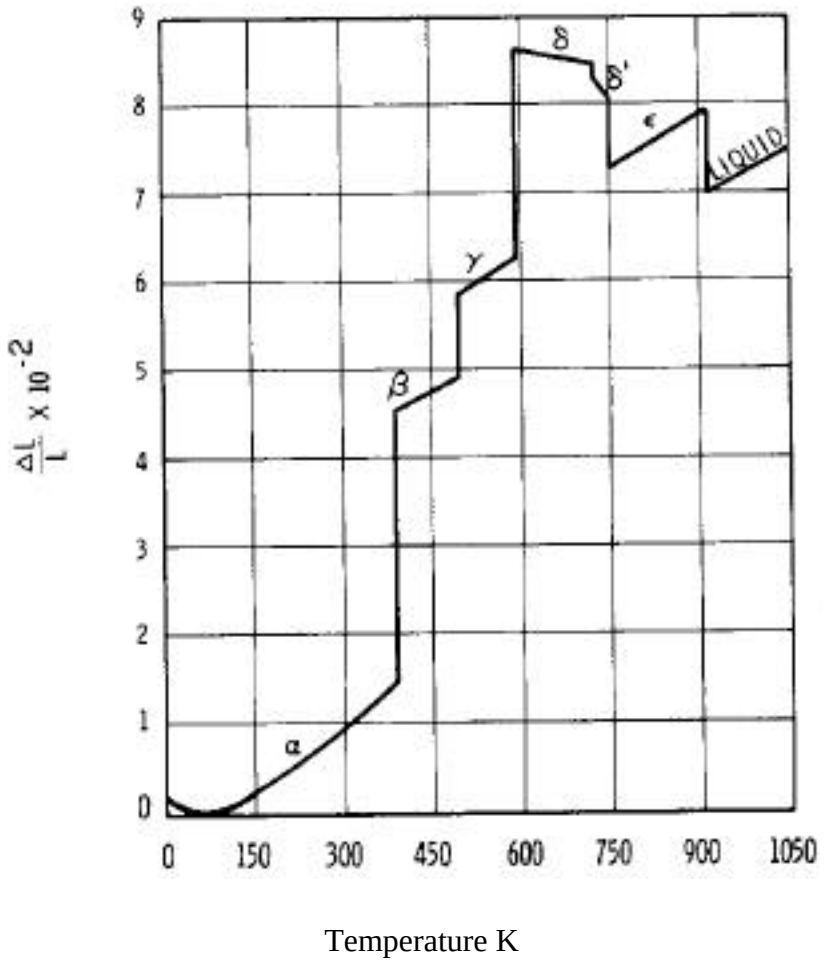

Figure 2. **Idealized expansion behavior of plutonium (1).**

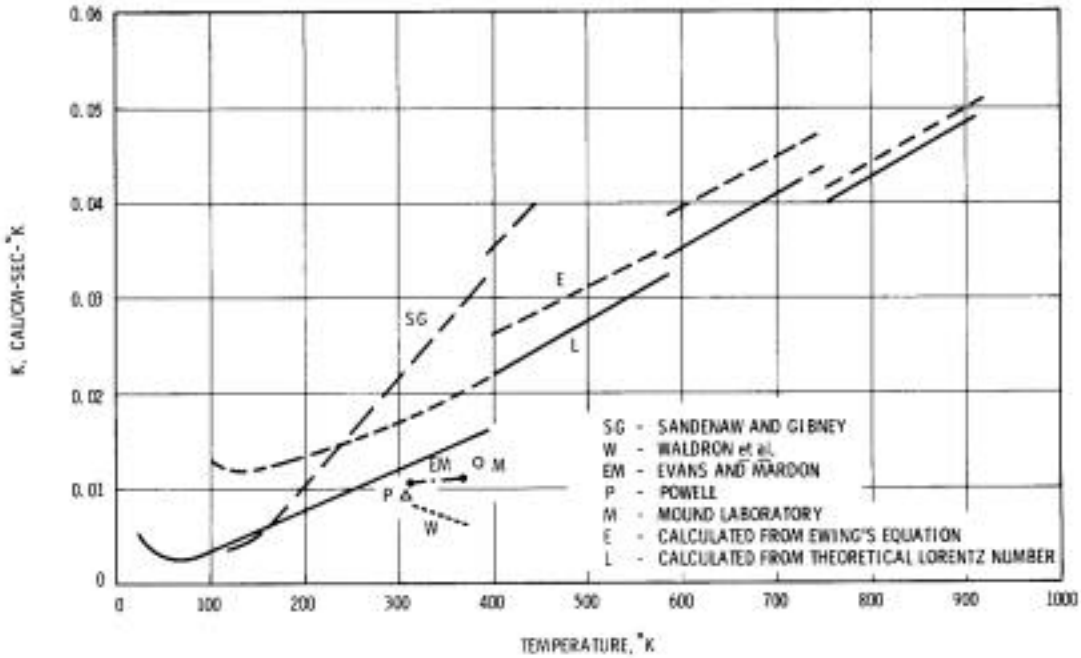

Figure 3. Thermal conductivity (experimental and calculated) for plutonium (1).

The presence of impurities in plutonium is known to influence a number of its physical properties. When beads of plutonium were first produced in 1943 by micrometallurgical techniques at the University of Chicago, it was observed that some beads were malleable and had a density of about 16 g/cm^3, while other beads were brittle and had a density closer to 20 g/cm^3. It was later determined that this apparent discrepancy was the result of impure elements stabilizing one of the lower-density allotropes of plutonium (2).

The most common and most studied element used to stabilize the plutonium δ-phase is gallium. The plutonium-gallium binary phase diagram taken from T. Massalski is shown in Figure 4 (3). The figure shows that adding gallium to pure plutonium raises the melting

point of the plutonium-gallium alloy. Figure 4 also shows the different phase-fields from the melting point down to room temperature.

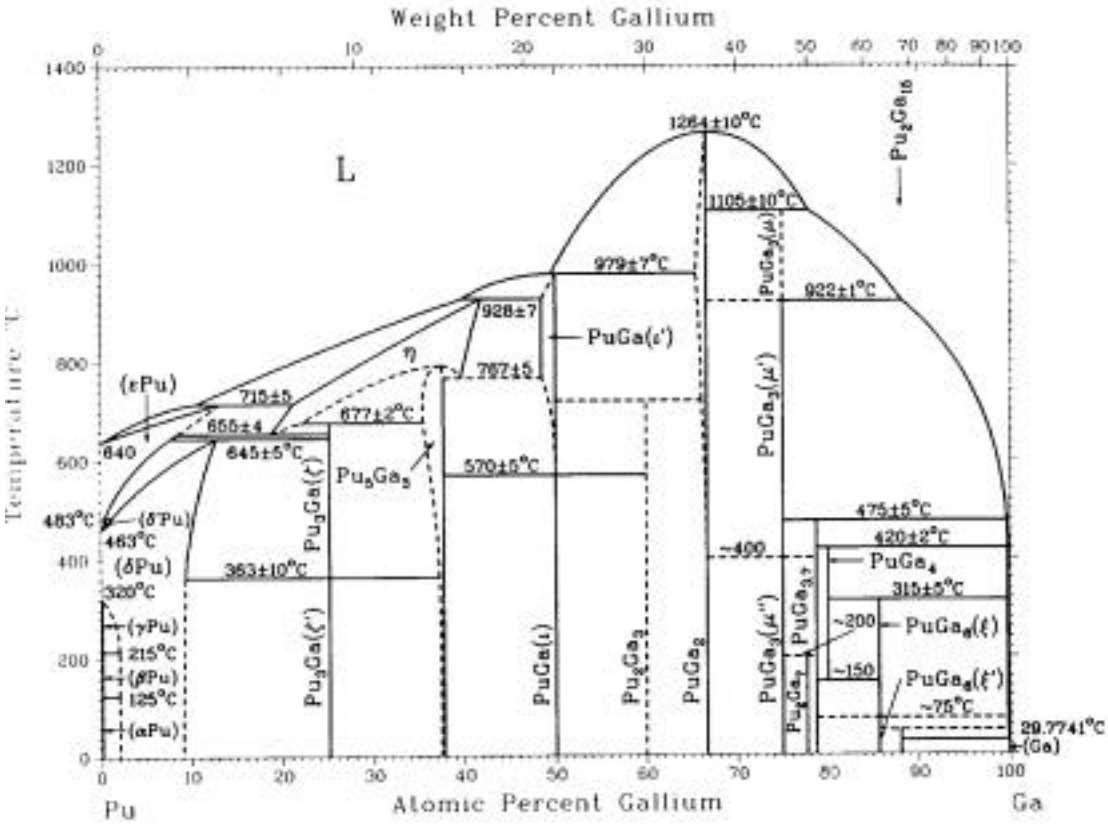

Figure 4. Plutonium-gallium binary phase diagram (3).

At the present time, basic material properties of plutonium metal are not accurately known (e.g., crystal structure, density, heat capacity, thermal expansion coefficient, isothermal compressibility, electrical resistivity, and elastic constants) because of the inability to produce even a small amount of plutonium metal of extremely high purity. To obtain the best possible measurements for plutonium properties would require Pu^{239} crystals that are at least 10 mm in two directions.

Knowledge of the basic material properties of plutonium metal is necessary for developing a robust understanding of the long-term performance of metallic weapon components in the aging nuclear weapons stockpile. Another reason for producing high-purity plutonium is the characterization of the plutonium phonon structure. This is the study of vibrational excitations, called "phonons," in the atomic lattice. Phonon spectra can be measured by inelastic neutron scattering. Such measurements require crystals of Pu^{242} at least 10 mm in all directions. The first step necessary for producing any large plutonium crystals is to produce the first plutonium metal of extremely high purity. As discussed above, the delta-prime phase of plutonium was discovered only after plutonium of relatively high-purity metal became available.

The current driving force for producing pure plutonium is the need for characterization of the plutonium phonon structure. Phonon spectra can be measured by inelastic neutron scattering. This leads to a detailed elucidation of the character of plutonium's atomic bonds to put equation-of-state modeling for plutonium on a sound theoretical footing. However, such measurements require large, single-crystal samples of Pu^{242}. But since there is no plutonium phase that remains stable from the melting point down to room temperature, any plutonium crystal will have to be made using a grain growth method. All grain growth methods require the starting material to be very pure because any impurities pin the grain boundaries and stop grain growth.

The two methods that will first be used to attempt to produce plutonium crystals once plutonium of high purity has been produced is solid-state zone refining and radial strain annealing. Solid-state zone refining will be done by passing a hot zone (lower than the δ to ε

phase transformation on heating) very slowly (0.01 in/h) along a rod of pure plutonium alloyed with 1 w/o gallium. Radial strain annealing will be accomplished by first forming a plutonium disk of a high-purity gallium alloy (1 w/o), then annealing the disk until the gallium is homogenous, followed by a 2% radial strain in the δ-phase field (the critical strain for maximum grain growth in δ-plutonium is 2%).

The current process used for plutonium metal purification is electrorefining molten plutonium metal in a molten salt ($MgCl_2$). The major problems with this process are that the product is not of high purity, the efficiency can be as low as 20% (average efficiency is 60%), and the process creates a large amount of salt and ceramic nuclear waste. Figure 5 shows a photo of a plutonium metal electrorefined ring. The blue color of the ring is due to the plutonium chloride on the surface of the ring. Because of this and other impurities in the ring, such as magnesium, an electrorefined ring cannot be cast directly into a part but must first be cast into rods under a vacuum to remove the chlorides and other impurities with high vapor pressures. Figure 6 shows the vacuum melting chamber of a standard plutonium casting furnace. The crucible containing the plutonium from an electrorefined ring is heated by induction. Above the crucible, one can see the formation of chlorides on the clear Vycor® tube as the molten plutonium outgases during vacuum melting. Figure 7a shows some of the impurities that outgas from an above average electrorefined ring on the Vycor® tube. Figure 7b shows some of the impurities that outgas from a poor electrorefined ring on the Vycor® tube. From these two figures one can see that the amount of volatile impurities

in a plutonium electrorefined ring is variable. This fact must be considered for casting of plutonium electrorefined rings.

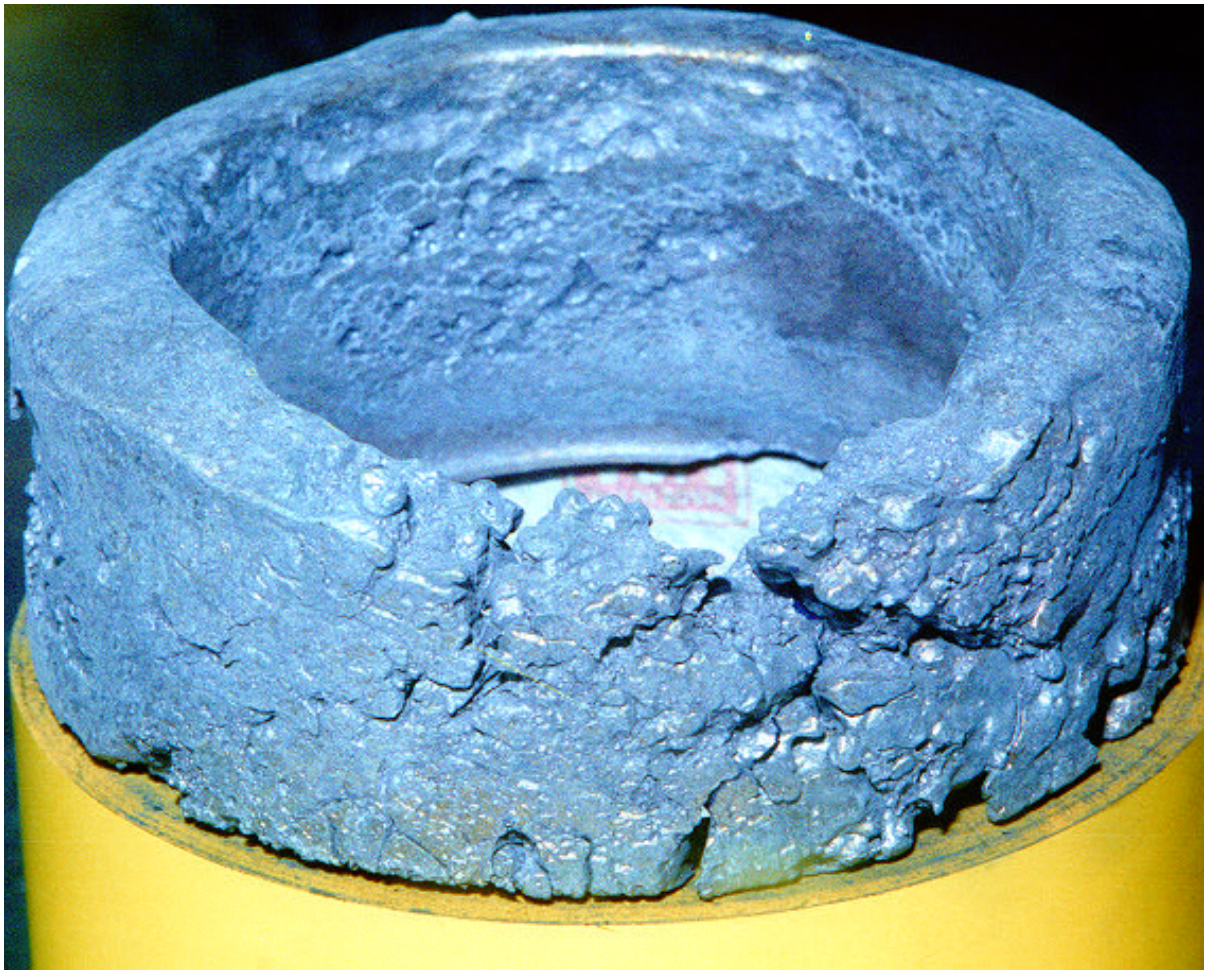

Figure 5. Electrorefined plutonium metal ring.

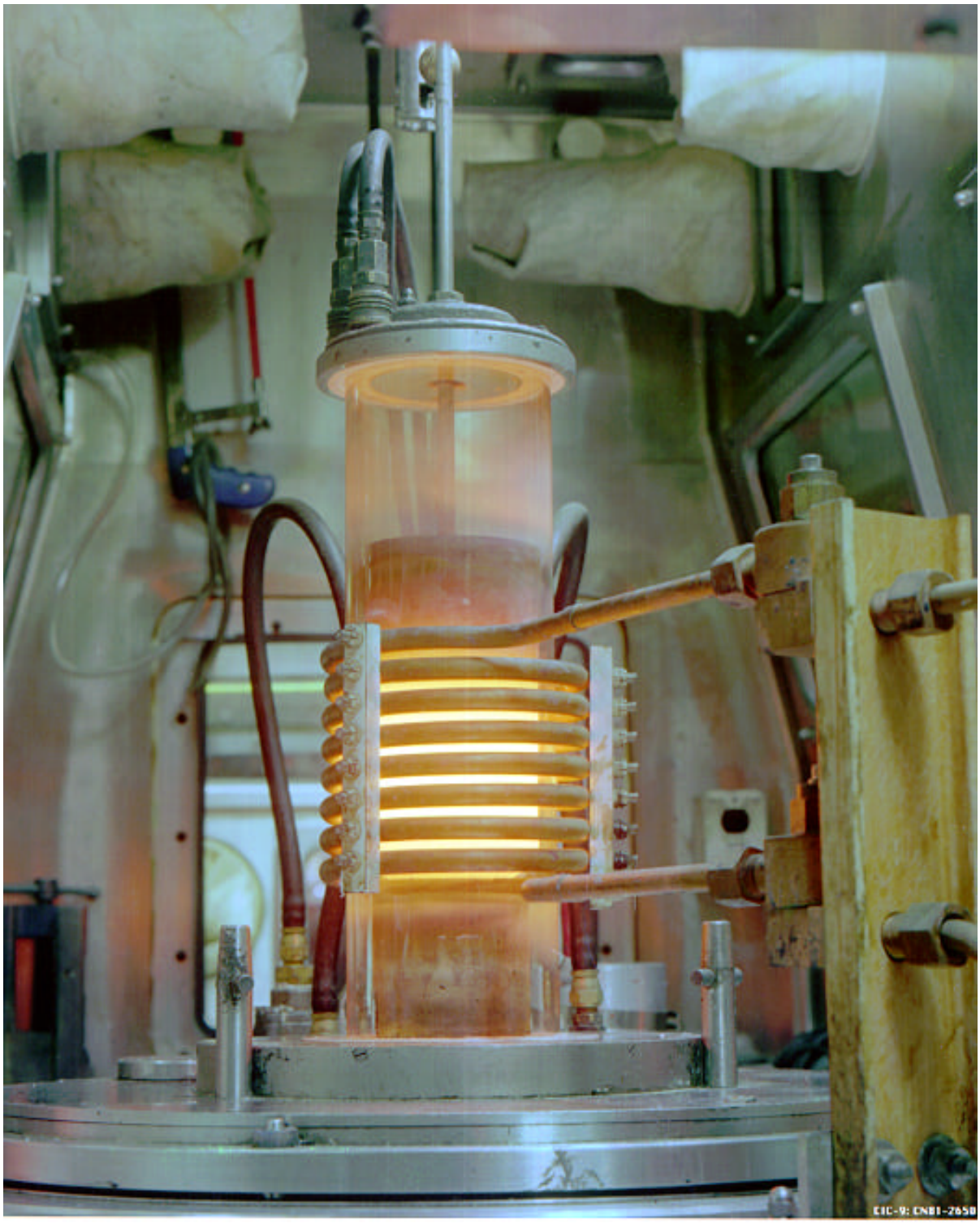

Figure 6. Top-half of standard plutonium metal vacuum casting furnace after the induction coil has heated the plutonium-containing crucible.

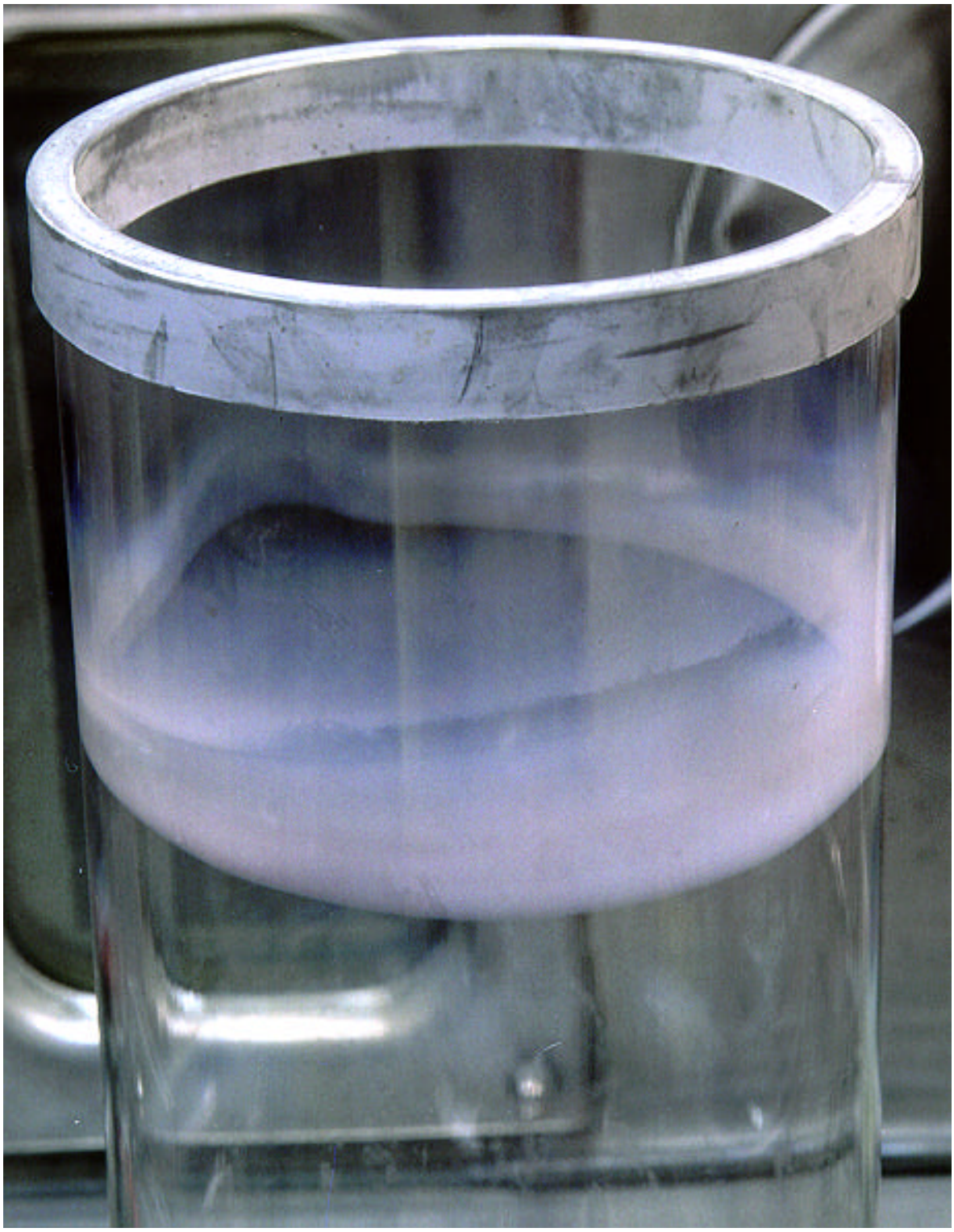

Figure 7a. Top-half of Vycor® tube used for vacuum containment of standard plutonium casting furnace after a single casting of an above average electrorefined ring into rods.

Figure 7b. Top-half of Vycor® tube used for vacuum containment of standard plutonium casting furnace after a single casting of a poor electrorefined ring into rods.

A zone refining technique might be capable of producing small amounts of extremely high-purity plutonium metal. Furthermore, a zone refining process for purifying plutonium would have a great advantage over the current electrorefining process because it would not create a large amount of salt and ceramic nuclear waste, and the product from zone refining could be cast directly into parts.

Zone refining is a well-proven technology used by the electronics industry to produce highly purified silicon and germanium. The technique for producing ultra-high purity materials has been greatly improved in the past 40 years, based upon the concept of zone melting processes conceived by W. G. Pfann (4). The use of zone refining has made possible the production of some extremely high-purity materials. For example, during zone refining of the elements silicon and germanium, the spectacular results were that most impurity elements were reduced to less than 1 in 10^{10} (one part in ten billion) (4).

The zone refining process is related to a fact that has been known to metallurgists for many years, i.e., the segregation found in alloy castings. Generally, constitutional segregation is considered a troublesome problem that foundrymen had to contend with, rather than a useful tool. Pfann, however, visualized a method of using segregation to move alloying elements about within a rod. The effectiveness of zone refining in reducing the concentration of unwanted impurities depends most importantly upon the way in which the impurity redistributes itself in the solvent during the melting and solidification processes. The zone refining process involves casting a rod of the substance to be purified, and then passing a molten zone serially through the rod in one direction. Impurities travel with, or opposite to, the direction of motion of the zones, depending on whether they lower or raise

the melting point of the rod metal, respectively. They tend to become concentrated in the ends of the rod, thereby purifying the remainder. The degree of separation (redistribution/purification) approaches a limit as the number of passes becomes infinite (4).

Two studies of plutonium zone refining have been documented at the Los Alamos National Laboratory. The first investigation in the late 1950s showed that the elements cobalt, chromium, iron, manganese, nickel, silicon, and aluminum moved in the directions predicted from the respective binary constitutional diagrams, but the elements beryllium, bismuth, boron, calcium, copper, lanthanum, lead, lithium, magnesium, silver, sodium, tin, and zinc did not move (2). The most recent plutonium zone refining study at Los Alamos was completed in 1994 (5). This was the first study done with high enough levels of impurities to clearly show any impurity movement during the zone refining process. The results of this study indicated that all ten of the added impurity elements (copper, chromium, cobalt, iron, nickel, neptunium, uranium, aluminum, americium, and gallium) moved as predicted by the respective binary constitutional diagrams (5).

This 1994 study demonstrated that zone melting of plutonium metal caused redistribution of impurity elements and implied that development of a zone refining process to purify plutonium metal is feasible. Also from this study, there was strong evidence that an amount of each impurity left the plutonium metal through some vaporization mechanism due to the vacuum conditions used in the experiments. However, based on the results obtained by this study, development of a plutonium metal zone refining purification process is hampered by two factors. First, the plutonium oxide layer that forms on the molten zone slows down the speed of impurity element redistribution. Second, molten plutonium metal is

difficult to contain; molten plutonium reacts with all metals and any inert ceramic cannot withstand the thermal shock it would be exposed to during the zone refining process.

To alleviate the latter and possibly the former, this study was carried out using a Crystalox® horizontal water-cooled cold crucible to contain the molten plutonium metal. The Crystalox® crucible is machined from a solid bar of high-conductivity copper that is subsequently gold-plated. During zone refining, the crucible is connected to a water manifold, which causes water to flow thoughout the crucible to keep it cool. The crucible is designed to provide a levitation force to the plutonium metal. The levitation force serves to suspend the molten material so that it will not come into contact with the crucible. Furthermore, since the crucible is cold, any molten material that contacts the crucible surface solidifies before it can react with the crucible surface.

An additional advantage of using the Crystalox® crucible is that it permits higher molten zone temperatures to be used in the material being purified. Higher temperatures in the molten zone produces greater mixing and greater release of impurities by vaporization. It may also affect the formation of the skin (plutonium oxide layer) on the exposed surface of the plutonium being zone-refined.

In order to better understand any impurity vaporization mechanism, a separate distillation apparatus was set up using a Crystalox® vertical water-cooled cold crucible. This apparatus was contained in a vacuum chamber designed for obtaining better vacuums than in the zone refining apparatus. The setup included a water-cooled condenser for condensing impurities that vaporized from the molten plutonium and a residual gas analyzer.

Distillation of impurities from a metal matrix at high temperature in a vacuum is a vacuum metallurgical process. This process is based on the principal of a liquid-to-vapor phase change at a specific temperature and reduced pressure (the lower the reduced pressure, the lower the temperature needed for the phase change). The vapor pressure of a metal is expressed by an equation of the type: $\log p = A - B/T$, where A and B are constants for a given metal within a certain temperature range. Due to the logarithmic character of this expression, it is evident that a considerable reduction in temperature can be realized when working at low pressures. For example, iron that boils at 2,735 C and 760 torr can readily be sublimed at 1,260 C and 0.001 torr (6).

To understand the theory of vaporization, consider water at the boiling point with external heat added. Boiling is a mechanical phenomenon caused by uneven temperature distribution in the bath. This phenomenon is best observed when one heats water to a boil. Gas bubbles first form at the bottom of the container because those water molecules are at the highest temperature and thus have enough energy to vaporize. If this were not the case and all the water molecules were at the same temperature, there would be no boiling but instead a sudden phase change of all the water from liquid to vapor once enough energy had been supplied to the container. The vapor pressure within these bubbles is equal to the external pressure at the surface of the bath, plus that exercised by the column of liquid above the bubbles. While this latter effect may be negligible with high external pressure, it is a decisive factor when boiling under vacuum. Furthermore, due to the logarithmic character of the vapor pressure curve, slight differences of pressure in a vacuum correspond to large variations in temperature (6).

However, normally when boiling takes place in a molten metal bath, it is much closer to the surface than with water. This is because the good thermal conductivity of metals does not permit large temperature differences within the bath. In fact, the principal law for evaporation of metals may be that evaporation is exclusively a surface phenomenon. Thus, to evaporate a metal rapidly in a vacuum, one must create the largest possible evaporating surface because there is no boiling within the body of the molten metal. Once the metal vapor is produced, it can be condensed at some desired location. The metal vapor coming from the surface being evaporated has to pass to the cool condensing surface, which is located at a certain distance from the place where the vapor is produced. This movement presumes the existence of a pressure difference between the main part of the metal bath and that next to the condenser surface (6).

The vapor pressure at the bath surface is the sum of all the partial pressures of the gases present and includes the partial pressure of the metal evaporated. It is evident that only the latter contributes to moving the metal vapor to the condenser, since this metal vapor is the only one that condenses. The vapor flow toward the condenser surface can be speeded up by increasing the metal vapor temperature, thus raising the pressure (6).

Purification of plutonium by distillation has been the subject of many studies over the past 45 years. For a plutonium distillation purification technique to work, the vapor pressure of the impurity must be larger than that of plutonium. Figure 8 shows plots of the vapor pressures of elements often found as impurities in metallic plutonium. From this figure, it is evident that distillation alone will not produce pure plutonium, but it will remove many of the impurities common in metallic plutonium (7).

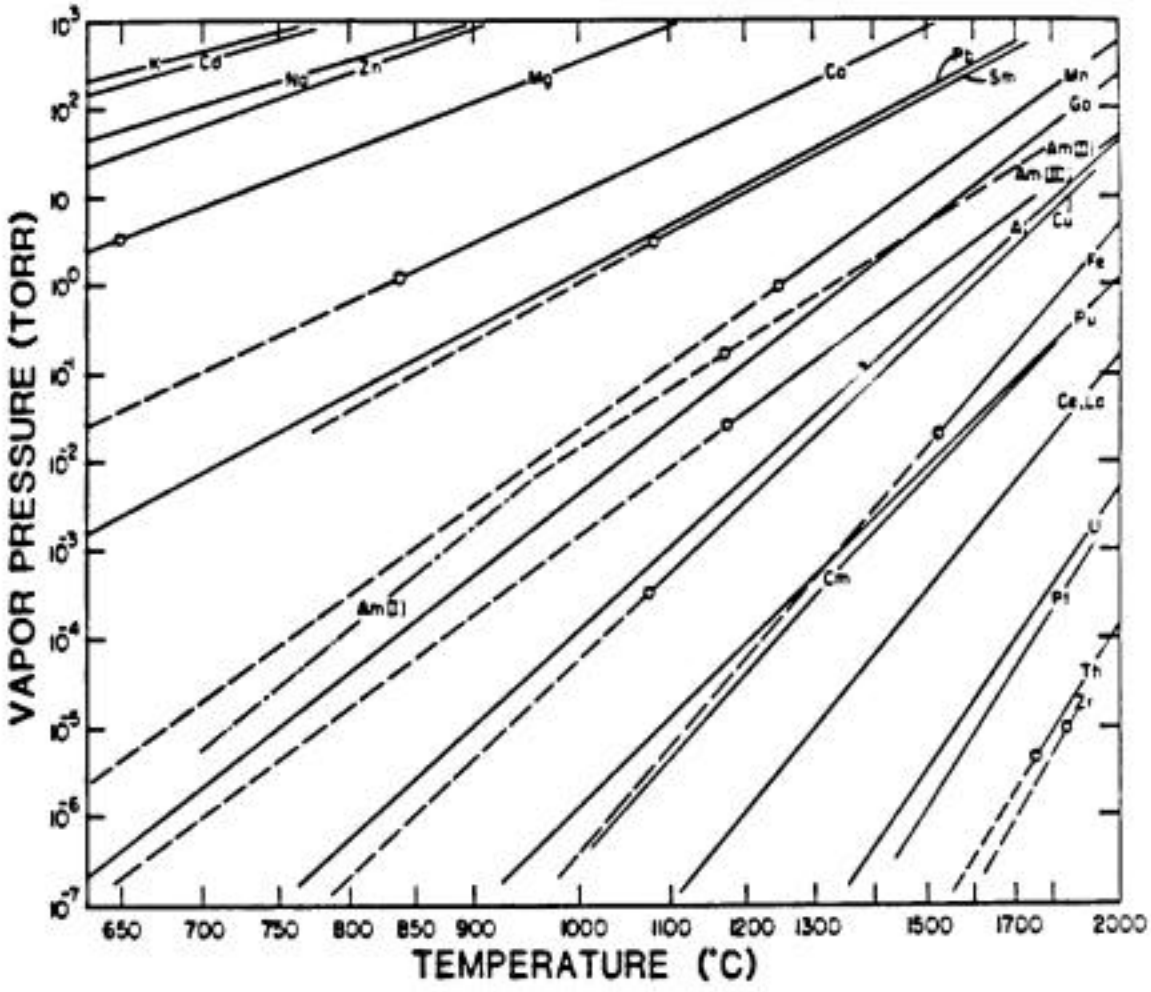

Figure 8. Vapor pressures of elements often found as impurities in metallic Plutonium (7).

Workers at the Rocky Flats Plant in Denver, Colorado, have used metal distillation as a technique for separating zinc from plutonium in one series of experiments, and americium from plutonium in another series. The results of these experiments revealed that the removal of zinc from plutonium was more than 10,000 times slower than the theoretical vaporization rate. On the other hand, the rate of distillation of americium from plutonium was found to be

of the same order of magnitude as the calculated rate. In fact, most americium used in smoke detectors was produced by distillation at Rocky Flats. Also, the main impurity in high-purity plutonium will be americium. Americium forms at a rate of approximately 30 ppm per month due to the decay of Pu^{241} to Am^{241}. Consequently, once plutonium metal of extreme purity is produced, distillation may be the best method of maintaining the high purity.

There are at least four known interrelated engineering problems in the process of plutonium distillation at high temperatures. These recognized problems are splattering, vapor trapping, plutonium reacting with the container, and slow vaporization rate (over 10 h). To alleviate these problems, this study was carried out using a Crystalox® vertical water-cooled cold crucible to contain the molten plutonium metal. The advantage of the Crystalox® cold crucible was that the molten plutonium metal was levitated as long as it was molten. The levitation prevented the molten plutonium from reacting with the crucible. Also, the amount of molten plutonium surface area was approximately five times greater due to the levitation (the greater the surface area, the more surface that vapors can escape through). Also, the molten plutonium received constant stirring from the induction field; the stirring presumably reduces vapor trapping. The amount of splattering was also reduced because of the high surface area, constant stirring, and shorter diffusion distance.

One further advantage of the Crystalox® vertical water-cooled cold crucible is that one of the first methods to be tried for producing plutonium crystals is by a radial-strain anneal technique using zone-refined δ-plutonium. The starting sample for this technique will be a thin 1 inch disk of delta-stabilized plutonium (1 w/o gallium). By using the Crystalox®

vertical water-cooled cold crucible to cast a half-sphere that the thin disk can be cut from, instead of using the standard plutonium casting furnace, there are many advantages. No impurity is picked up from the crucible or mold of the standard casting furnace. During the casting with the Crystalox® crucible, the impurity level in the plutonium improves due to the impurity distillation effect of the crucible. Also, the gallium distribution in the plutonium half-sphere is presumably better due to the stirring effect produced by the magnetic fields from the induction coil and crucible.

The purpose of this study was to develop an experimental plutonium purifying process that could be used to produce a small amount of plutonium metal of extremely high purity. This experimental process was based on levitation zone refining and that included levitation distillation of plutonium metal. Consequently, this thesis demonstrates whether or not levitation zone refining with or without levitation distillation can purify plutonium metal. Also, this thesis demonstrates whether or not levitation distillation can remove americium from plutonium metal. If this purpose is accomplished, it may be possible to perform fundamental property experiments on plutonium metal that have not yet been done. Current methods for purifying plutonium do not produce plutonium metal of high-enough purity to carry out such experiments.

A secondary purpose of this paper is to prove that the Crystalox® crucibles can contain molten plutonium from long periods without any crucible-plutonium interaction. At the present time, there is no crucible (many different materials and materials with coatings have been tested) that can be used to contain molten plutonium without crucible-plutonium interaction.

CHAPTER 2

THE THEORY OF ZONE REFINING

2.1. Theory of Solidification

Zone refining is based on the principle that a difference in solute concentration exists between the solid and the bulk liquid at the liquid-solid interface at the solidifying end of the molten zone. This difference is a consequence of the equilibrium that exists between the liquid and solid phases of a binary system. During solidification, equilibrium can be closely approached between the liquid and solid at the liquid-solid interface. However, most metals do not freeze under equilibrium conditions. As an alloy is cooled from the liquid state, it reaches a point at which a solid begins to form. The solid that forms generally has a different composition than the liquid from which it is freezing. This redistribution of the solute produced by solidification is frequently termed segregation (4,8).

Alloy solidification can take place under four distinct sets of conditions as discussed below. In practice, Case 3 dominates solidification with no diffusion in the solid and partial mixing in the liquid (4, 8, 9).

2.1.1. Equilibrium Solidification (Case 1)

Consider a hypothetical alloy, indicated by the dot-dash line in the eutectic-type phase diagram shown in Figure 9. The way that such an alloy solidifies in practice depends in rather a complex way on temperature gradients, cooling rates, and growth rates. The alloy whose composition is C_o begins to solidify at temperature T_1, if no nucleation barrier interferes, with the formation of a small amount of solid of composition C_s or KC_o. It is

useful to define the equilibrium distribution coefficient K as the ratio of the composition of the solid to that of the liquid at any temperature of interest:

$$K = \frac{C[solid]}{C[liquid]} = \frac{C_s}{C_o} \tag{1}$$

with values of C_s and C_o taken from the binary phase diagram. The equilibrium distribution coefficient is K < 1 for systems in which the solute element lowers the melting point and is K > 1 for systems in which the solute element raises the melting point of the alloy as the temperature is lowered more solid forms. If cooling is slow enough to allow extensive solid-state diffusion, the solid and liquid will each be homogeneous and in equilibrium with compositions following the solidus and liquidus lines, as in Figure 9. The relative amounts of solid and liquid at any temperature are given by the inverse lever rule. At temperature T_2, the last drop of liquid has a composition C_o /K and the average composition of the solid is C_o, the same as that of the original melt (8,9,10).

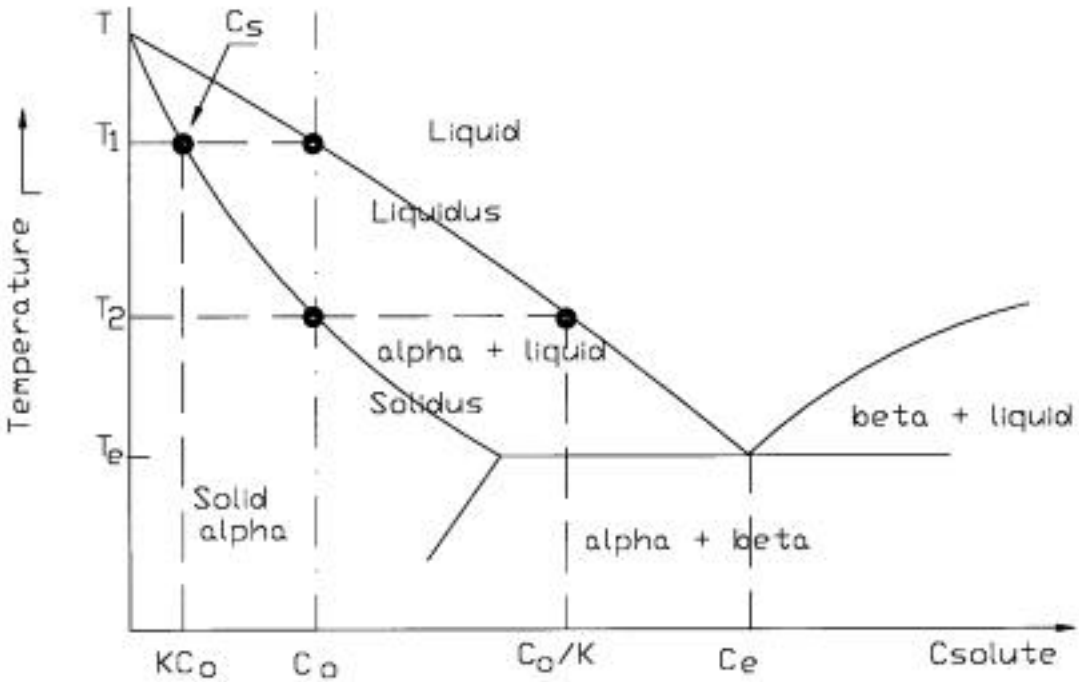

Figure 9. Hypothetical solid-liquid region of a eutectic-type phase diagram.

2.1.2. Solidification with No Diffusion in Solid and Perfect Mixing in Liquid (Case 2)

If the rate of cooling is rapid enough, no diffusion takes place in the solid. Assuming that the liquid is kept homogeneous during solidification by efficient stirring, then, as in Case 1, the first solid to appear when T_1 is reached has a composition C_s, Figure 9. This first solid contains less solute than the liquid from which it forms. The solute atoms are rejected into the liquid and increase the solute concentration above C_o. The temperature must therefore decrease below T_1 before further solidification can occur, and the second layer of solid is slightly richer in solute than the first. As this sequence of events continues, the liquid becomes progressively richer in solute, and solidification takes place at progressively lower

temperatures. However, since there is no diffusion in the solid, the separate layers of solid retain their original compositions. Thus, the mean composition of the solid (C_{sm}) is always lower than the composition at the solid-liquid interface, as shown by the marked line that starts at C_s in Figure 10. It follows that the liquid can become much richer in solute than C_o/K, and it may even reach a eutectic composition, C_e. Solidification thus tends to terminate close to T_e with the formation of a eutectic structure. This case begins to show the principle of purifying a metal (removing the solute) by zone refining (10).

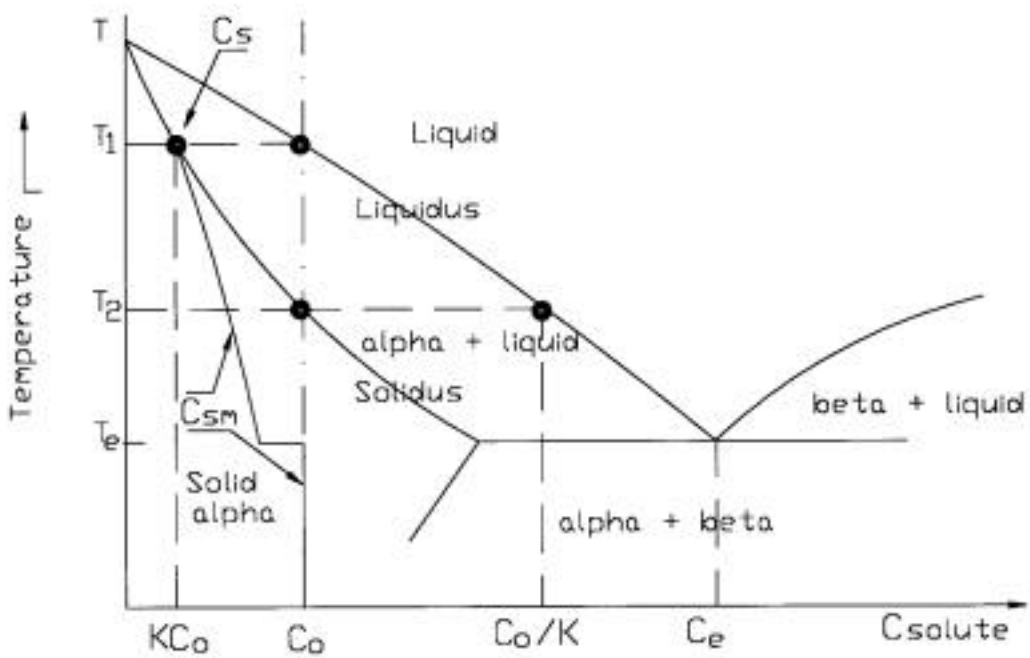

Figure 10. Hypothetical solid-liquid region of a eutectic-type phase diagram.

2.1.3. Solidification with No Diffusion in Solid and Partial Mixing in Liquid (Case 3)

As solidification occurs with partial mixing in the liquid, by far the most common case, the liquid is no longer uniform. Again, consider the molten alloy in the hypothetical phase diagram shown in Figure 9. When alloy C_o begins to solidify at T_1, the advancing solid rejects solute more rapidly than can mix into the main body of liquid, hence a layer of liquid enriched with solute builds up ahead of the interface. The solute concentration in this layer, rather than that in the main body of liquid, determines the solute concentration of solid forming at the liquid-solid interface. The solute concentration in the bulk liquid, C^{ℓ}, can be described by an effective distribution coefficient K_e equal to the ratio C_s/C^{ℓ} (4).

2.1.4. Solidification with No Diffusion in Solid, Diffusion in Liquid and No Stirring (Case 4)

If there is no stirring or convection in the liquid phase, the solute rejected from the solid is only transported away by diffusion. Cases of completely diffusion-dominated transport in the liquid are rare in practice, for metals at least. Hence, there is a rapid build-up of solute ahead of the solid and a correspondingly rapid increase in the composition of the solid formed. If solidification is made to occur at a constant rate, it can be shown that a steady state is finally obtained when the solid-liquid interface temperature reaches T_2 in Figure 9. The liquid adjacent to the solid then has a composition C_o/K, and the solid forms with the bulk composition C_o (4,9).

2.1.5. Segregation During Normal Freezing

No segregation remains after equilibrium solidification because sufficient time is allowed for complete diffusion in the solid. In practice, solidification occurs fast enough that there is usually little or no diffusion in the solid and thus segregation results. The degree of

segregation depends on transport conditions in the liquid, as in Cases 2, 3, and 4. If the freezing rate is not slow and the degree of mixing is not rapid, the advancing solid rejects solute more rapidly than it can diffuse into the liquid phase, hence an enriched layer builds up ahead of the interface. Under this condition, the enriched concentration rather than that in the main liquid phase determines the concentration of solute in the solid. The distribution coefficient in this condition is called the effective distribution coefficient, K_e. This K_e can be determined only by taking all the operational conditions into account. Thus, the equilibrium distribution coefficient K is the extreme value of the effective distribution coefficient K_e for a given system; freezing conditions for which the K_e is equal to K are those corresponding to maximum segregation.

2.2. Theory of Single-Pass Zone Refining

During zone refining, the direction of impurity travel and how well the impurity moves depends on the equilibrium distribution coefficient. When K is larger than unity, the solute accumulates at the front end of the rod; whereas when K is smaller than unity, it will accumulate at the back end. The greater the difference between K and unity, the easier the purification will be.

Consider a rod of length L of the hypothetical alloy whose composition C_o is shown in Figure 9 and cause a molten zone of length l to traverse the rod slowly, as shown in Figure 11. Since $K < 1$, by passing the zone through the ingot, it is possible to distribute the solute as shown in Figure 12. The curve has three distinct regions: an initial region (purified region) starts with composition KC_o and ends with composition C_o at the start of the central region; the central region ends at the start of the end region when the composition begins to

increase above Co; the end region is a short region of length l (molten zone width) where the solute has concentrated.

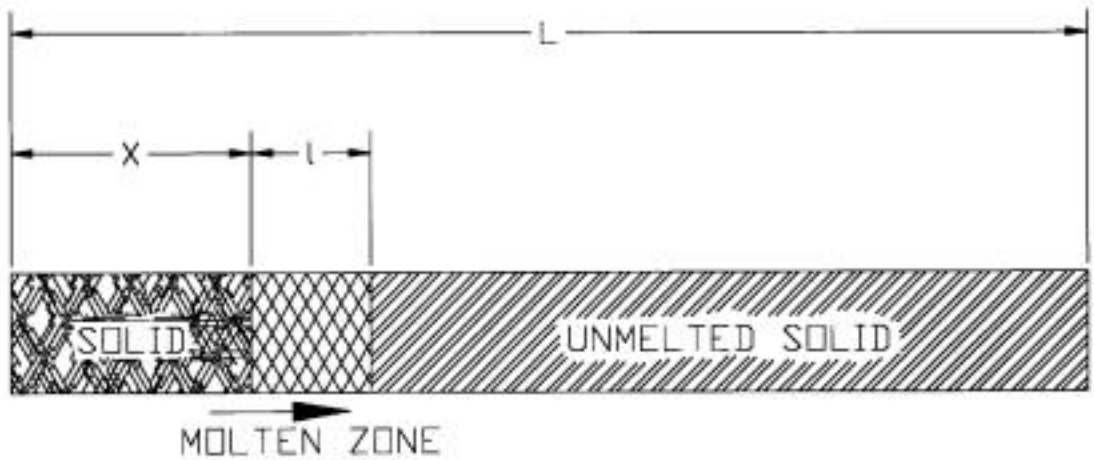

Figure 11. Molten zone traversing a rod.

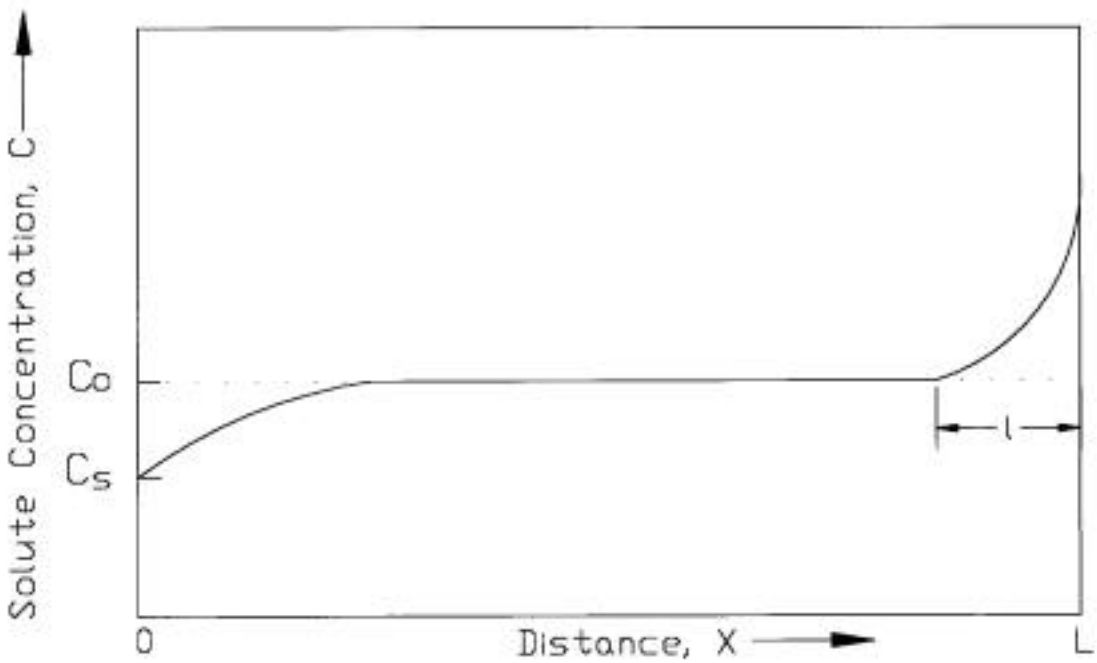

Figure 12. Variation of composition along a rod produced by zone melting after one pass (K<1).

As the molten zone moves from the front end of the rod (head-end) to the back end of the rod (tail-end), the solute accumulates at the freezing interface. If there is no fluid flow in the molten zone, diffusion is the only transport process. When the accumulation reaches a maximum, a steady state is reached, where the solute amount entering and leaving the molten zone is equal. At this point, $K_e = 1$ and there is no purification except in the first few molten zone lengths. To purify efficiently, the molten zone speed must be slow enough (less that 10 in/h), which fixes the growth rate, and uses rapid stirring to minimize the diffusion layer thickness (δ), beyond which transport by fluid motion dominates. Burton, Prim, and Slichter (10) found the relation of K_e and K considering the atomic motion at the freezing interface. As explained in Section 2.1.1.:

$$K = \frac{C[solid]}{C[liquid]} = \frac{C_s}{C_o} \tag{1}$$

The relation is described more generally as depending upon s, and possibly other quantities such as acceleration:

$$\frac{C_s}{C_o} = K^*(s, \frac{ds}{dt}.....) \tag{1a}$$

where K* is a general distribution coefficient with a value between K_e and K. The conservation of solute atoms in the melt is expressed by the continuity equation:

$$\frac{fC}{ft} = - \quad (CV \quad -D \quad C) \tag{1b}$$

where V is the vector fluid velocity, with $= (i\frac{f}{fx} + j\frac{f}{fy} + k\frac{f}{fz})$, and D is the diffusion coefficient of the solute. For a one-dimensional treatment in steady state, Equation 1b reduces to:

$$D\frac{d^2C}{dX^2} - V_x\frac{dC}{dX} = 0 \tag{1c}$$

Beyond a distance, δ, from the growing interface of the fluid, the liquid flow keeps the concentration equal to the solute concentration in the molten zone (C_o). Within δ, the normal flow velocity is s. Thus:

$$D\frac{d^2C}{dX^2} + S\frac{dC}{dX} = 0 \tag{1d}$$

with $C = C_o$ at $X = \delta$

The concentration at the interface is then given by the following equation:

$$\frac{Co - Cs}{C - Cs} = e^{\frac{s\delta}{D}} \tag{1e}$$

where δ depends upon the following relation:

$$\delta = 1.6 D^{\frac{1}{3}} \nu^{\frac{1}{6}} \omega^{-\frac{1}{2}}$$

where ω is the angular velocity of crystal rotation in the molten zone and ν is the kinematic viscosity of the liquid (10).

Using Equations 1a through e, the equation for the effective distribution coefficient in steady state can be deduced as:

$$K_e = \frac{K^*}{K^* + (1 - K^*)e^{-\frac{s\delta}{D}}} \tag{1f}$$

For the case in which equilibrium prevails at the interface independent of the growth rate:

$$K_e = \frac{K}{K + (1 - K)e^{-\frac{s\delta}{D}}} \tag{1g}$$

Thus, it is practical to find the effective distribution coefficient, K_e, through the knowledge of s, δ, D, and K (9).

The concentration at any point in the rod after one pass can be expressed as a function of the volume solidified up to that point. Assuming that the volume of the solution is unity and f, S, and C are:

f = the volume fraction solidified;

S = the amount of solute in the liquid;

S_t = the total amount of solute in the system;

C = the solute concentration in the solid at the solid-liquid interface; and

$C\ell$ = the solute concentration in the liquid.

If it is assumed that there is no diffusion in the solid and complete diffusion in the liquid, and that K_e is constant no matter how the solute concentration changes, then by definition:

$$C = K_e C_o \tag{1h}$$

$$C\ell = \frac{S}{1-f} \tag{1i}$$

$$C = \frac{K_e S}{1-f} \tag{1j}$$

and the concentration, C, in the frozen layer of volume, df, is:

$$C = -\frac{dS}{df} \tag{1k}$$

The minus sign is because as f increases S decreases. Combining Equations 1j & 1k:

$$-\frac{dS}{df} = \frac{K_e S}{1-f} \tag{1l}$$

Integration produces:

$$\int_{S_t}^{S} \frac{dS}{S} = \int_{0}^{f} -\frac{K_e}{1-f} df \tag{1m}$$

$$\ln \frac{S}{S_t} = K_e \ln(1-f) \tag{1n}$$

$$S = S_t(1-f)^{K_e} \tag{1o}$$

Combining Equations 1o & 1j:

$$C = \frac{K_e S}{1-f} = \frac{S_t K_e (1-f)^{K_e}}{1-f} = K_e S_t (1-f)^{K_e - 1} \tag{1p}$$

Since the volume was unity, $S_t = C_o$ and thus:

$$C = K_e C_o (1-f)^{K_e - 1} \tag{2}$$

After a single molten zone pass, the solute concentration can be obtained as a function of the distance from the rod head-end (X), using the same assumptions as in Equation 2. However, some of the variables have slightly different meanings than in Equation 2.

C = the concentration of freezing solid at any distance X,

ℓ = the molten zone length (constant),

S_x = the quantity of solute in the molten zone at X,

S_i = the quantity of solute in the molten zone at X=0.

Assuming unit cross-sectional area, the amount of solute in a length dX of the solid is $K_e C\ell$ dX, where $C\ell = S_x/\ell$, with C_odX the quantity entering the molten zone. The solute increase in the molten zone in moving a distance dX is:

$$dS_x = C_o dX - \frac{K_e S_x dX}{\ell} \tag{2a}$$

Combining and integrating produces:

$$\frac{dS}{dX} + \frac{K_e}{\ell} S_x = C_o \int_{S_i}^{S_x} d(S_x e^{\frac{K_e X}{\ell}}) = C_o \int_0^X e^{\frac{K_e X}{\ell}} dX \tag{2b}$$

$$S_x e^{\frac{K_e X}{\ell}} - S_i = \frac{C_o \ell}{K_e}(e^{K_e X} - 1) \tag{2c}$$

Since $S_i = C_o \ell$ then:

$$S_x = C_o \ell \frac{K_e - 1}{K_e} e^{\frac{K_e X}{\ell}} + \frac{\ell C_o}{K_e} \tag{2d}$$

Since $C = K_e S_x / \ell$

$$C = C_o - C_o(1 - K_e) e^{-\frac{K_e X}{\ell}} \tag{2e}$$

or

$$\frac{C}{C_o} = 1 - (1 - K_e)e^{-\frac{K_e X}{\ell}} \tag{3}$$

This equation is valid in all but the last zone length (Figure 12). See Figure 13 for the curves of single-pass zone refining showing solute concentration in the solid versus distance in zone lengths (rod length is 10 zone lengths) from beginning of charge, for various distribution coefficients ranging from 0.01 to 5 (4).

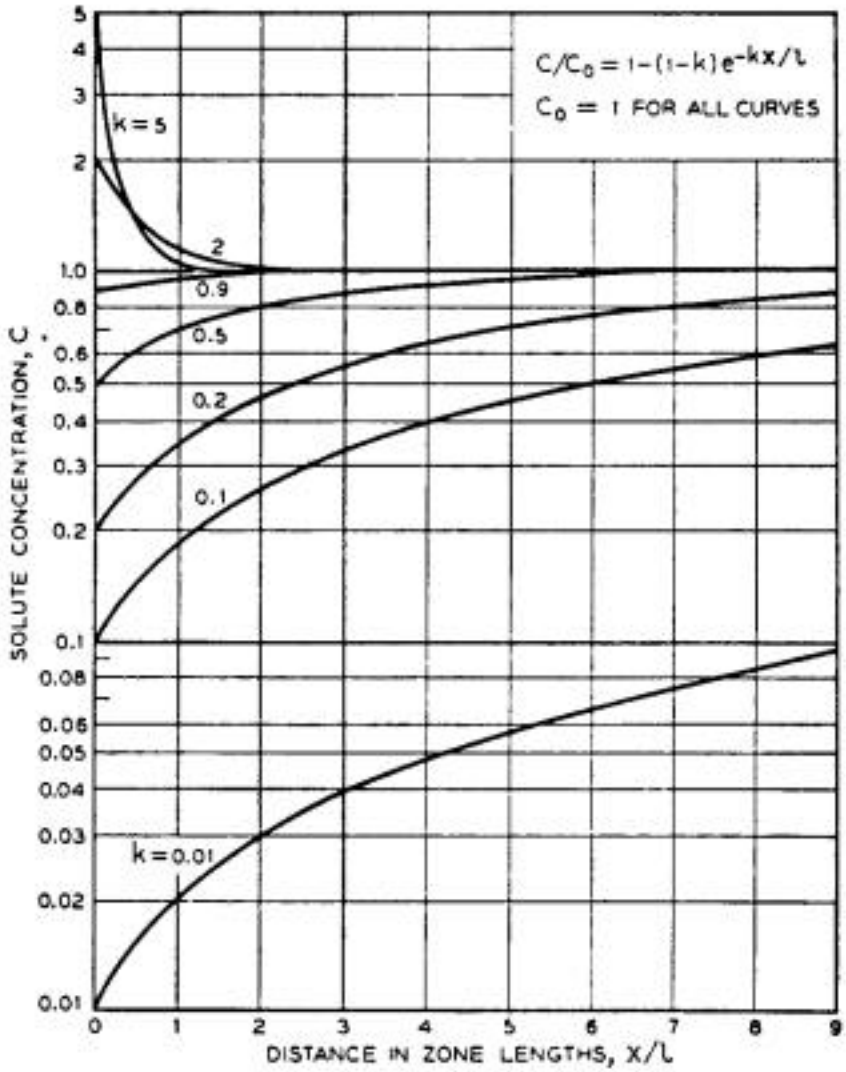

Figure 13. Curves for single-pass zone refining showing solute concentration in the solid versus distance in zone lengths from beginning of charge, for various values of K (4).

2.3. Multiple Pass Zone Refining

The merits of zone refining become evident when multiple passes of a molten zone (n) are made along a rod. During a second pass through the rod, the first solid to form is further depleted of solute, enriching the solute liquid. In each successive pass, the first solid to form is increasingly depleted of solute, and the total amount of solid depleted in solute also increases. Pfann shows examples of multiple zone refining passes (Figures 14a through c) (4). Upon examination of the figures, one can see the importance of the effective distribution coefficient. When K_e is near unity ($0.9 < K_e > 1.1$), a large number of passes may be required before any appreciable redistribution of solute can be effected (Figure 14c). Nevertheless, the ultimate redistribution may be considerable, and so zone-melting processes are important in such cases.

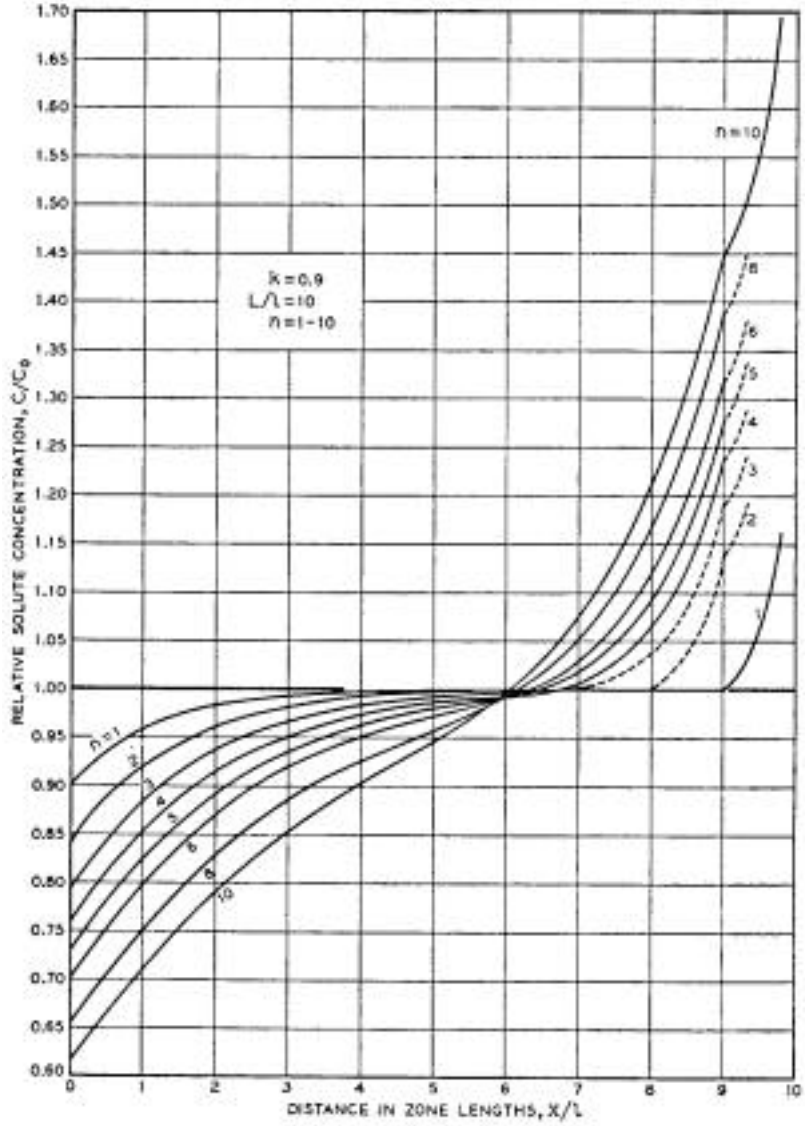

Figure 14a. Relative solute concentration C/C_0 versus distance in zone lengths X/l from rod head-end for various numbers of passes n. Parameters: $K_e = 0.9$, $L/l = 10$; and n= 1-10 (4).

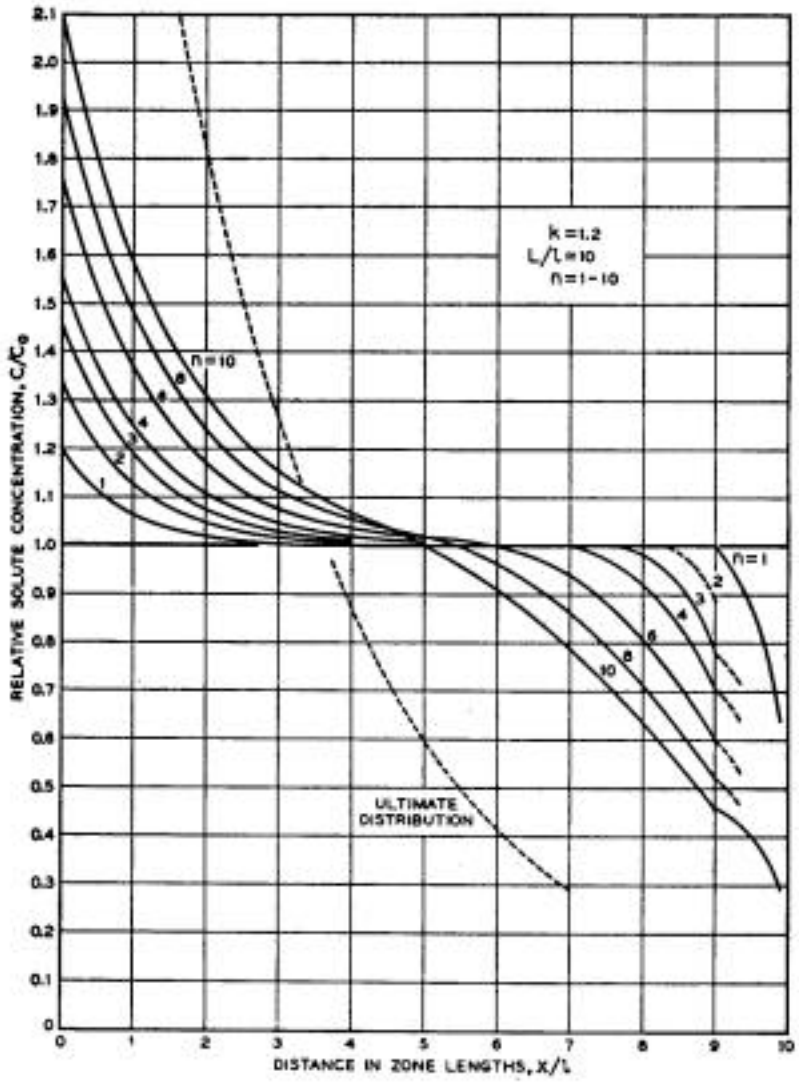

Figure 14b. Relative solute concentration C/C_0 versus distance in zone lengths X/l from rod head-end for various numbers of passes n. Parameters: $K_e = 1.2$, $L/l = 10$; and n= 1-10 (4).

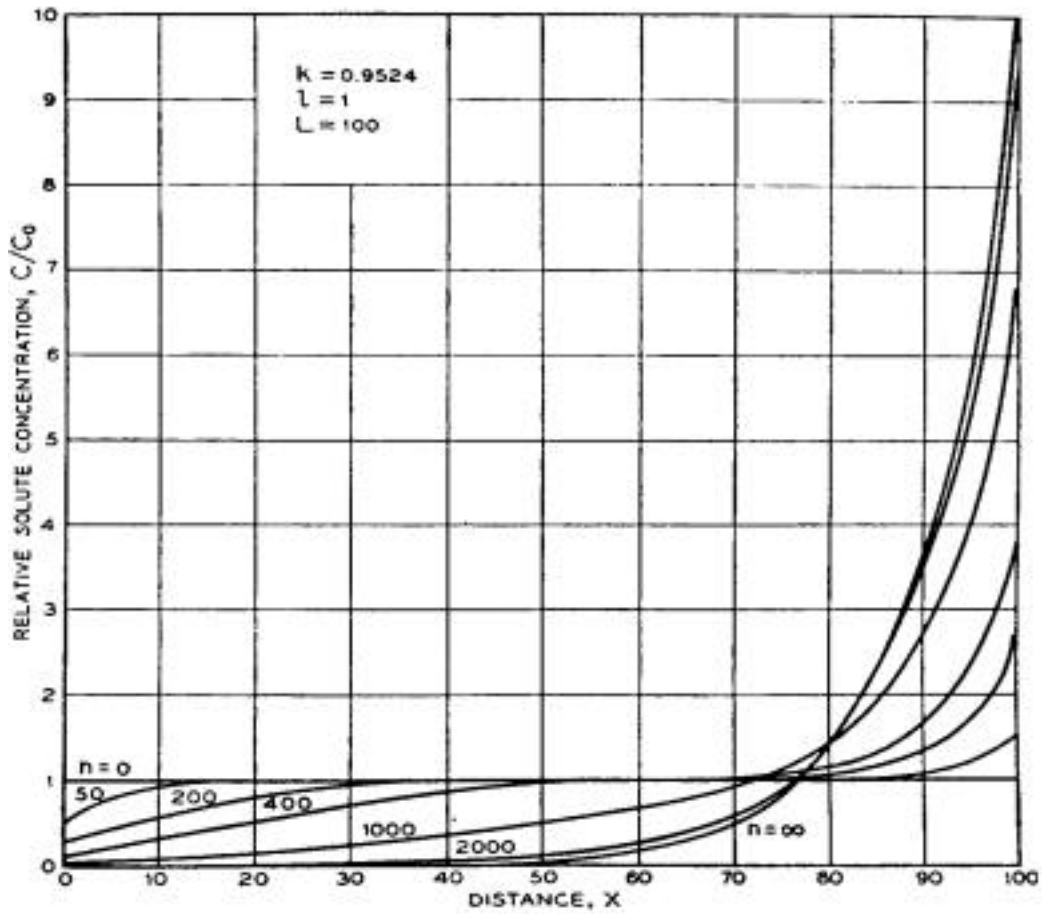

Figure 14c. Relative solute concentration C/C_0 versus distance X with number of passes n as a parameter for Ke = 0.9524, l = 1, and L = 100 (4).

For this study, there is a need for an equation that expresses solute concentration as a function of distance from the head-end of the rod for any number of passes through the rod. A complex expression for solute concentration as a function of distance in molten zone lengths and number of passes was derived by Lord (11). This equation unfortunately does not account for backward reflection of the pile-up at the rod tail-end. Thus, it is only applicable to the region ($0<x<L-n\,l$).

To derive the noncomplex part of Lord's (11) equation, one must start with the effective distribution coefficient K_e and assume that it is constant throughout the rod for all passes considered. This assumption does not cause much error as long as the initial impurity concentration is below 1%. The effective distribution coefficient is then defined as:

$$K_e = \frac{C_n(X)}{C_{nL}(X)} \tag{3a}$$

where $C_n(X)$ is the impurity concentration in the solid rod at distance X during the nth passing of a molten zone, and $C_{nL}(X)$ is the impurity concentration of the liquid zone from which the solid at distance X is formed. $C_{nL}(X)$ remains the same after passage of the molten zone (no solid diffusion). The constant K_e may be either greater or less than unity, but Lord's (11) derivation is based on the former.

Each $C_n(X)$ can be determined from the condition that the amount of solute added to the molten zone during an incremental advance, dX, is due to the melting in of a solid portion $C_{n-1}(X)dX$ and the freezing out of $K_e C_{nL}(X)$, that is:

$$\frac{d}{dX}C_n(X) + \frac{K_e}{l}C_n(X) = \frac{K_e}{l}C_{n-1}(X+l) \tag{3b}$$

This is based on the assumption that l is constant and that the total impurity content previously present up to X + l is constant (11).

2.4. Molten Zone Speed and Width

In deciding upon the optimum speed of zone refining, one must take into account both theoretical and economic aspects. However, theoretical considerations may override those of time and expense. On the other hand, where zone refining has important commercial applications, it may be necessary to go to great lengths in order to develop continuous rather than batch processes (12).

For theoretical purposes, it has been assumed that solid-state diffusion is so slow relative to liquid diffusion that it can be considered as negligible. On the other hand, it has been convenient to imagine diffusion in the liquid as being complete. However, this is not particularly so in practice as rejected solute atoms entering the molten zone near the freezing face have to be continuously transported away into the liquid by diffusion, convection, or mechanical stirring. Thus, the rate of solidification that depends on the speed of zone travel must be much more rapid than the rate of solid diffusion, and yet not too rapid to prevent reasonably efficient diffusion of the impurity into the molten zone. Any mechanical aid to liquid diffusion, such as stirring, increases the efficiency to the process. For example, zone speeds can be increased by ten-fold or larger for a given degree of purification if efficient stirring of the molten zone can be accomplished (12).

Zone velocity may also be governed by practical considerations, and the optimal speed that should be adopted to ensure maximum efficiency is a balance between these and theoretical considerations. Zone velocities are slow, particularly in metals, and vary between 0.25 and 6 in/h (12).

Zone width is usually governed by practical considerations and in particular by the physical properties of the material in question. A stable and compact zone with the sharpest possible demarcation between the liquid and solid phases gives the best chance of success. Such an ideal molten zone depends upon the degree to which it is possible to focus the heat input. This in turn depends upon the melting point, specific heat, latent heat of fusion, emissivity, and thermal conductivity of the material being purified. It is thus easier to produce a narrow molten zone in a material having a high melting point and poor thermal conductivity than in a material having a melting point near room temperature and good thermal conductivity (12).

2.5. Molten Zone Heating

The problem of producing and maintaining a molten zone amounts to establishing a temperature in the zone that is above the melting point of the solid, and establishing on either side of the zone a cool region whose temperature is below the melting point of the solid. If the zone length is to remain constant, this temperature profile must be held correspondingly constant (4).

The problem of moving a zone amounts to moving both the heat source and heat sink; i. e., furnishing heat of fusion at the melting interface and removing heat of fusion at the freezing interface. Even at the low travel rates used in zone refining, the heats of fusion and freezing can markedly change the temperature profile when an established zone begins its travel (4).

2.5.1. Molten Zone Heating Techniques

Many techniques can be used for heating the molten zone, from the simple method of resistance heating to the more complex laser heating methods. An ideal means for generating a molten zone in a bar of metal is induction heating. This method is applicable only to substances that conduct electricity and so has particular use in the zone refining of metals. If the material concerned is surrounded by a coil that carries a high-frequency current, energy in the form of heat is produced in the surface layers by the induced current that flows around the bar. The temperature to which the metal rises for a given power input is governed by the frequency employed, the rate of heat conduction to the center of the bar, time, and heat losses due to normal conduction, convection, and radiation. This method has another natural advantage for zone melting as it ensures continual self-stirring within the molten zone, which aids diffusion of the impurity atoms away from the solidifying face into the molten pool (12).

2.6. Containers

Finding a container suitable for zone refining may be either easy or difficult, depending on the charge substance. For many chemicals, metals, and semiconductors, the job is relatively simple. For reactive substances, it is not. In fact, techniques of zone melting without a container had to be devised to zone-refine highly reactive substances such as silicon, iron, beryllium, and molybdenum. It is essential to find a material that contaminates the melt as little as possible. Contaminants may be agents on the surface of the container, gases in interstices of the porous container, impurities occluded or in solid solution in the container material, or the material of the container itself. For physical reasons as well as chemical ones, the liquid should not wet the container material, since this may result in

adhesion of the solidified charge to the container, which may cause fracture of either or both by differential thermal contraction (4).

CHAPTER 3

THE THEORY OF VACUUM METALLURGY (DISTILLATION)

3.1. Introduction

The part of the science of metallurgy that is concerned with the extraction and refining of metals deals largely with the properties whereby metals may be distinguished and separated from other nonmetallic elements and from each other. An important property that separates one metal from another is volatility. The boiling points of metals range from 39 C for mercury to approximately 6000 C for tungsten, with the boiling points of other metals well scattered in between. This indicates that it should be possible, in principle, to separate any mixture of metals existing in the metallic state by selective distillation. The more volatile metals, such as mercury and zinc, are recovered from their ores by reduction and distillation. Distillation at atmospheric pressure requires temperatures approaching the boiling point of the metal to be distilled. However, if the pressure of the residual gas is decreased, the partial pressure of the vapor required for distillation is correspondingly decreased (13).

In the 1950s, there were important developments in the technique of evacuating large enclosures. This resulted in the ability to produce metallic magnesium and calcium by reduction and distillation in an evacuated retort. Furthermore, a method was developed for removing zinc from molten lead by distillation in an evacuated bell that was emerged in the molten metal. It should be mentioned that evacuation offers the further advantage of protecting the metal vapor from reacting with the gaseous constituents of the atmosphere,

thereby allowing reactive metals to be recovered in the pure state, uncontaminated by oxides or nitrides (13).

3.2. Vapor Pressures of Metals

Thermodynamics in vacuum metallurgy is a useful tool to predict the equilibrium state of any metallurgical system, but it does not predict the rates of reactions. It tells us what reactions are possible, under what conditions they will proceed, and what the final state will be (13).

The relationship between vapor-pressure and temperature can be derived from the Clausius-Clapeyron equation:

$$\frac{dp}{dt} = \frac{\Delta H}{T \Delta V} \tag{4}$$

where p is the vapor pressure, H is the enthalpy, T is temperature, and V is volume. An approximate solution of this equation gives the logarithm of the pressure as a linear function of the reciprocal absolute temperature:

$$\log p = A - \frac{B}{T} \tag{4a}$$

where A and B are constants (13). A better approximation of the vapor-pressure is given by a more complex form of Equation 4a:

$$\log p = \frac{A}{T} + B \log T + CT + D \tag{4b}$$

where A, B, C, and D are constants.

3.3. Partial Pressures of Metals

Vapor pressures of metals in the pure state represent the relative volatility under conditions of immiscibility. But when two or more metals are mixed as solid or molten solutions, the vapor pressure is decreased approximately proportional to the mole fraction. The partial pressures, p_1 and p_2, of components 1 and 2 are then:

$$p_1 = p_{01} x_1 \text{ and } p_2 = p_{02} x_2 \tag{4c}$$

where p_{01} and p_{02} are the vapor pressures of the two metals in the pure state, and x_1 and x_2 are their respective mole fractions assuming ideal gases (13).

If a mixture of approximately equal proportions of two metals is distilled, the vapor is composed almost entirely of the more volatile constituent, but as distillation proceeds, the proportion of the more volatile constituent decreases. Therefore, the composition of the residual metal eventually becomes such that the vapor contains an appreciable proportion of the less volatile metal. Since the molal proportion of the two constituents is proportional to their partial pressures, the composition of the vapor can be estimated as follows:

$$c_2 = \frac{p_2}{p_1 + p_2} = \frac{x_2 p_{02}}{x_1 p_{01} + x_2 p_{02}} \tag{4d}$$

where c_2 is the fraction of the less volatile metal in the vapor (13).

3.4. Rate of Evaporation

At any given temperature, there is a maximum rate at which a volatile substance evaporates from an exposed surface. This rate is difficult to calculate from kinetic theory but can be estimated from the observed vapor pressure or partial pressure of the volatile substance in question. At equilibrium, the rate of evaporation is equal to the rate of condensation of the vapor on the evaporating surface. From kinetic theory, the rate of collision of molecules of vapor with the surface can be calculated from the pressure of the vapor. The mass of vapor molecules (μ) striking a square centimeter of surface per second is given by:

$$\mu = \frac{\rho\nu}{4} \tag{5}$$

where ρ is the density of the vapor and ν is the average molecular velocity. The average molecular velocity and density is also given in the following equations:

$$\nu = 4\sqrt{\frac{RT}{2\pi M}} \tag{5a}$$

$$\rho = \frac{pM}{RT} \tag{5b}$$

where p is the vapor pressure, R is the gas constant, M is the molecular weight, and T is temperature. Combining Equations 5, 5a, and 5b gives:

$$\mu = p\sqrt{\frac{M}{2\pi RT}} \tag{5c}$$

In general, the number of molecules returning to the surface is the same fraction α of the number striking it so that the rate of return is $\alpha\mu$. At equilibrium, this is the same as the rate of evaporation; therefore, the maximum rate of evaporation (ω_o) is:

$$\omega_o = \alpha p_o\sqrt{\frac{M}{2\pi RT}} \tag{6}$$

where p_o is the vapor pressure at equilibrium (13).

However, the observed value of α for metals is very nearly unity; therefore, the rate of evaporation can be estimated by:

$$\omega_o \quad p_o\sqrt{\frac{M}{2\pi RT}} = 3.50\, p_o\sqrt{\frac{M}{T}} \tag{6a}$$

with the units (atm) for pressure, (g) for molecular weight, (K) for temperature, and (g per cm^2 per min) for the rate of evaporation (13).

Evaporation can occur at rate ω_o only in a perfect vacuum and when the rate of evaporation is so small that the mean free path of the vapor molecules exceeds the distance between the evaporating and condensing surfaces. Under these conditions, evaporation is known as molecular evaporation (13).

At appreciable rates of evaporation, the vapor molecules collide with each other; some rebound from the surface, so that the actual rate of evaporation is the difference between ω_o and the rate of return from the surface, ω_1. The net rate of evaporation is then:

$$\omega = \omega_o - \omega_1 \tag{6b}$$

As already discussed, the two rates, ω_o and ω_1, are related to the corresponding pressures p and p_o. Therefore, the net rate of evaporation is given by:

$$\omega_o = 3.50(p_o - p)\sqrt{\frac{M}{T}} \tag{6c}$$

where p is the partial pressure of the vapor at the evaporating surface (13).

The ratio between p and p_o is the degree of saturation of the vapor. It varies from 0 to 1.00 as the evaporating conditions vary from molecular evaporation to equilibrium. The degree of saturation is related to the observed and maximum rate of evaporation:

$$\frac{p}{p_o} = 1 - \frac{\omega}{\omega_o} \tag{6d}$$

The actual rate of distillation is determined not so much by the rate of evaporation from the surface as by the rate of transfer of vapor away from the surface. This rate of transfer is not as easy to calculate as the rate of evaporation. The factors that must be considered are:

(1) Pressure gradient of the vapor.

(2) Effective pressure of permanent gas in the system.

(3) Dimensions of the distillation chamber and condensing system.

When the distance between the evaporating and condensing surfaces is small with respect to the diameter of the chamber, the walls of the chamber have little effect and the rate of transfer is determined primarily by the rate of diffusion of the vapor. When the residual gas pressure is less than the partial pressure of the vapor, the rate of transfer is determined primarily by the pressure gradient of the vapor. The rate of distillation is equal to the rate of diffusion down the pressure gradient:

$$\omega = DM \frac{p_1 - p_2}{Z} \tag{7}$$

where p_1 is the partial pressure of vapor at the evaporating surface, p_2 is the partial pressure of vapor at the condensing surface, Z is the effective distance between the two surfaces, D is the effective diffusion constant, and M is the molecular weight (13).

An important point to consider is that the effective pressure of permanent gas (all gases other than distilling vapor) in the system is much less than the observed pressure in the condenser. The distilling vapor acts as a diffusion pump and sweeps the gas molecules away from the evaporating surface toward the condenser. Therefore, the effective pressure of the

permanent gas is always less than the observed pressure in the system. For this reason, the rate of evaporation usually becomes independent of the gas pressure after the pressure in the system has been decreased to a few tenths of a millimeter. Very low pressures are required only when the metal vapor tends to react strongly with the permanent gases (13).

When the pressure of the permanent gas is large enough to be taken into account, the rate of transfer is limited by the rate of diffusion of the vapor through the permanent gas. Under these conditions, the rate of distillation is related to the pressures of the vapor and gas in the following way:

$$\omega = \frac{DM}{Z} \log \frac{p_3 - p_2}{p_3 - p_1} \tag{7a}$$

where D is the diffusion constant and p_3 is the pressure of residual gas, which is different from that in the previous Equation 13.

For practical purposes, the rate of distillation is determined by the rate at which heat is transferred to the evaporating surface. All other factors adjust themselves to the conditions in which the heat required for evaporation is balanced by the rate at which thermal energy is transferred to this surface. Usually this heat is transferred by conduction from the body of the liquid, so that the temperature has a strong positive gradient below the surface (bulk liquid is hotter than the liquid at the surface). This temperature gradient is equal to:

$$\frac{dT}{dZ} = \frac{\Delta H_v \omega}{60 M \lambda} \tag{8}$$

where ΔHv is the heat of vaporization, M is the molecular weight, λ is the thermal conductivity of liquid metal, and ω is the rate of evaporation (13).

Another important factor to be considered is the effect of films on the evaporating surface, which often have a profound effect in inhibiting evaporation. These films may be composed of extraneous impurities or they may be formed from the metals being separated. Films may result from premature condensation of the vapor. As previously pointed out, during rapid evaporation, the vapor leaving the surface is only partially saturated with respect to the surface temperature. As it moves into a zone of lower temperature, it approaches saturation. If condensation occurs below the melting point, the condensed phase is a fine powder that settles on the surface as a loosely compacted film with low thermal conductivity and is therefore not readily absorbed by the liquid.

It is also possible for a film to form from the liquid phase when the less-volatile component has the higher melting point. For example, in the distillation of zinc from aluminum, the surface may become so depleted of zinc that the composition reaches the liquidus composition. In this case, a thin layer of liquid phase crystallizes at the surface of the bulk liquid (13).

3.5. Selective Distillation

Since the real purpose of distillation is to separate one metal from an other, it is pertinent to inquire into the selectivity of the evaporation process and the factors that affect selectivity. The two most important factors that determine selectivity have already been discussed; they are relative vapor pressures and the molal proportions of the constituents

remaining in the residual metal. The effect of these factors is shown by Equation 4d, which was derived by assuming that partial pressures over metallic solutions obey Raoult's law. This is approximately true for pairs of metals having similar properties such as lead and tin. The agreement with Raoult's law usually improves as the distillation temperature is raised. However, when the metals show a tendency toward immiscibility, the partial pressures show a positive deviation from Raoult's law, i.e., they are greater than that predicted by Equation 4d. On the other hand, metals that show a tendency to combine into intermetallic compounds undergo a mutual decrease in activity when mixed, and their vapor pressures show a negative deviation. The extent of the deviation increases as the molal ratio between the constituent metals increases (13).

A fourth and very important factor affecting the selectivity of distillation is the rate of diffusion of the volatile metal from the interior to the evaporating surface. As the volatile constituent is rapidly distilled, the surface layer becomes depleted and a concentration gradient is established with respect to the interior. The relationship between the rate of diffusion and concentration gradient is expressed by Fick's law:

$$J = -D\frac{dc}{dX} \tag{9}$$

where J is the flux diffusing through unit area in unit time, c is the concentration of diffusing component, X is the distance in direction of diffusion, and D is the diffusivity (13).

The concentration gradient adjusts itself to the value required to balance the rates of diffusion and evaporation. In other words, the concentration gradient is proportional to the net rate of evaporation. When the volatile metal has a low diffusivity and is sufficiently

depleted, the concentration of the volatile metal at the surface may become so low that metals are evaporated in nearly the same ratio found in the residual metal (13).

3.6. Engineering Problems of Distillation

There are at least four known interrelated engineering problems in the distillation process at high temperatures. These recognized problems are bumping or splattering, vapor trapping, metal/container reactions, and long distillation times. Bumping, or splattering, appears to be a serious problem encountered in vacuum distillation of plutonium metal. The phenomenon involves formation of a gas bubble at some depth (often at the bottom) in the liquid and the rising of the bubble to the surface, with rapid expansion because of the much lower pressure at the surface of the dense liquid (molten plutonium has a density of approximately 16.5 g/cm^2). The amount of vapor inside the bubble also increases rapidly throughout its lifetime because of the large temperature of superheating that occurs before bubble nucleation. Whereas water may require superheating of about 50 C at a clean surface to initiate bubble formation, superheating temperatures required for bubble formation in plutonium metal are much higher. In the case of water, superheating is usually restricted to a relatively thin film at the surface because the low thermal conductivity of water causes high thermal gradients. The thermal conductivity of molten plutonium metal is about 50 times greater than that of water (Figure 3), so the whole body of liquid metal is superheated before bubble nucleation at the heated surface. The combination of these effects can produce vaporization of a large mass of molten metal on the subsecond time scale. The first bubble may produce an acoustic wave and disrupt the geometry of the pool to produce areas of reduced pressure, with both effects leading to nucleation of additional bubbles. The net

effect is to produce almost explosive forces that may mechanically disrupt the weaker parts of the apparatus and throw a spray of droplets of unfractionated liquid into the condenser and vacuum system The bumping problem can be relieved somewhat by heating slowly, pumping with a system that produces a poor quality ultimate vacuum, or equipping the system with an inert gas bleed-in and pressure control system. Stirring is another technique that has been little used in molten metal distillation, but might be effective. This bumping phenomenon of molten plutonium metal in a vacuum was observed during the first pass of each zone refining run in Blau's study. This bumping caused small amounts of plutonium metal to splatter out of the crucible (5,7).

Another problem encountered in vacuum distillation is the difficulty of achieving efficient vapor trapping. To minimize the time required for true vacuum distillation, the pathway for evacuation of the distillation chamber should be relatively open to achieve a low ultimate pressure, but if that pathway is open too far, the vapor spreads throughout the system and is difficult to recover. This loss can be minimized by avoiding bumping and by operating a very cold condenser (7).

Reactions between the molten metal and the container cause serious problems because this contaminates the melt, damages the container, and makes it impossible to remove the solidified product from the container without breaking the container. The higher the temperature, the faster the container/metal reaction. This containment problem was overcome by using a Crystalox® crucible, which levitates the molten plutonium zone using a magnetic field that is produced by the induction field used to heat the plutonium impurities being distilled.

CHAPTER 4

REVIEW OF THE LITERATURE

4.1. Zone Refining of Plutonium

There have been two documented studies of plutonium zone refining at the Los Alamos National Laboratory.

4.1.1. First Investigation

Modest success in the zone refining of plutonium was reported by Tate and Anderson in 1958 at the Los Alamos National Laboratory (2). They made zone refining runs on five different plutonium rods (10 passes each) at five different speeds (0.23 to 1.3 in/h). The starting plutonium contained impurities averaging less than 100 ppm per impurity. They used a 450-kHz power supply to run a single-turn coil. This induction setup produced a large molten zone compared to rod diameter, with little stirring in the molten zone.

The results showed that the impurities cobalt, chromium, iron, manganese, nickel, silicon, and aluminum were moved in the direction predicted by the respective binary constitutional phase diagrams. The experimenters also confirmed that the slower the molten zone speed, the greater the segregation. However, in most cases, a speed of 1.3 in/h had poor separation, a speed of 0.9 in/h had better separation, and slower speeds down to 0.23 in/h did not improve the separation. The elements beryllium, bismuth, boron, calcium, copper, lanthanum, lead, lithium, magnesium, silver, sodium, tin, and zinc did not appear to move.

This study had three deficiencies. All five rods used had different compositions. The impurity levels were low, making it difficult to measure element movement. The induction frequency was so high that there was little induction stirring in the molten zone.

4.1.2. Latest Investigation

Modest success in the zone refining of plutonium was reported by Blau in 1994 at the Los Alamos National Laboratory (5). This study showed that after 10 passes of six different bars of a molten zone in a zone refining operation through a bar of plutonium metal, moderate movement of certain elements was achieved. Blau used a 3-kHz power supply to run a three-turn coil. The plutonium was zone refined in tantalum boats that moved through the coil at either 1 or 2 in/h. The impurity elements cobalt, copper, chromium, iron, nickel, neptunium, and uranium moved in the direction of zone travel. Aluminum, americium, and gallium moved in the opposite direction. These results were in accord with anticipated element movement based on the distribution coefficient determined from the binary phase diagram of each element with plutonium. While this study demonstrated that zone refining can be used to redistribute impurity elements in plutonium metal, it could have been improved with better containment and stirring of the molten plutonium metal.

4.2. Zone Refining of Similar Metals

As already discussed, plutonium is an unique metal. The most readily available metal with properties similar to plutonium is uranium. The most obvious difference between them is their melting points, 1132 C for uranium compared to 640 C for plutonium. Modest success has been documented in zone refining of uranium metal. Both natural impurities and fission products have been redistributed by this method. There have been several studies on zone refining of uranium using many different techniques and with starting materials

containing impurities ranging from 50 ppm to over 1000 ppm. In all cases, there was some degree of uranium purification (4, 14,15, 16).

One of the best examples of uranium zone refining using uranium with moderate impurity levels (1000 ppm) was by Bieber, Schreyer, and Williams (14). Using an electron-beam zone refining technique, they purified uranium from 1000 ppm to about 50 ppm in six passes using different speeds (0.75 to 5.0 in/h). However, they determined that the oxide layer that formed during each molten zone pass had to be removed before the next pass or poor zone refining resulted.

The most current uranium zone refining work is that of Suzuki, Shikama, and Ochiai (15). Using an induction zone refining technique under high vacuum, they were able to obtain uranium purity of 99.99 weight percent (100 ppm total impurity content).

4.3. Special Issues with Plutonium

Many challenges must be faced in order to process plutonium because of its toxicity, reactivity, pyrophoricity, and criticality hazards. Therefore, plutonium experimentation must be conducted inside gloveboxes, making even the simplest tasks difficult, time-consuming, and costly. The reactivity of molten plutonium severely limits the container that is suitable for experimenting with molten plutonium to either a few ceramics or refractory metals, or metals with certain coatings. Also, plutonium metal is highly pyrophoric when heated or finely divided, thus molten plutonium must be kept away from oxygen. Because of the criticality hazard, metallic plutonium experiments must be conducted using less than 4.5-kg batches.

4.3.1. Glovebox

The greatest health hazard from plutonium arises from the emission of alpha particles. Plutonium forms an extremely fine particulate oxide, which readily disperses in air and is easily respirable. Therefore, gloveboxes are required to keep the plutonium contained. Shielding for the other types of radiation, such as beta, gamma, neutrons, and x-rays, must also be provided (17).

When a glovebox must be used for containing radioactive material, many compromises must be made. All hands-on tasks are done using lead-lined gloves attached at glove ports that may not always be in the best location for the particular experiment. This is especially true for research, because in many cases research gloveboxes must be designed for many different projects. In general, performing research-type tasks in a glovebox takes at least ten times longer than if they were performed in the open. Also, for the person performing the glovebox tasks, the effort required is approximately fifteen times that of performing the same task in the open. One reason why it takes so much effort is because of all the required training before a person is allowed to work in a glovebox, as well as the continuous required training.

4.3.2. Reactivity

Molten plutonium metal is very reactive (it is a better oxygen-getter than titanium) and is also a pyrophoric substance when finely divided. The biggest obstacle to over come in developing a zone refining or distillation process for plutonium metal is containment of the molten metal. This is because all metals react with molten plutonium, and ceramics cannot withstand the thermal shock associated with zone refining. This containment problem may be overcome by using a Crystalox® crucible, which levitates the molten plutonium zone

using a magnetic field that is produced by the induction field used to heat the plutonium being zone refined. Furthermore, because of the reactivity of plutonium with atmospheric gases at elevated temperatures, any operations conducted at elevated temperatures must be done in a protective atmosphere. High vacuum has been found to be the most practical environment in which to melt plutonium. But vacuum melting further increases the difficulty of zone refining or distillation of plutonium because this now requires another air-tight chamber within the glovebox to contain the zone refining or distillation apparatus. However, additional purification results from evaporation of volatile impurities from the molten zone when the zone refining is accomplished in a high vacuum.

4.4. Distillation of Plutonium Impurities

Analytical data taken during Blau's study (5) indicated that an amount of each impurity in the plutonium metal vaporized under the vacuum conditions of the experiments. The data accounted for an apparent total impurity loss in excess of 25%. Because of the enhanced purification resulting from vaporization of impurities, vaporization studies were conducted concurrently with the zone refining studies.

4.4.1. Impurity Distillation

Purification of plutonium by vaporization of impurities has been the subject of many studies over the past 45 years. For such a technique to be useful, the vapor pressure of the impurity must be greater than that of plutonium, as discussed previously. Vaporization alone does not produce pure plutonium because some impurity elements have vapor pressures less than that of plutonium. Therefore, it may prove useful to measure the reducing levels of some impurities commonly found in metallic plutonium (7).

The first step in purification is to determine the maximum rate of evaporation (ω_o). Starting with Equation 6a from Section 3.4 and putting ω_o into units of (g per cm^2 per s) produces:

$$\omega_o = 0.058 p_o \sqrt{\frac{M}{T}} \tag{10}$$

where p_o is the vapor pressure at equilibrium in torr, M is the gram molecular weight, and T is the absolute temperature in K.

Equation 10 is valid for a pure substance. Impure plutonium is a dilute solution; therefore, Equation 10 must be modified to take this into account. The modifying factor is the area of the vaporizing surface reduced by the mole fraction of the vaporizing species. Equation 10 then becomes:

$$\omega_1 = 0.058 A X_1 p_1 \sqrt{\frac{M_1}{T}} \tag{10a}$$

where ω_1 is the weight loss of component 1 (g s^{-1}), A is the total exposed surface area (cm^2), X_1 is the mole fraction of component 1, p_1 is the vapor pressure for pure component 1, and M_1 is its gram-molecular weight (7).

However, Equation 10a assumes a large mean free path. Collisions of vaporizing molecules with molecules of a gas blanket above the condensed phase can significantly

reduce of the rate of vaporization of material from the condensed phase. Such collisions significantly reduce the mean free path of the vaporizing species, the distance a molecule travels before it undergoes a collision. In the low-pressure region (molecular flow), which is of greatest interest in vacuum distillation processes, an approximation of the mean free path (L) in (cm) is:

$$L = \frac{0.005}{P} \tag{10b}$$

where P is the pressure in the vaporizer in torr (7).

The validity of Equation 10a was examined using zinc and americium as impurities in plutonium (7). The results of these experiments indicated that the removal of zinc from plutonium was more than 10,000 times slower than the calculated rate (Equation 10a). On the other hand, the rate of distillation of americium from plutonium was found to be of the same order of magnitude as the calculated rate. Therefore, Equation 10a may not be valid for estimating the rate of removal of some impurity elements from plutonium.

4.4.2. Vacuum Distillation of Americium Metal

Berry, Knighton, and Nannie performed a study on vacuum distillation of americium metal from plutonium metal at the Rocky Flats plant in 1981 (18). Differences in vapor pressures provide the basis for separation of americium and plutonium by vacuum distillation. In the temperature range of 1175 C to 1400 C, the difference in vapor pressures of americium and plutonium is greater than three orders of magnitude. The constants for Equation 4a for plutonium and americium in the desired range for vapor pressure (atm) are:

$$\log P = A - \frac{B}{T} \tag{4a}$$

For plutonium in the temperature range 1210 to 1620 K, A = 4.592 and B = 17120.

For plutonium in the temperature range 1724 to 2219 K, A = 9.74 and B = 17066.

For americium in the temperature range 1450 to 1820 K, A = 4.14 and B = 11300.

For americium in the temperature range 990 to 1358 K, A = 6.578 and B = 14315.

The relative concentration of the two components in the vapor phase can be determined by the ratio of their partial pressures (Section 3.3) to produce Equation 4d, the mole fraction of the component in the vapor phase:

$$c_2 = \frac{p_2}{p_1 + p_2} = \frac{x_2 p_{02}}{x_1 p_{01} + x_2 p_{02}} \tag{4d}$$

Figure 15 is a plot of Equation 4d with the above plutonium and americium vapor pressure data. This figure shows the americium content of the americium-plutonium vapor phase and the liquid phase as a function of the total pressure at 1200 C. Any horizontal line on the plot represents a condition of constant pressure. The intersections of the horizontal lines with the two curves graphically show the americium-plutonium separation that is possible by distillation. For example, at a pressure of 2.5 X 10^{-6} torr, americium concentration in the vapor phase is approximately 96 mole percent while the americium concentration in the liquid phase is approximately 1 mole percent (18).

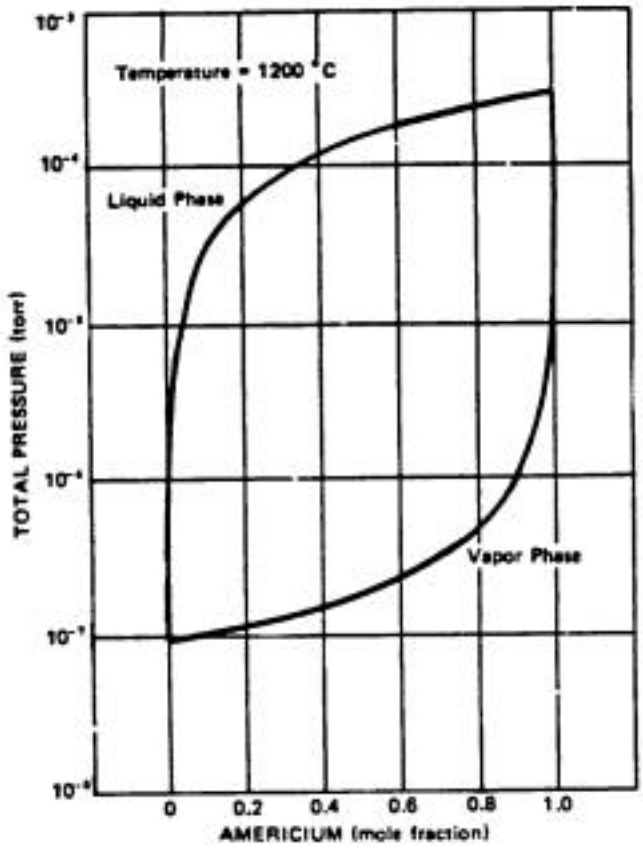

Figure 15. Americium content of the americium-plutonium vapor phase and the liquid phase as a function of the total pressure at 1200 C (18).

The distillation apparatus used for this work is shown in Figure 16. This apparatus was mounted in a 12-in vacuum feed-through collar and a water-cooled steel bell jar. The vacuum pumping system consisted of a 4-in oil diffusion pump backed with a 17-cfm mechanical pump. The vacuum system could maintain a vacuum of 10^{-6} at 1250 C. The distillation assembly consisted of a yttria (Y_2O_3) crucible, tantalum collimator, and yttria

receiver. The crucible and receiver were identical and could be used interchangeably. The receiver was cooled by use of a copper heat radiator and was supported by a tantalum support

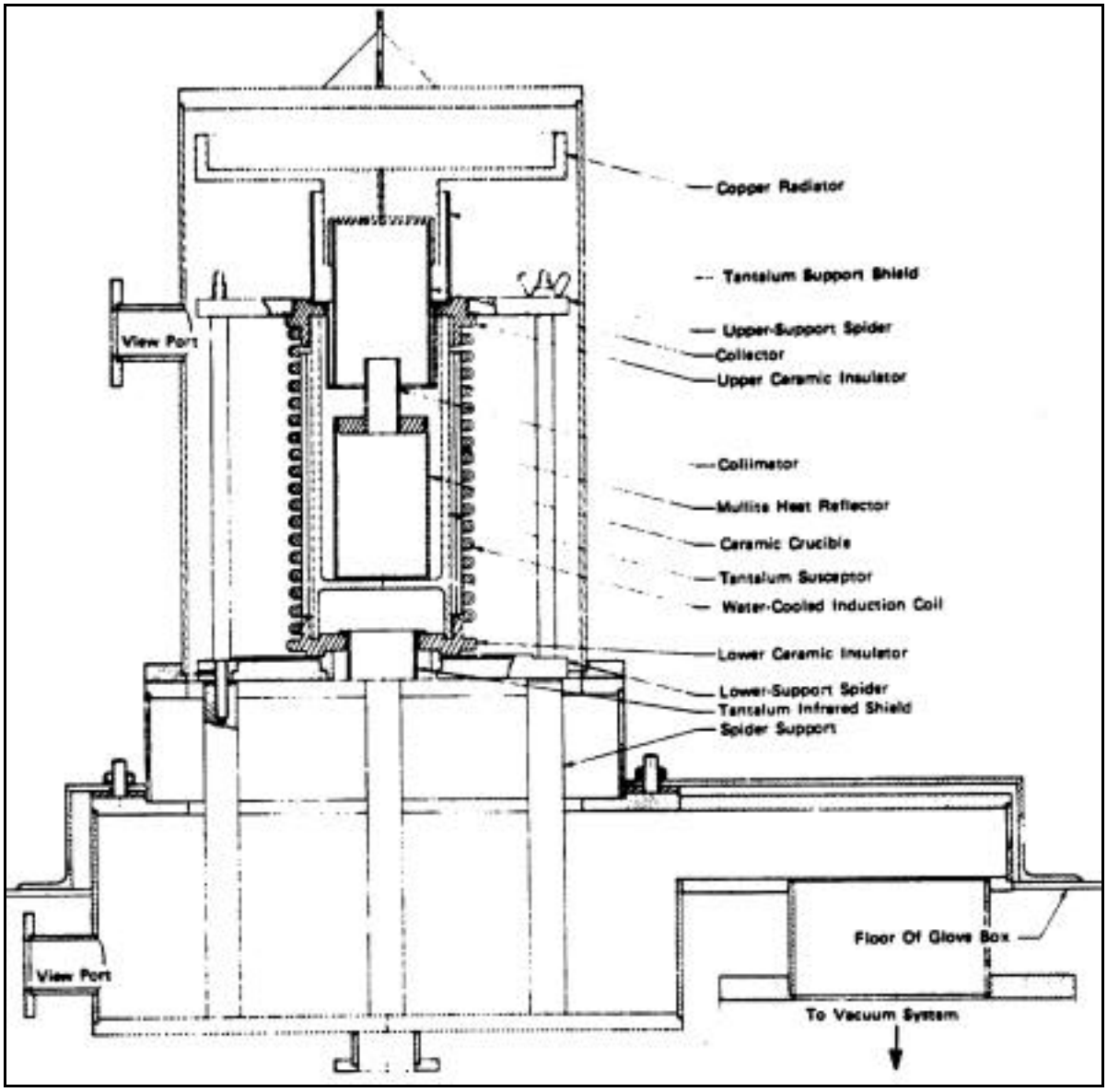

Figure 16. Americium distillation apparatus used for the Rocky Flats study (18).

shield. The size of the crucible limited the distillation assembly to 800 g of plutonium-americium alloy. The heating system consisted of an 18-turn, water-cooled induction coil with a tantalum susceptor. The power supply was a 20-kW, 9.6 kHz motor-generator set. The apparatus was in a standard plutonium handling glovebox (18).

The distillation procedure started with loading of the plutonium-americium alloy in the americium distillation apparatus (Figure 16). The vacuum chamber was purged with argon, followed by a pump down to 10^{-6} torr. The heat-up rate was controlled at approximately 400 C per h up to 1200 C. The melt was then held at 1200 C for 4 h, during which the condenser temperature would reach 600 C. After the 4-h hold, the furnace was cooled at a rate of about 600 C per h to 500 C and then allowed to cool uncontrolled overnight. The results of four runs made during this study were that in each case gram quantities of americium condensed on the condenser. The average americium purity of the condensed americium was 99.7 w/o, with an average plutonium impurity content of 0.31 w/o. The americium rate of evaporation was approximately 50% of the maximum rate of evaporation predicted by Equation 10a for americium (18).

4.4.3. Separation of Zinc from Plutonium by Vacuum Melting

Sandvig performed a study on vacuum distillation of zinc metal from plutonium metal at the Rocky Flats plant in 1980 (19). The interest in separation of zinc metal from plutonium metal came about because of a proposed pyroredox process to purify plutonium that would leave residual zinc metal (0.1 to 10 w/o) in the purified plutonium metal product. The apparatus used was comparable, but a more simple apparatus than the one used by Berry,

Knighton, and Nannie (18). The procedure used was similar to the one used by Berry, Knighton, and Nannie (18) except that the hold temperature was 800 C instead of 1200 C, and the runs were made using 12 different zinc-plutonium alloys (1, 2, 3, 4...11, 12 w/o Zn). The results were that the theoretical rate of evaporation for zinc (Equation 10a) was about four to five orders of magnitude greater than the experimental rate as shown if Figure 17 (19).

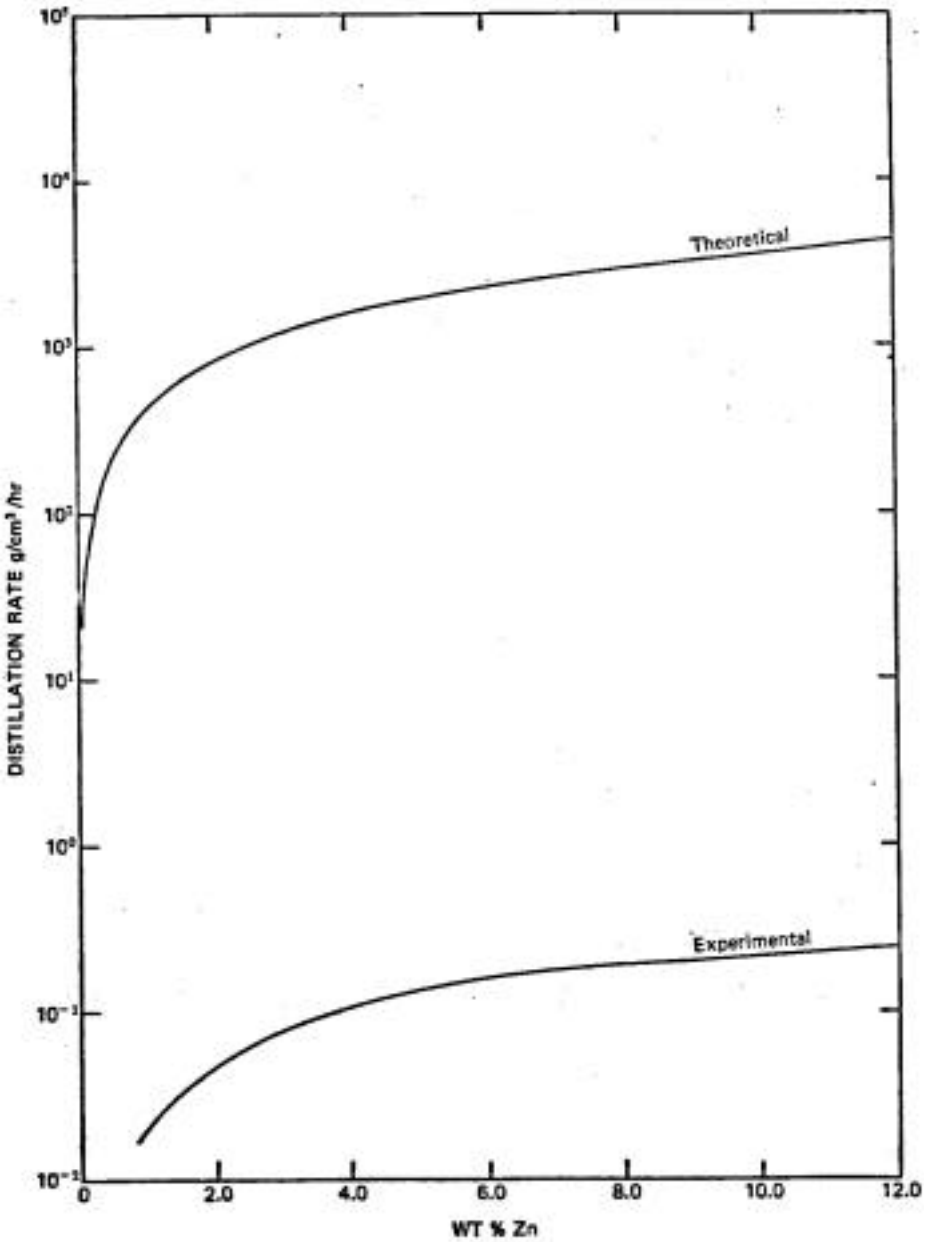

Figure 17. Distillation rate (theoretical and experimental) of zinc from a zinc-plutonium alloy at 800 C (18).

4.5. Induction Heating

Because the reactivity of molten plutonium forces the use of levitation containment of molten plutonium for both zone refining and distillation, the best heating method becomes induction heating. The basis for induction heating lies in the ability to induce electric currents in electrical conductors. Resistance to the electric currents leads to heating of the conductor. Associated with the current, I, is a voltage drop, V, which, for a pure resistance, R, is given by Ohm's law ($V = IR$). When a drop in potential occurs, electrical energy is converted into thermal energy (watts, W), ($W = VI = I^2R$), or heat (20).

In designing an induction heating system, the major consideration is the power supply frequency. Induction heating is efficient if certain basic relationships between the frequency of the magnetic field and the properties of the conductor produce a suitable degree of skin effect. Skin effect is the phenomenon by which the eddy currents flowing in a cylindrical conductor tend to be most intense at the surface, while currents at the center are nearly zero. There is no induction heating unless the power developed near the surface is larger than the power induced near the center of the conductor (20,21).

The mathematics needed to explain the skin effect are beyond the scope of this discussion, but an important benefit obtained from the solution of the differential equation describing induction heating is that it gives an “effective” depth of the current-carrying layers. This depth, which is known as the “skin depth,” d, depends on the frequency of the alternating current field and on the electrical resistivity and relative magnetic permeability of the work piece. The skin depth is useful in gauging the suitability of various materials for induction heating. The definition of d is:

$$d = 3160 \sqrt{\frac{\rho}{\mu f}} \qquad (11)$$

where d is the skin depth, in inches; ρ is the resistivity of the work piece, in ohm-inches; μ is the relative magnetic permeability of the work piece (dimensionless); and f is the frequency of the coil, in hertz. Skin depth is defined as the distance from the surface of a given material at which the induced field strengths are reduced to 37% of their surface values. Ideally, for melting operations, the skin depth should be three to four times the diameter of the work piece. When using the skin depth concept for zone refining applications, the lower the frequency, the more stirring of the molten zone. The more stirring in the molten zone, the higher degree of purification per molten zone pass during zone refining and the better the separation during vacuum distillation (20,21).

4.6. Levitation Cold Crucibles

To process reactive metals at elevated temperatures without contamination, a suitable crucible material must be used. By a combining induction heating and cold metal containers, which are themselves part of the work coil inductance, this problem has been solved in a novel way. The earliest work on cold-crucible melting is described in a German patent filed in 1926, but the technique was not further developed at that time. In 1960, Sterling and Warren (22) reported on their extensive investigations of contamination-free, high-temperature melting in several versions of cold crucibles. Sterling (22) later showed that by modifying the shape of a water-cooled silver hearth, the interaction between the inducing and

induced current could produce varying degrees of electromagnetic levitation of the liquid metal from the surface of the hearth.

4.6.1. Important Results from Sterling and Warren

Initial experiments with noncontaminating crucibles were based on the idea that a water-cooled metal container could be used to melt and process reactive materials. In the first application of this principle, a boat for zone melting was made from a silver tube by pressing a longitudinal depression into its surface for most of the length. When such a boat is placed in an induction field, the metal boat itself forms part of the work coil inductance and therefore assists in supplying the energy for melting the contained charge. Silver was chosen as the preferred boat material because it has a high electrical and thermal conductivity, coupled with good surface reflectivity. The silver boat is mounted on a carriage that is power-driven; the boat moves in the horizontal direction. The radio frequency (RF) coil surrounds the boat and is fixed. When power is applied to the coil, a narrow molten zone is formed in the bar of material contained in the boat. Movement of the carriage at a low speed effectively passes a molten zone along the bar and zone refining may be carried out (22).

A most important aspect of the method is that the liquid charge does not wet the cold silver surface, and that no skin or solid shell of material is present between the silver surface and the melt. The liquid, in fact, can be made to run on the silver surface, like mercury on glass. An essential part of the zone refining process is that the traveling molten zone must be completely liquid. This is because the segregation process for removing impurities would be virtually inoperative if even a shell of solid material remained under the molten zone. This

shell effect is probably what slowed down the zone refining effect after the first few passes during the Blau investigation (5).

The first silver boats were made so that the cooling water flowed straight through them, but in some circumstances it is advantageous to arrange the inlet and outlet pipes for the cooling water at the same end of the boat, thus making a single-ended assembly. If the boat is then enclosed in a sealed-end silica tube, it can be operated in a vacuum. However, the vacuum pressure is limited by the mechanical strength of the thin-walled tube. An alternative design of a boat that overcomes this limitation can be constructed from a number of parallel tubes of small diameter mounted in a semicircle, as shown in Figure 18.

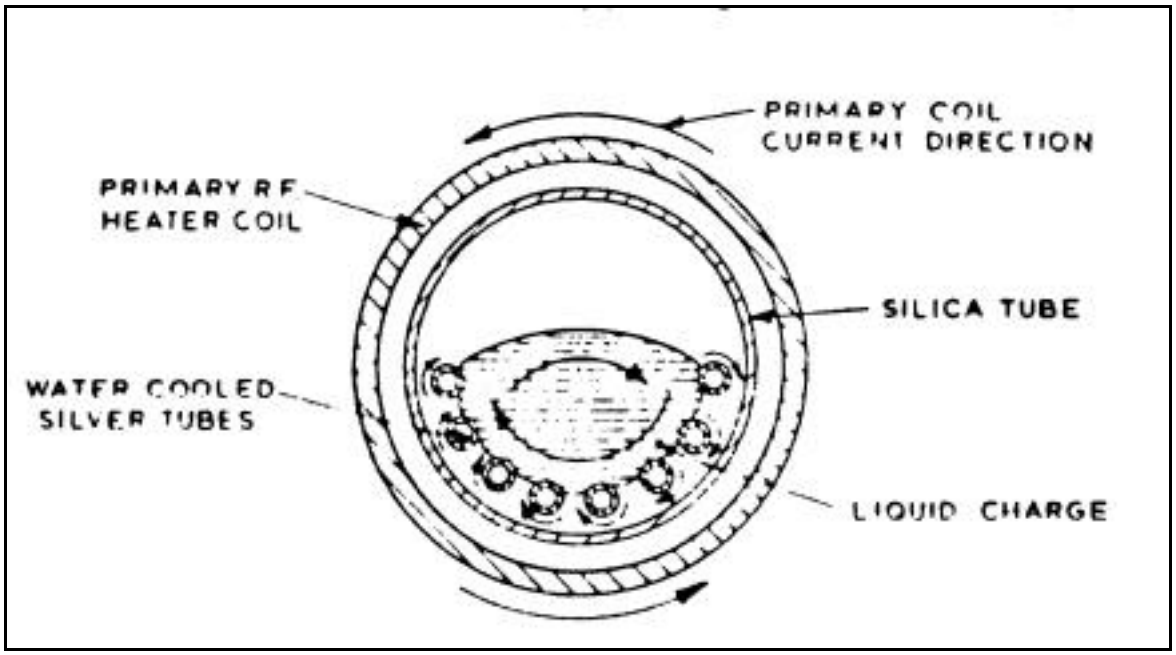

Figure 18. Section through a horizontal silver boat (22).

These silver tubes are closely spaced so that the melt can be contained in the boat by surface tension. RF power from a primary coil is induced in the charge, directly through the gaps and indirectly from the current that flows circumferentially in each tube. Furthermore, this device permits electromagnetic stirring. This effect, which is frequency dependent (the lower the frequency, the more stirring), can be desirable in zone refining processes. Zone refining using the multiple-tube boat has been successful with silicon, iron, titanium, vanadium, and zirconium, causing segregation of impurities according to their receptive distribution coefficients. A feature of the multiple silver-tube boat is that the temperature gradient in the solid material adjacent to the liquid zone is large. The molten zone is therefore smaller; and in consequence, any back diffusion of impurities from the molten zone into the refined part of the bar is less than would be expected where normal hot containment is used.

With an RF current flowing in the primary coil, a secondary current is induced into that part of the silver boat that is within the influence of the primary field. Within this region, the boat itself acts as a secondary turn, and the complete system acts as an RF transformer. Although the induced current in the boat is of opposite phase to that in the primary coil, the re-entrant nature of the boat ensures that the currents that appear in the charge from the primary coil above it and the secondary coil below it (i.e., the boat) are in phase. Because the currents induced into the charge from both the primary coil and boat are in phase, the charge receives much more heat than if the primary coil and boat-induced currents were out of phase. This is because the two induced currents would tend to cancel each other.

4.6.2. Important Results from Sterling

An induction coil is usually made of copper tubing that is cooled with water, and it remains quite cold even when used to heat material to above 2000 C. The coil can be thought of as a cold transmitter of energy. With this idea in mind, Sterling (23) constructed a crucible that was itself the coil, and that could hold a melt without turns of its coil being short-circuited. This results in a silver crucible that, when placed inside a suitable RF coil becomes the secondary coil of a transformer (Figure 19). A current of some hundreds of amperes flows in the outer surface of the crucible and causes a heating current to flow in a suitable charge of metal placed in the cavity.

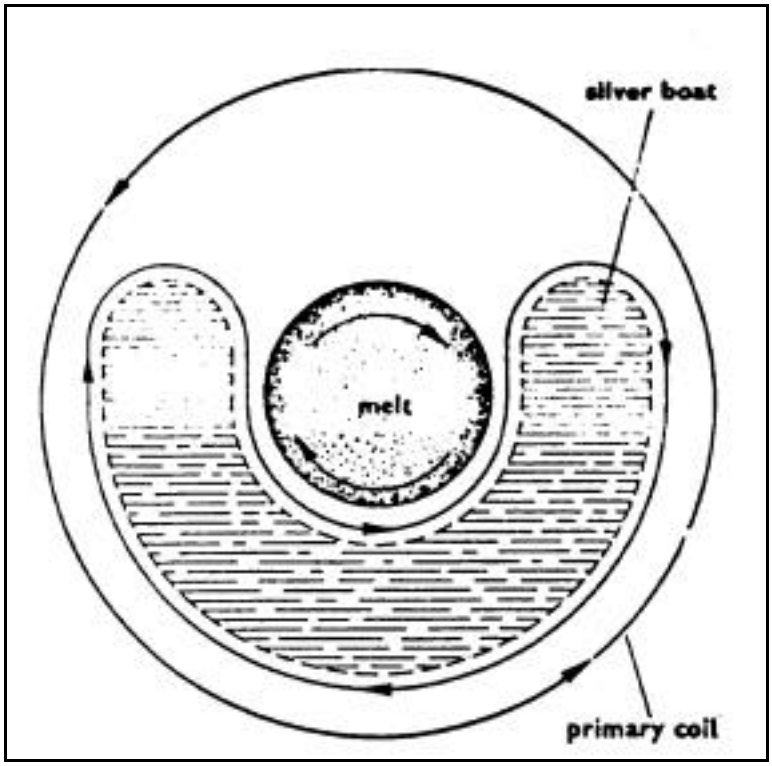

Figure 19. Section through a horizontal silver boat (23). The silver crucible acts as an inductance coil. The primary coil induces current in the crucible, which itself induces current in the melt. Repulsion cushions the melt and hence

prevents contamination.

The primary coil induces a high current in the silver crucible, and the crucible in turn induces the heating current in the material that it holds. Some current is also induced directly from the primary coil into the same material, but these two currents reinforce each other. However, the currents in the silver boat surface and in the material next to it are opposed, and so repel each other. This electrical force tends to push apart the silver boat and the material that it contains. Gravity, as well as a downward force of repulsion from the primary coil, opposes this repulsive force, and as a result the melting material is merely repelled from the silver surface.

Since processing is normally carried out in an inert atmosphere, one would expect that a gas film would fill the space between the melt and the silver crucible, but the roles played by the strong electromagnetic repulsion and this gas film in the cushioning effect are not fully understood. In practice, the white-hot liquid metal runs on the cold surface like mercury on

glass, despite the enormous difference in temperature between the two. From its physical effect on the molten metal, the silver surface of the boat-shaped container (Figure 19) can be regarded as thermally cold. From the electrical point of view, the induced current gives it a "hot" status. Complete melting occurs when a large-enough induced current is flowing in the system. The material used for the crucible must be a very good conductor of electricity to allow induction of the electric current in the material, and also a good conductor of heat to

ensure efficient cooling by the water. Either copper or aluminum are possible alternatives to silver for use as crucibles.

This type of crucible can be used to melt and process the most refractory metals, such as niobium (melting point 2500 C), molybdenum (melting point 2620 C), and tantalum (melting point 2997 C); as well as those whose melting points are below 2000 C, such as the extremely reactive metals zirconium and titanium. The ability to melt these materials satisfactorily, and to retain and improve their purity, makes this a technique of great importance in modern metallurgy and solid-state physics. No evidence of contamination of the metals by silver has been found, even with radio-chemical tracer techniques of analysis. From the point of view of retaining material purity, these containers are ideal.

4.6.3. Crystalox® Cold Crucibles

Based upon the principles discussed above, Crystalox® (24) manufactures a vertical (HCC-50) and a horizontal (HCB-150) water-cooled levitation cold crucible, and a water manifold for both crucibles (Figures 20a, b, c). Both crucibles are machined from solid bars of high-conductivity copper to give them an axially symmetrical array of either vertical or horizontal segments, each having integral water cooling (approximately 5 gpm). The water enters each segment through a tube and then returns along the outside of the tube within each segment. The water flow is directed to each segment by the water manifold (Figure 20c). All the outside surfaces as well as the cavities are gold-plated. This design optimizes both the amplitude of the induced currents and the profile of the field that they produce. Close electrical coupling can be achieved among the RF coil, the crucibles, and the charge,

resulting in significantly improved levitation and lower power requirements than conventional crucibles made from assemblies of copper tubes.

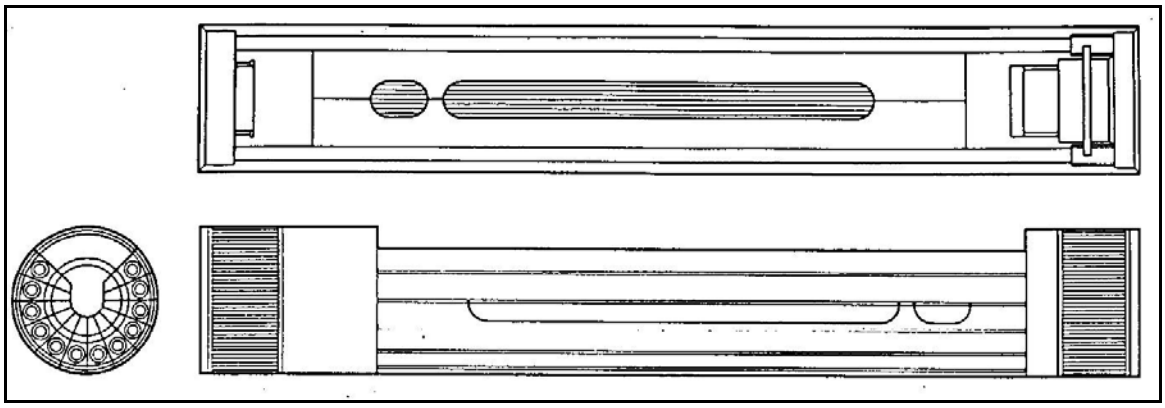

Figure 20a. Crystalox® HCB-150 horizontal cold boat (24).

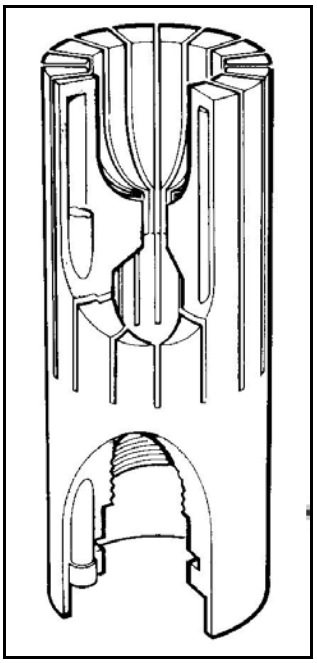

Figure 20b. Crystalox® HCC-50 vertical cold boat (24).

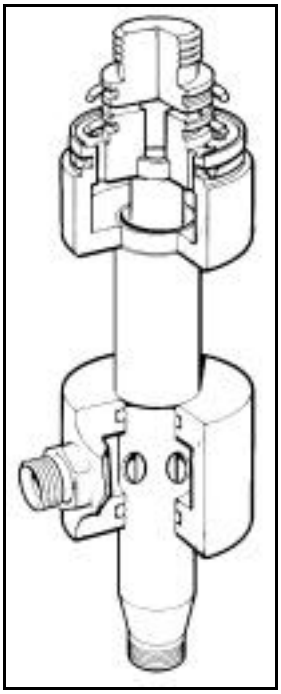

Figure 20c. Water manifold for both Crystalox® cold boats (24).

The material to be melted is held in a water-cooled, electrically conducting container in which currents are induced from a surrounding RF coil. These currents in turn induce eddy currents in the surface of the charge, which are both ohmically heated and electromagnetically repelled from the inner surface of the crucibles, thus producing concurrent melting and levitation of the charge with total freedom from contamination or reaction with the water-cooled crucible.

The Crystalox® HCB-150 horizontal water-cooled cold boat (Figure 20a), can be used for melting and purifying a large range of metals, alloys, and intermetallic compounds, in inert atmospheres or under vacuum, including aluminum, silicon, copper, cobalt, zirconium, uranium, titanium, germanium, nickel, iron, thorium, and rare-earth metals. Figure 20a also shows the 12 horizontal segments, with each segment containing its own water channel in the cross-section view. This crucible holds charges up to 150 mm long x 13 mm diameter. For this study, the HCB-150 cold boat was used for containment of molten plutonium metal during zone refining.

The Crystalox® HCC-50 vertical, water-cooled cold boat (Figure 20b) can be used with the same conditions as the HCB-150 cold boat. This crucible holds charges up to 24 ml (top cavity shown in figure). Figure 20b also shows the inner detail of some of the vertical segments in the top cut-away view. For this study, the HCC-50 cold boat was used for containment of molten plutonium during the distillation of volatile impurities in plutonium metal.

4.7. Coil Design

For zone refining to be performed efficiently, the length of the molten zone should be minimized (4). This may be accomplished by optimizing coil design. Fluxtrol® Manufacturing, a manufacturer of flux-field concentrators, has examined this engineering problem. They designed a water-cooled, three-turn copper pancake coil with a proprietary Fluxtrol® flux-field concentrator. A pancake coil has a higher density of flux lines over a smaller volume than a single turn coil such as the one used by Tate and Anderson (2). The Fluxtrol® flux-field concentrator increases the flux density even more and thus reduces the flux-field volume, producing a smaller and much hotter heated zone in the work piece and thus a smaller molten zone. This can be seen by comparing the flux lines with and without a Fluxtrol® flux-field concentrator for the same water-cooled, three-turn copper pancake induction coil, shown in Figures 21a and b, respectively (25).

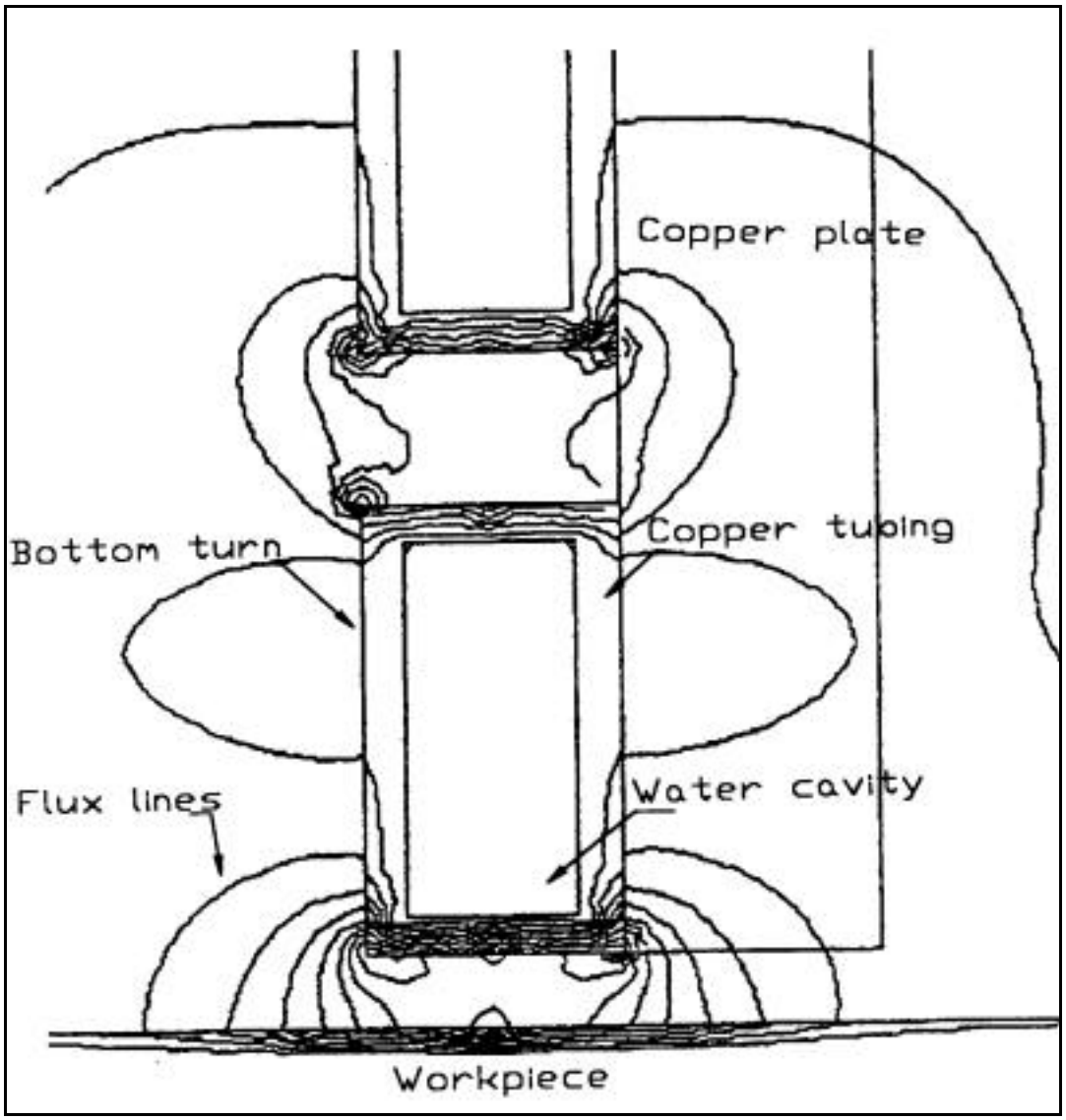

Figure 21a. Flux lines of a proposed three-turn pancake coil without Fluxtrol® flux-field concentrator. This figure was generated by Fluxtrol® (25).

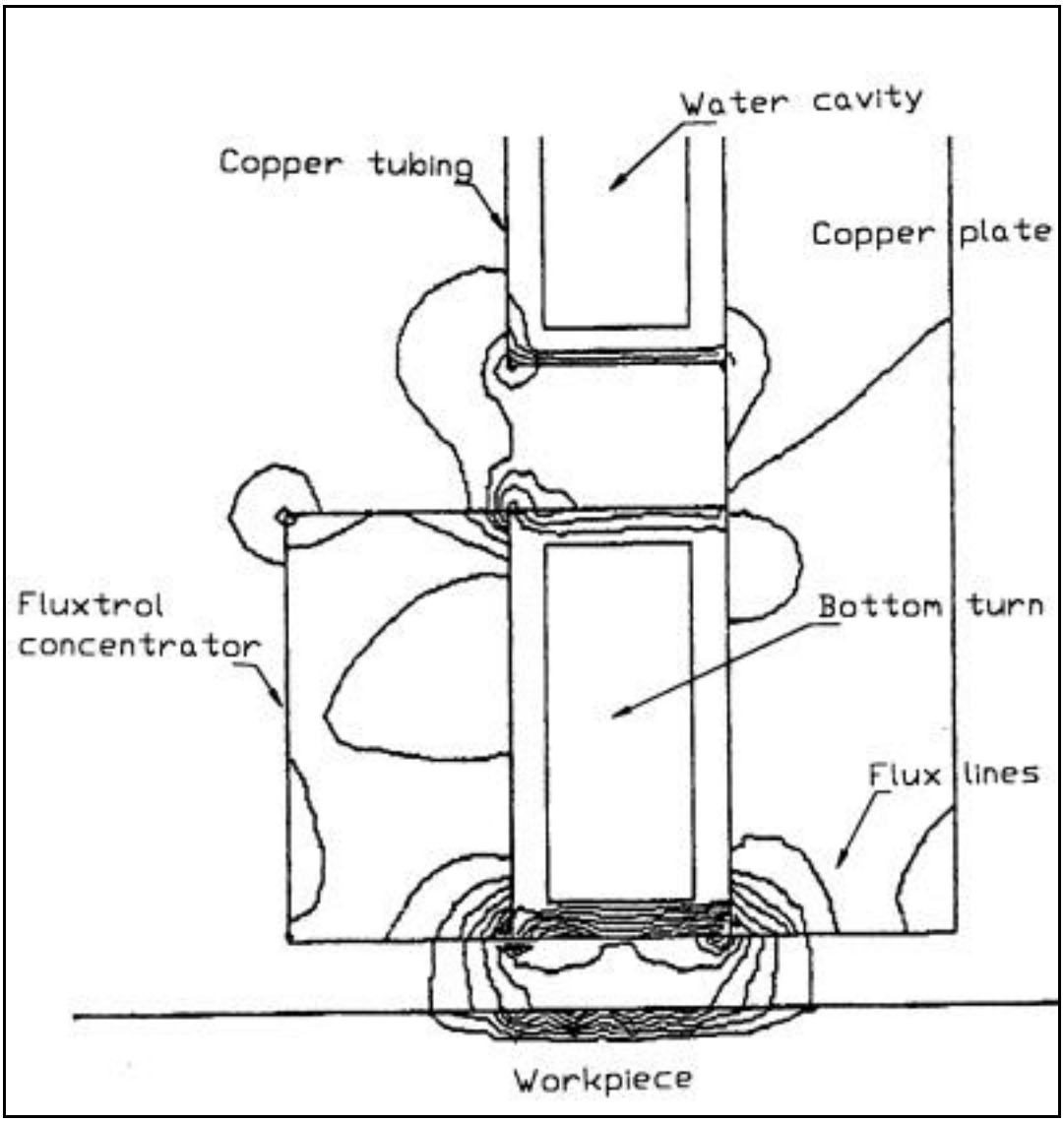

Figure 21b. Flux lines of proposed three-turn pancake coil with Fluxtrol® flux-field concentrator. This figure was generated by Fluxtrol® (25).

Coil design is not much of an issue with distillation because the crucible does not move with respect to the coil, and all the material is melted at once instead of a small zone. For this study, the frequency of the power supply connected to the coil was most important

because the lower the frequency, the more induction stirring and larger the amount of levitation force produced. Thus, as long as the coil was designed such that it induced the vertical crucible at the frequency of the power supply, there was no coil design issue.

4.8. Molten Zone Speed

The optimum rate of zone travel during zone refining depends on many factors and cannot be reduced to a simple mathematical Equation. One important factor is the amount of stirring in the molten zone. For example, to obtain the same level of separation during zone refining if there were no stirring in the molten zone, the speed would need to be about one one-hundredth of the case with vigorous stirring. Furthermore, when several impurity solutes are involved, the travel rate is likely to be determined by the impurity whose K_e is closest to unity. Based upon the analysis by Kristofova, Kuchar, and Wozniakova (26), K_e for most of the impurity elements of interest in plutonium are 0.6 or higher for those elements for $K < 1$. Based on the work of Tate and Anderson (2) and Pfann (4), work, an optimum rate should be less than 4 in/h. In the case of plutonium zone refining, economic aspects limit the minimum zone speed to 0.5 in/h because personnel must be present during any experimental zone refining, and a single pass must be less than 11 h (maximum work-day length). However, with a high economic cost, a molten zone speed of less that 0.5 in/h could be used in an automatic zone refining apparatus by making use of programmable logic controllers.

4.9. Statistically Designed Experiments

The purpose of conducting experiments is to determine the values of the properties of a material or to determine how changing the values of the variables affecting a process alter the process. Purposeful selection of values for the variables of the process is the most

important part of experimental design. An efficient process can be worked out with or without a statistical design. The only "value added" by statistical design is the minimization of the effort involved in finding the most efficient set of values for the variables tested. There is no value added to the intrinsic efficient process. An efficient experiment is one that derives the required information with the least expenditure of resources (27).

4.9.1. Experimental Factorial Designs

A full-factorial experiment is an experiment in which the response *y* is observed at all factor-level combinations of the independent variables. One approach for examining the effects of two or more factors on a response is called the "one-at-a-time approach." To examine the effect of a single variable, an experimenter changes the levels of this variable while holding the levels of the other independent variables fixed. This process is continued until the effect of each variable on the response has been examined while the other independent variables are held constant. If any independent variables interact, this approach does not work. Also, the inadequacies of the one-at-a-time approach are even more salient when investigating the effects of more than two factors on a response. Factorial experiments are useful for examining the effects of two or more factors on a response y, whether or not interaction exists. Consequently, factorial designs yield information concerning factor interactions, when there are no interactions, yield the same amount of information about the effects of each individual factor using fewer observations (28).

4.9.2. Analysis of Variance for Experimental Factorial Designs

Thoroughly reviewing analysis of variance for experimental factorial designs is beyond the scope of this thesis. Presented here are, those equations needed to do an analysis

of variance for experimental factorial designs up to a three-factor factorial experiment with fixed effects and more than one replication per cell are presented. The following notation is used for the needed equations (28).

G: total for all sample observations (all y's added together)

n: total number of sample measurements

a: number of levels factor A is investigated at

b: number of levels factor B is investigated at

c: number of levels factor C is investigated at

n_A: number of observations at each level of factor A

n_B: number of observations at each level of factor B

n_C: number of observations at each level of factor C

A_i: sum of the n_A observations receiving the ith level of factor A

B_j: sum of the n_B observations receiving the jth level of factor B

C_k: sum of the n_C observations receiving the kth level of factor C

n_{AB}: number of observations at each combination of levels of factors A and B

n_{AC}: number of observations at each combination of levels of factors A and C

n_{BC}: number of observations at each combination of levels of factors B and C

$(AB)_{ij}$: sum of the n_{AB} observations receiving the ith level of A and jth level of B

$(AC)_{ik}$: sum of the n_{AC} observations receiving the ith level of A and jth level of C

$(BC)_{jk}$: sum of the n_{BC} observations receiving the ith level of B and jth level of C

n_{ABC}: number of observations at each combination of levels of the three factors A, B, and C

(ABC)ijk: sum of the n_{ABC} observations receiving the ith level of A, jth level of B, and kth level of C

The appropriate analysis of variance formulas for a k-factor factorial experiment with r observations per cell can be subdivided into sums of squares for main effects (variability between levels of a single factor), two-way interactions, and three-way interactions are shown below.

The sums of squares for main effects are:

$$SSA = \sum_i \frac{A_i^2}{n_A} - \frac{G^2}{n} \tag{12a}$$

$$SSB = \sum_j \frac{B_j^2}{n_B} - \frac{G^2}{n} \tag{12b}$$

$$SSC = \sum_k \frac{C_k^2}{n_C} - \frac{G^2}{n} \tag{12c}$$

The sums of squares for two-way interactions are:

$$SSAB = \sum_{ij} \frac{(AB)_{ij}^2}{n_{AB}} - SSA - SSB - \frac{G^2}{n} \tag{13a}$$

$$SSAC = \sum_{ik} \frac{(AC)_{ik}^2}{n_{AC}} - SSA - SSC - \frac{G^2}{n} \tag{13b}$$

$$SSBC = \sum_{jk} \frac{(BC)_{jk}^2}{n_{BC}} - SSB - SSC - \frac{G^2}{n} \qquad (13c)$$

The sum of squares for a three-way interaction is:

$$SSABC = \sum_{ijk} \frac{(ABC)_{ijk}^2}{n_{ABC}} - SSAB - SSAC - SSBC - SSA - SSB - SSC - \frac{G^2}{n} \qquad (14a)$$

Total sum of squares is:

$$TSS = \sum y^2 - \frac{G^2}{n} \qquad (14b)$$

The sum of squares for an error is:

SSE = TSS - SSA - SSB - SSC - SSAB - SSAC - SSBC - SSABC (14c)

The mean sum of squares in each case is the sum of squares divided by the degrees of freedom for that sum of squares. The F value for main effects and interactions then becomes the mean sum of squares for main effects or interactions divided by the error mean sum of squares.

Once the analysis of variance is complete using the above equations, the calculated F values can be compared with values from the appropriate F distributions to conclude whether

or not there are differences among the main effects and if there are interactions between the main effects (27). A Statistical Analysis System (SAS) computer program was used to calculate an analysis of variance from the data generated in each part of this experiment. From these results, it was determined if there were significant differences among the main effects and if there were interactions between the main effects.

For this thesis, experimental factorial designs were used because obtaining each datum point is costly. By using factorial designs, the number of data points is greatly reduced. For this experiment, the response y in most cases was the absolute percent change in impurity concentration from the head-end to the tail-end of the zone refined rod. The first reason for using this as the response y was that it gave the best measure on how well the impurity elements moved during the zone refining process. Second, since the chemical analysis from each individual rod (three samples per rod) were done together, the error produced due to different analysis batches was eliminated. In other cases, the response y was the impurity concentration in the plutonium metal. The fixed effects were the number of zone refining passes, molten zone speed, impurity alloy (two different alloys), wire brushing the rod before each pass, holding the rod under good vacuum between passes, and position along the rod where the sample was taken. In all cases, no more than three fixed effects were used at once and with two replications. Given the fact that the low number of data points were used in each case, it was difficult to obtain significant results from the analysis of variance because of the low number of degrees of freedom. However, in each case, there were more than double the number of degrees of freedom than used by Blau (5).

CHAPTER 5

EXPERIMENTAL PROCEDURES

5.1. Material Preparation

The best way to achieve the main objective of this experiment would have been to start with rods cast from electrorefined plutonium metal and use different zone refining variables to develop the best process for producing the first high-purity plutonium. However, this could not be done easily because the analytical analysis needed to track the different plutonium impurities (a few ppm each element) cost $60,000 per sample and would have taken approximately 3 to 6 months to accomplish. This problem was overcome by creating two different alloys (one α-phase and one δ-phase) that contained high-impurity compositions of a number of impurities that could by tracked by using a simple X-ray fluorescence method that cost $2,000 per sample and took less than a month to accomplish. One draw back of the simple X-ray fluorescence method was the accuracy (± 10%).

Two plutonium alloys were prepared, a low-impurity alloy and a high-impurity alloy. The plutonium starting material was electrorefined plutonium metal, typically 99.5% pure by weight exclusive of americium (Figure 5). Americium-241 grows into plutonium by the beta decay of plutonium-241 (half life = 14.4 years). The in-growth of americium with the plutonium metal used for this study was approximately 30 ppm per month. The low-impurity alloy contained seven impurity elements other than americium at about 400 ppm by weight of each. The high-impurity alloy contained approximately 1 w/o gallium. In addition, it contained eight impurity elements at about 1000 ppm each by weight and americium at 3000

ppm, making it a stabilized δ-phase alloy. The high-impurity alloy was similar to the impurity alloy previously used by Blau (5).

Flow diagrams presented in Figures 22a and b illustrate the experimental procedure that was followed for the two alloys.

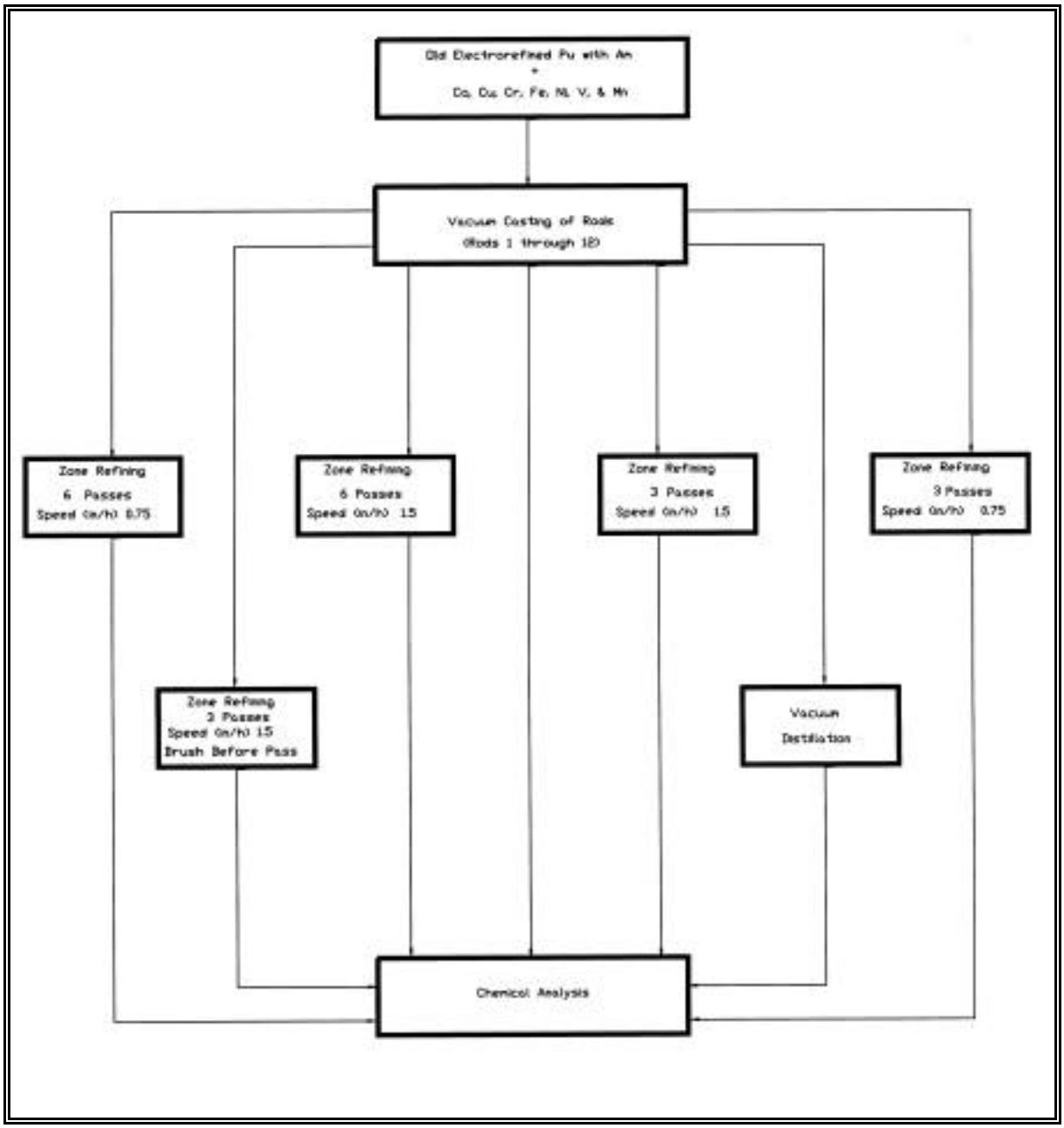

Figure 22a. Experimental procedure flow diagram for the low-impurity alloy.

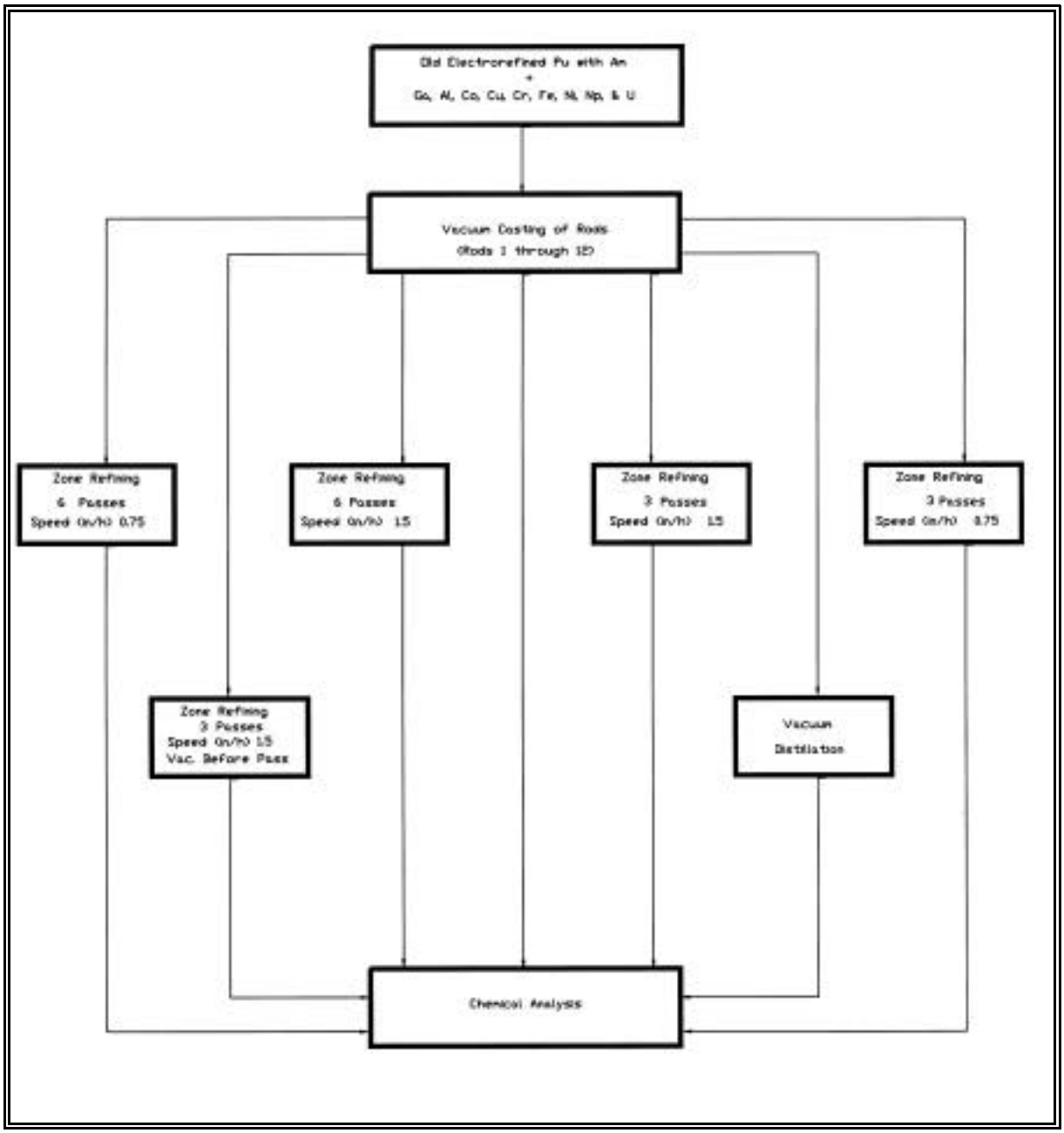

Figure 22b. Experimental procedure flow diagram for the high-impurity alloy.

5.1.1. Low-Impurity Alloy

This alloy was fabricated using the following procedure:

- Electrorefined plutonium metal that contained about 1000 ppm (0.1 w/o) americium was used.
- Amounts of cobalt, copper, chromium, iron, nickel, vanadium, and manganese were added to produce an alloy containing 400 ppm (0.04 w/o) of each element.
- The charge was vacuum-cast into rods (1/4-in in diameter and 8 in long) using the standard plutonium casting furnace (Figure 6).

The following schedule was used:

-the charge was heated to 900 C and held for 20 minutes with constant stirring (the molten metal was stirred using a manual stirring rod) under a vacuum of about 5 x 10^{-3} torr.

-the charge was bottom-poured into a cold titanium rod mold.

-one-gram samples were taken from near the end of two of the rods for chemical analysis.

5.1.2. High-Impurity Alloy

This alloy was fabricated using the following procedure:

- Electrorefined plutonium metal that contained about 3000 ppm (0.3 w/o) americium was used.

- Gallium was added to this material to produce a nominally 1 w/o of alloy (approximately 3.4 a/o).
- Amounts of aluminum, cobalt, copper, chromium, iron, nickel, neptunium, and uranium were added to produce an alloy containing 1000 ppm (0.1 w/o) of each element.
- The charge was vacuum-cast into rods (1/4-in in diameter and 8 in long) using the standard plutonium casting furnace (Figure 6).

The following schedule was used:

-the charge was heated to 900 C and held for 20 minutes with constant stirring (the molten metal was stirred using a manual stirring rod) under a vacuum of about 5 x 10^{-3} torr.

-the charge was bottom-poured into a cold titanium rod mold.

-one-gram samples were taken from near the end of two of the rods for chemical analysis.

5.2. Experimental equipment

The experimental equipment was based on the processes of zone refining and distillation, with both processes being contained in a single glovebox.

5.2.1. Zone Refining Apparatus

The zone refining equipment was built specifically for this experiment and placed in an existing glovebox adapted for the experiment. A 50-kW, 50-kHz power supply was acquired and installed. This is because, based on the skin-depth equation (Equation 11), the best workpiece diameter is 1/4-in or larger for a frequency of 50-kHz for the plutonium metal rod to be induced by the induction coil.

To move the cold boat containing the plutonium rod at a very slow controlled speed (0.75 or 1.5 in/h) through the induction coil, Micro Kinetics Corporation designed and built a linear precision table (translation table). The zone refining speeds were selected based on results obtained from Tate and Anderson (2) and Blau (5). The table translates on a single-axis with 9-in of movement, driven by a motor controlled by a remote hand-held computer (RHHC) external to the glovebox. The induction coil was designed and built by Fluxtrol Manufacturing specifically for the Crystalox® HCB-150 cold boat. The coil consists of a water-cooled, three-turn, copper pancake with a Fluxtrol® flux-field concentrator This design minimized the size of the molten zone. A vacuum chamber was designed and built at Los Alamos to contain the entire zone refining apparatus and fit inside the glovebox.

Drawings of the zone refining apparatus and a illustration of the cold boat on the translation table are shown in Figures 23a, b, c, d respectively. Figure 23a shows a side view of the vacuum chamber with the lid closed. This figure also shows the vacuum chamber position in the glovebox and a view of the glovebox induction pass-through and the vacuum chamber induction pass-through. The induction pass-through supplies both the induction power and water cooling to the induction coil. This figure also shows the position of the two vacuum chamber view ports. From this figure, one can see where the chamber lid and body separate. An O-ring seal at this separation in the vacuum chamber makes the chamber vacuum-tight. The water cooling lines that keep the vacuum chamber cool during processing can also be seen in this figure.

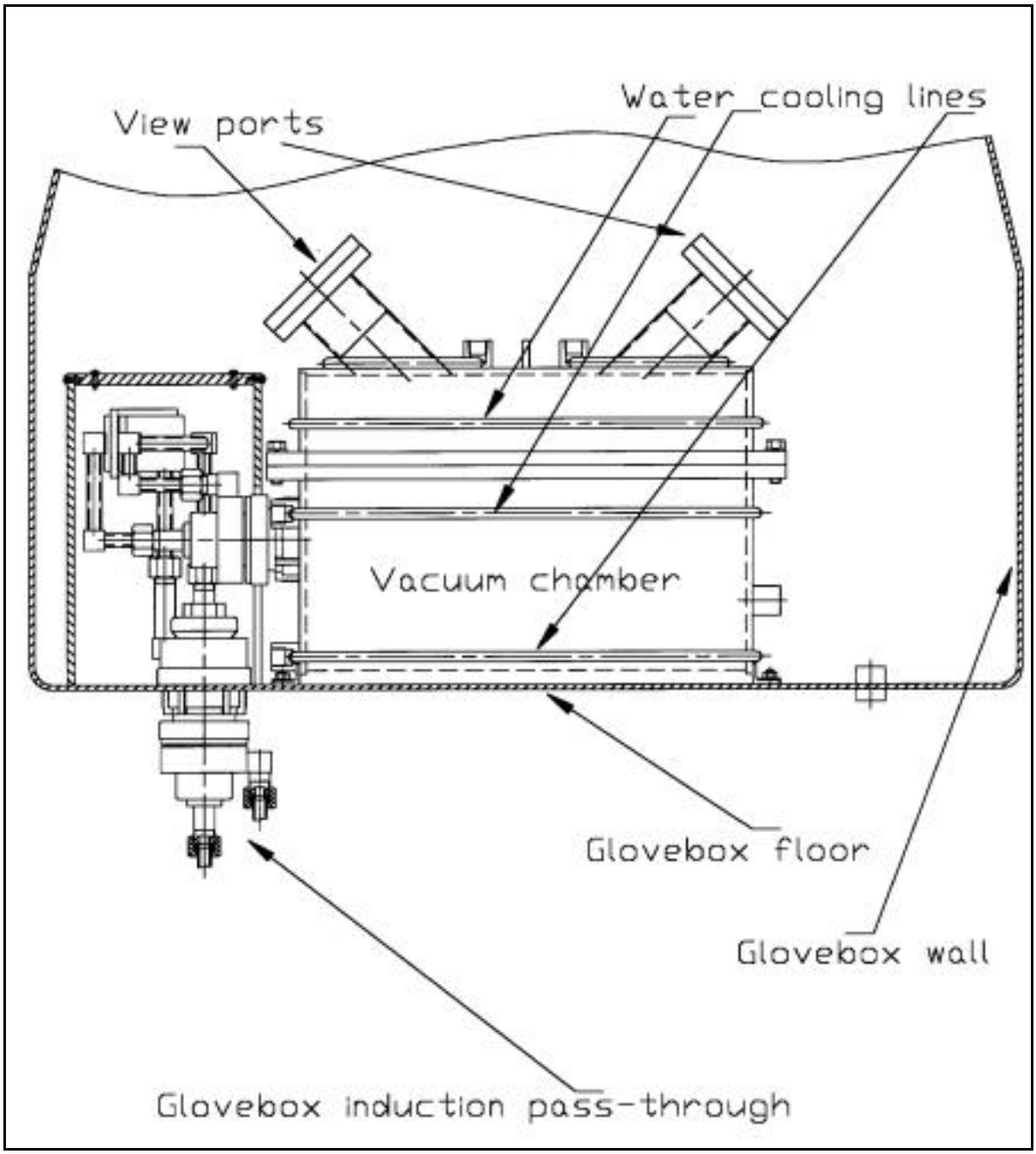

Figure 23a. Side-view drawing of the zone refining apparatus.

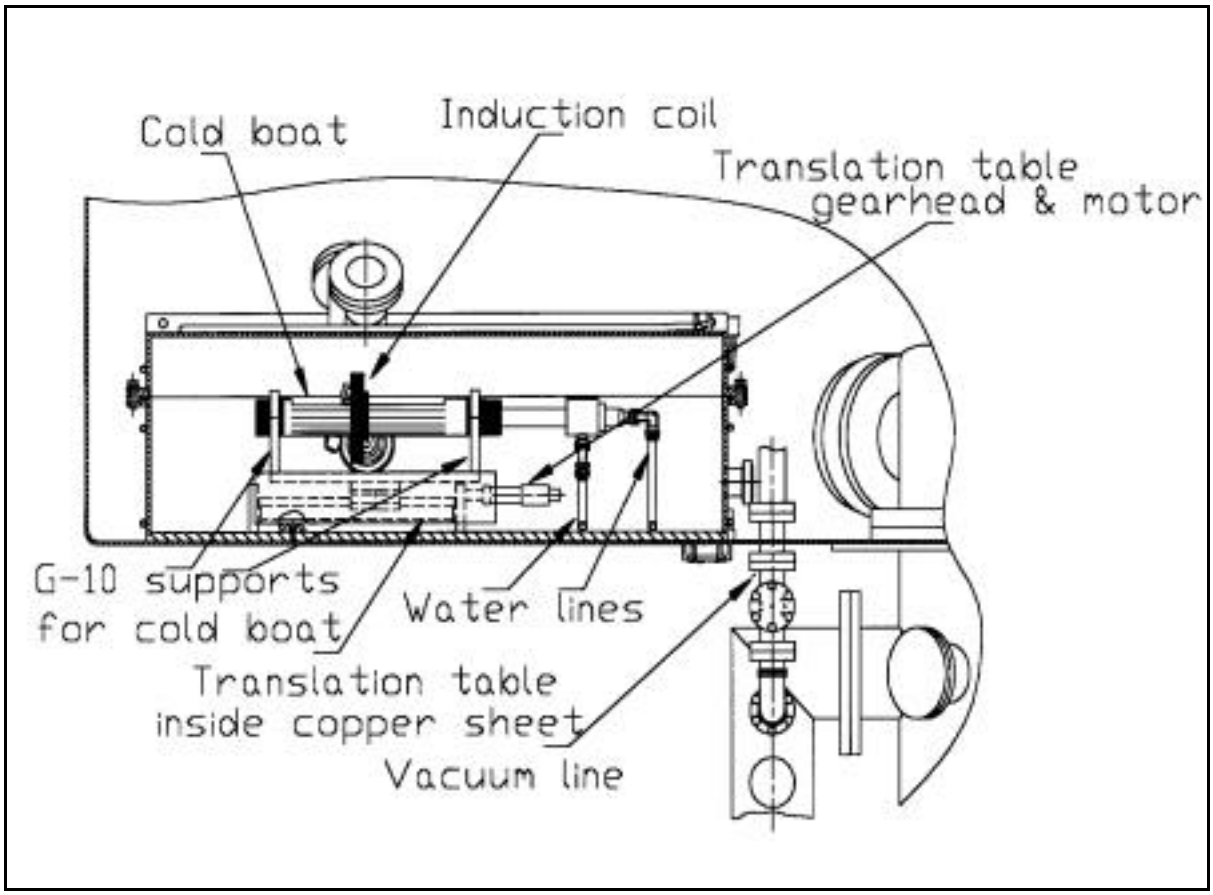

Figure 23b. Front-view drawing of the zone refining apparatus.

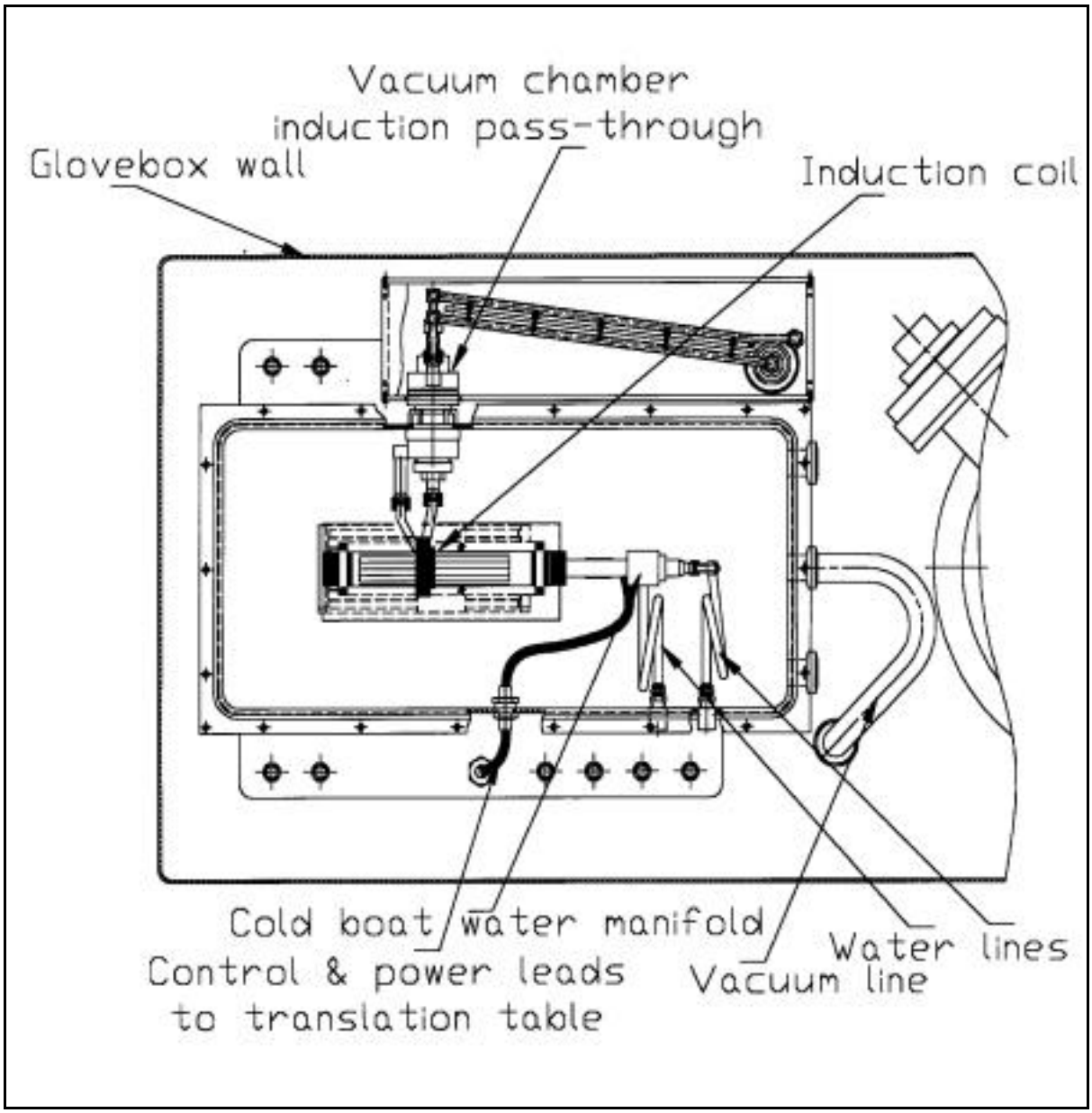

Figure 23c. Plan-view drawing of the zone refining apparatus.

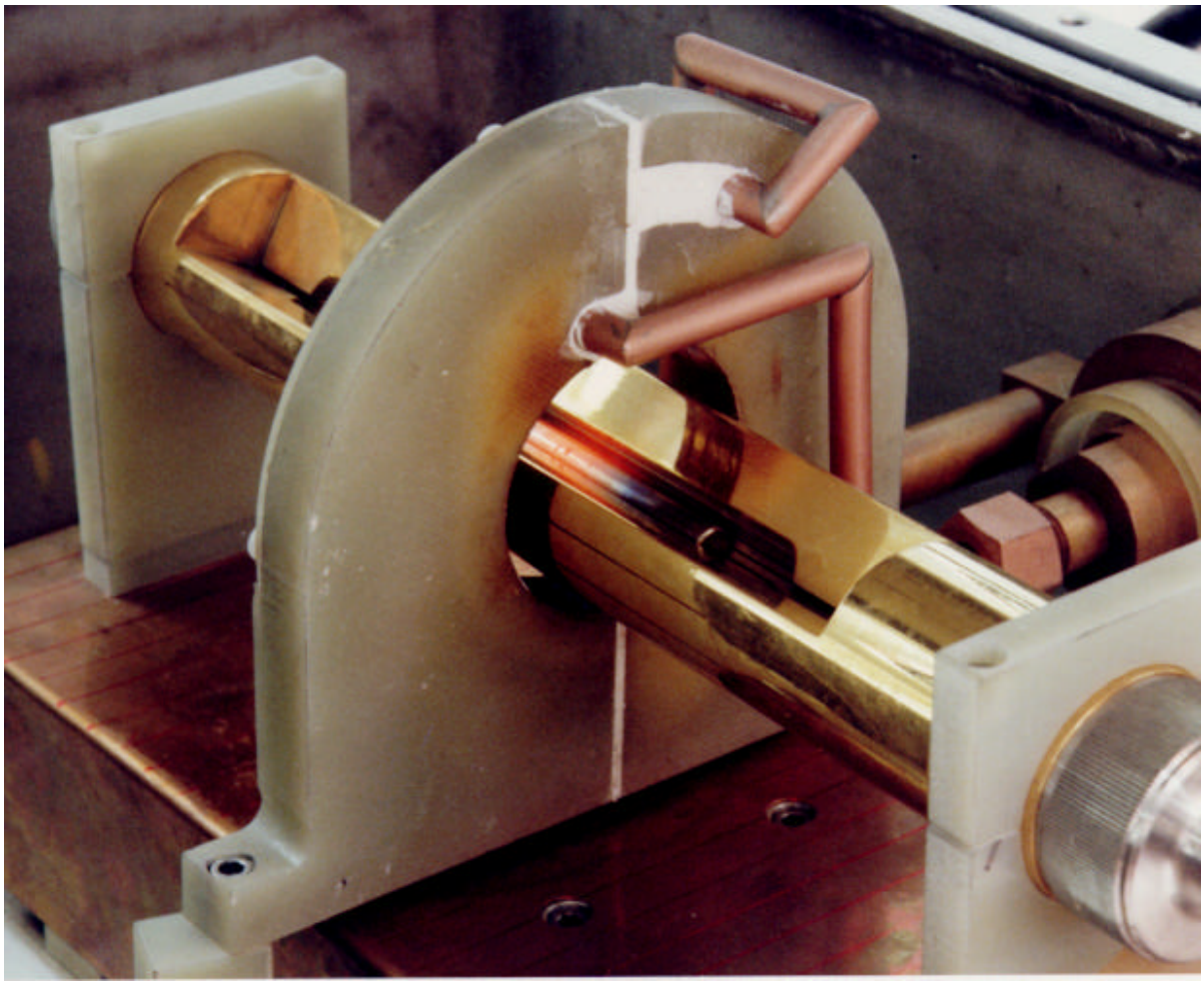

Figure 23d. Zone refining apparatus with stainless steel rod in the Crystalox® cold boat at a power setting of 10 kW.

Figure 23b is a front-view drawing of the zone refining apparatus as it is positioned in the glovebox. This figure shows the induction coil around the Crystalox® cold boat. The supports for the cold boat are made of G-10 (an insulator) for isolating the electrical contacts from the chamber. As can be seen in the figure, the translation table is covered by a thin copper sheet, which is required to shield the translation table from the induction field

produced by the coil. The encoder motor and gear-head assembly are visible on the right side of the translation table. The vacuum line is also shown in the figure. This vacuum line is connected to a large chamber in the glovebox. The vacuum equipment consists of a roughing pump, valves, and an 8-in cryo-pump.

Figure 23c shows a drawing of the plan view of the zone refining apparatus as it is positioned in the glovebox. One can see the points of entry of the induction power leads and their connection to the induction coil. They are made of copper tubing and supply both power and cooling water to the coil. The vacuum line that penetrates both the vacuum chamber and the glovebox is also shown. The cooling water lines to the cold boat water manifold are also shown, as well as the control and power leads to the translation table. The induction coil is shown in both this figure and the previous figure.

Figure 23d shows a illustration of the zone refining apparatus with a stainless steel rod loaded in the Crystalox® cold boat. The hot zone on the rod can be clearly seen from the red glow caused by the induction from the coil (approximately 10 kW). Infrared thermometer readings taken on the rod showed the temperature gradient to be approximately 200 C/in. The highest temperature of the rod was 900 C, while the temperature of the water flowing out of the crucible was only 25 C. Because stainless steel, unlike plutonium, does not oxidize in air, it was possible to take this illustration with the vacuum chamber in the open position.

5.2.2. Distillation Apparatus

The distillation apparatus was built specifically for this experiment and placed in the same glovebox as the zone refining apparatus. The vacuum chamber for the distillation

apparatus used the same vacuum system as the zone refiner. However, since the vacuum piping has a larger diameter and takes a shorter path to the cryo-pump, the vacuum that can be reached in the distillation vacuum chamber is much better. The power supply that was used with the distillation apparatus was a 75-kW unit that ran at a frequency of around 4 kHz, the power setting that was used for this experiment (40 kW). Based on the skin depth equation (Equation 11) the best workpiece diameter is 1 in or larger for a frequency of 4 kHz.

A drawing and a illustrations of the distillation apparatus are shown in Figures 24a, b, and c Figure 24a shows a front view of the distillation apparatus with the vacuum lid closed. The vertical crucible (Crystalox® HCC-50), which contains the plutonium, sits in the middle of the chamber surrounded by a standard water-cooled induction coil made from copper tubing. The vertical crucible is connected to the Crystalox® water manifold by vacuum-tight O-ring seals. The water manifold is resting on a lift that can be used to adjust the height of the vertical crucible with respect to the top of the induction coil. The lift goes through a series of O-rings in order to keep the chamber vacuum-tight. Above the vertical crucible is the water-cooled copper condenser. Since the condenser is the coldest object near the molten metal during distillation, any metal vapors tend to condense on the condenser. The induction and water pass-through can be seen on the right side of the vacuum chamber. The vacuum port on the left side of the chamber is connected to an elbow, followed by a gate valve and an 8-in cryo-pump. The elbow can be seen in the lower right of Figure 23b. Also in Figures 23b and 24a, the glovebox floor can be seen as being at almost the same level as the vacuum chamber lid. The two view ports shown in Figure 24a are, in reality, rotated 90 degrees out of the page, giving a view of inside the chamber for the front of the chamber.

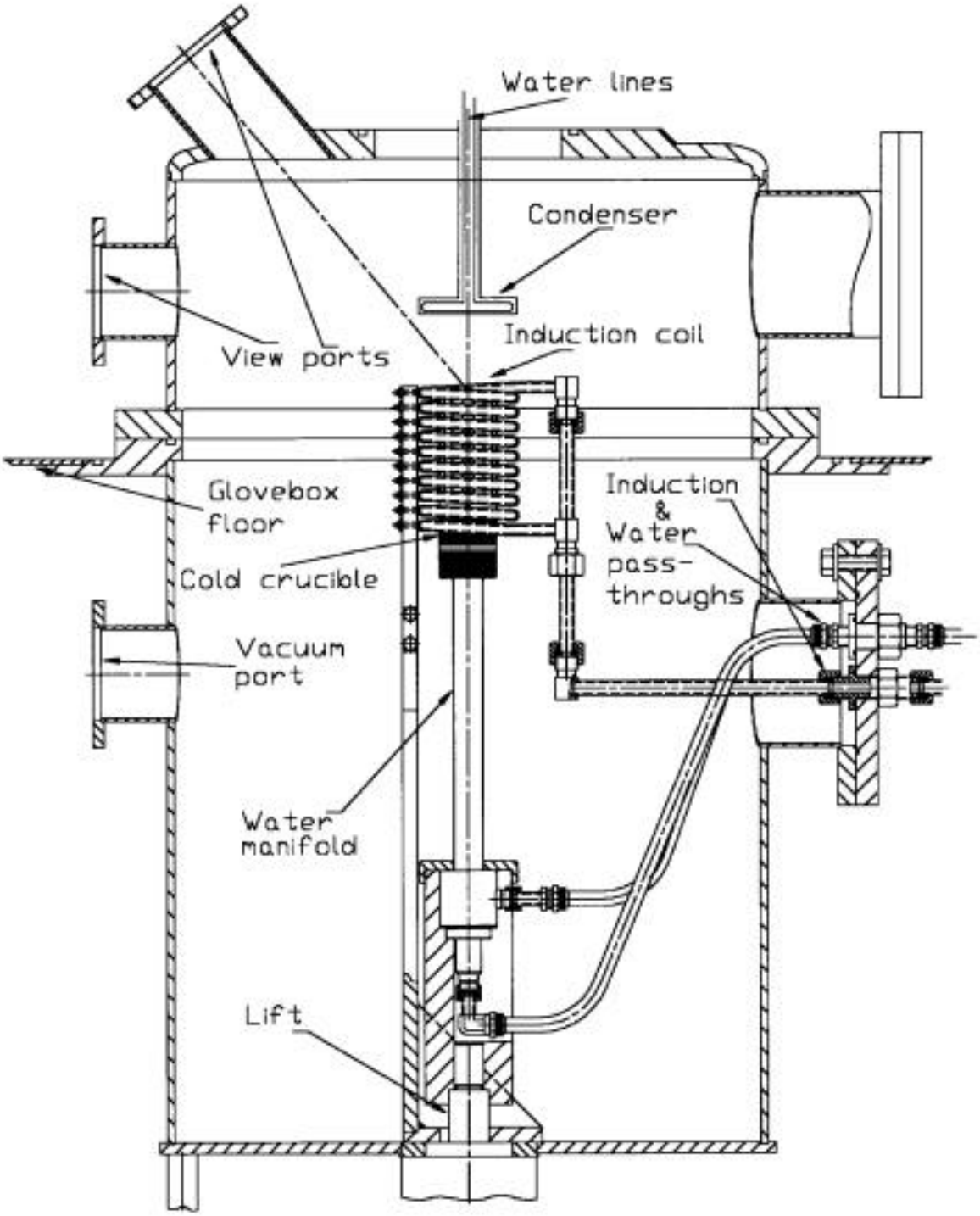

Figure 24a. Front-view drawing of the distillation apparatus.

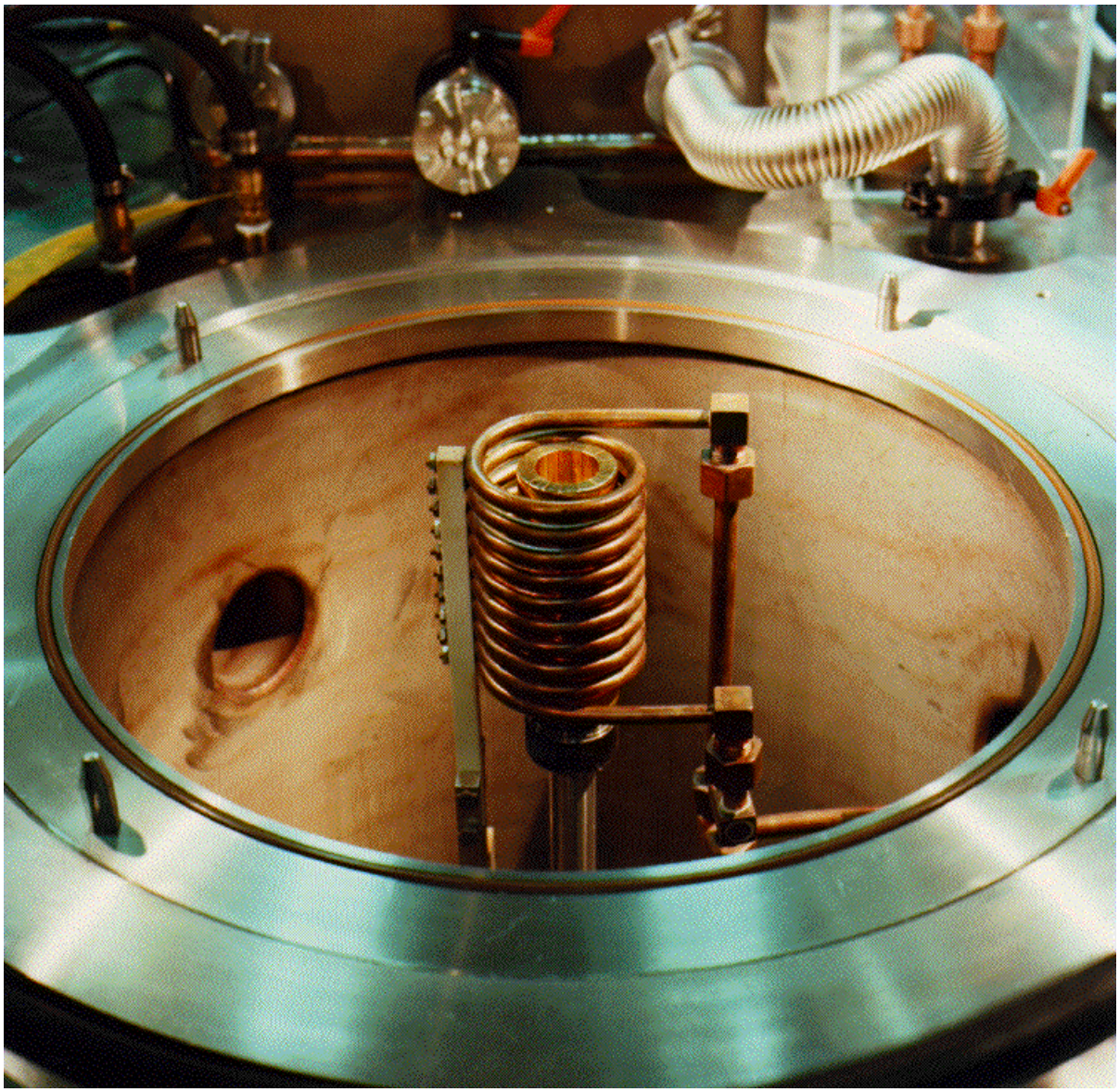

Figure 24b. Distillation apparatus with vacuum chamber lid raised.

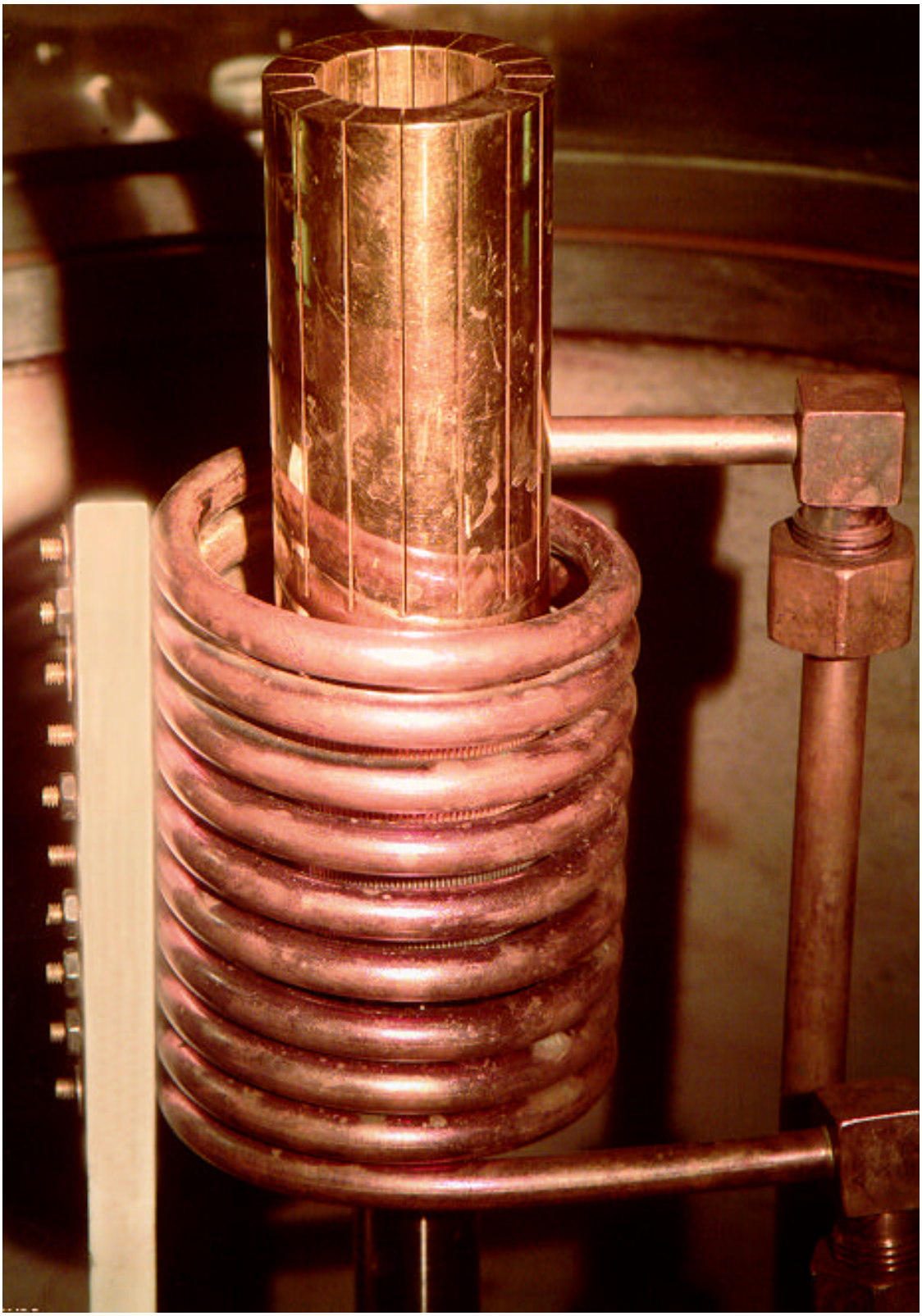

Figure 24c. Distillation apparatus with crucible raised.

Figure 24b is a illustration of the distillation apparatus with the lid raised, taken from the left side shown in Figure 22a. At the top of the illustration, one can see the flexible vacuum line that is connected to the zone refining vacuum chamber. Towards the center of the illustration, the top of the vertical crucible within the induction coil can be seen. The O-ring used to make the vacuum-tight seal between the lid and vacuum chamber can be seen in the figure. On the left side of the chamber, the vacuum port can be seen. Figure 24c is a close-up illustration of the induction coil and crucible, with the crucible in the raised position.

5.2.3. Experimental Glovebox

Illustrations of the front and back of the experimental glovebox are shown in Figures 25a and b, respectively The glovebox is constructed of 304 stainless steel and lined with lead. The glove ports in the middle and near the top of the glovebox are fitted with lead-lined gloves. A pressure gauge (inches of water) near the top of the glovebox monitors the difference between the internal glovebox pressure and room pressure. This is important because the pressure in the glovebox must be less than the room pressure, so that if there is a breach in the glovebox, the air will flow in instead of the contamination flowing out of the glovebox. Below the glovebox are insulated water cooling lines and the water interlocks. The water interlocks monitor water flow and water temperature. If either gets out of the desired range, the interlock shuts off power to the zone refining coil. The top of the vacuum chamber lid and the electric hoist used to raise the vacuum chamber lid appears on the left inside the glovebox. The main body of the distillation vacuum chamber with the view port

can be seen on the right side of the illustration below the glovebox floor. The top of the raised distillation lid with view port can be seen through the large rectangular window.

Below the glovebox floor in the center is the head of the Stanford Research System® RGA 300 residual gas analyzer (RGA). The RGA was used for characterization of the vacuum environment. It is a mass spectrometer that is connected directly to the vacuum system above the cryo-pump; its function is to analyze the gases inside the vacuum chamber as they are sucked into the cryo-pump. The principle operation of the RGA 300 is that a small fraction of the gas molecules in the instrument are ionized (positive ions); and the resulting ions are separated, detected, and measured according to their molecular masses. For instance, one species of interest in this experiment is americium-241 and that was the reason for installing an RGA 300. On the floor below the RGA are two thermocouple pressure gauges used to monitor the pressure in different parts of the system. These pressure gauges do not work at high vacuum, when only the ion-gauge or the RGA can read a pressure below 10^{-3} torr.

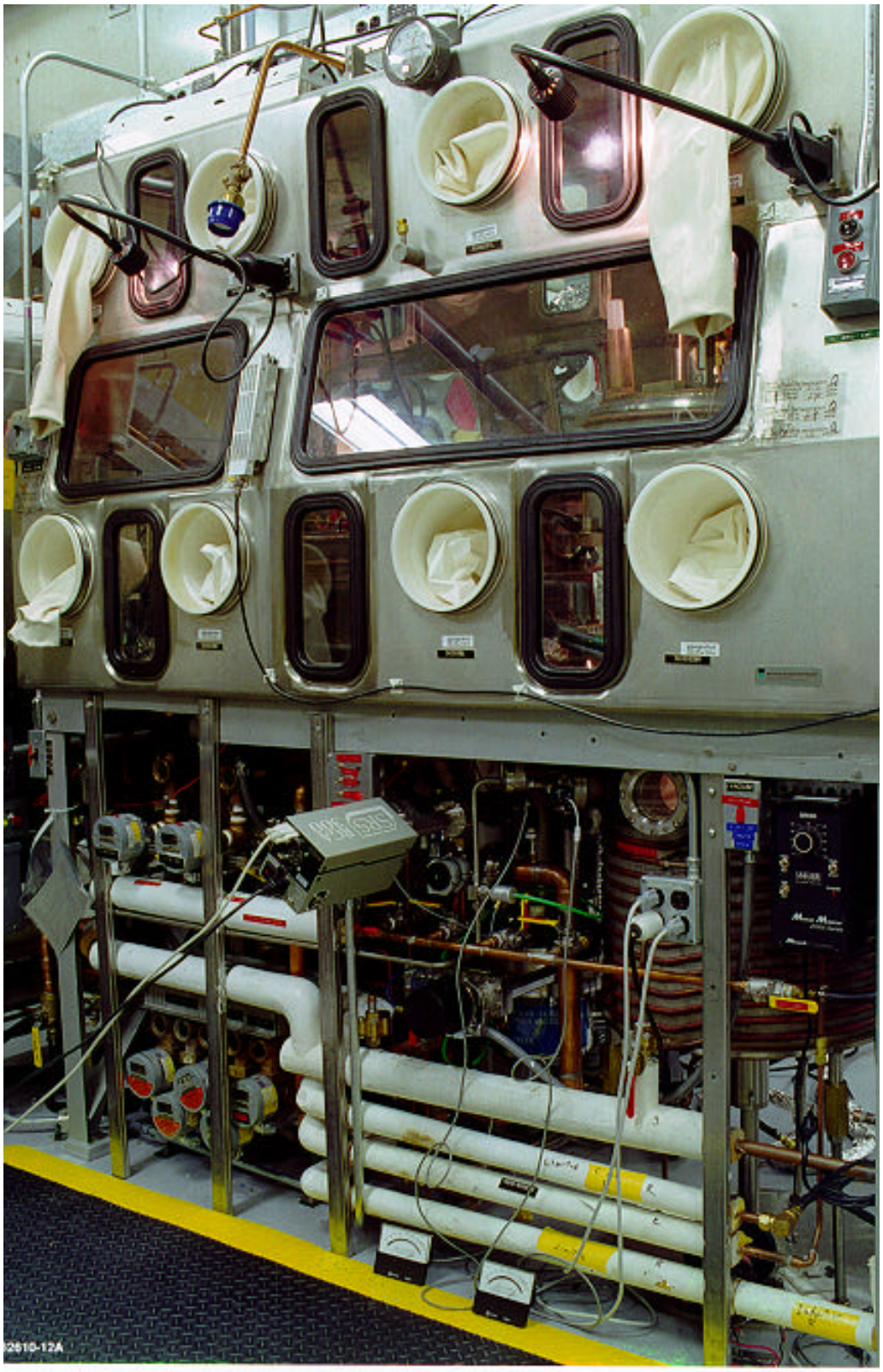

Figure 25a. Front-side of zone refining glovebox.

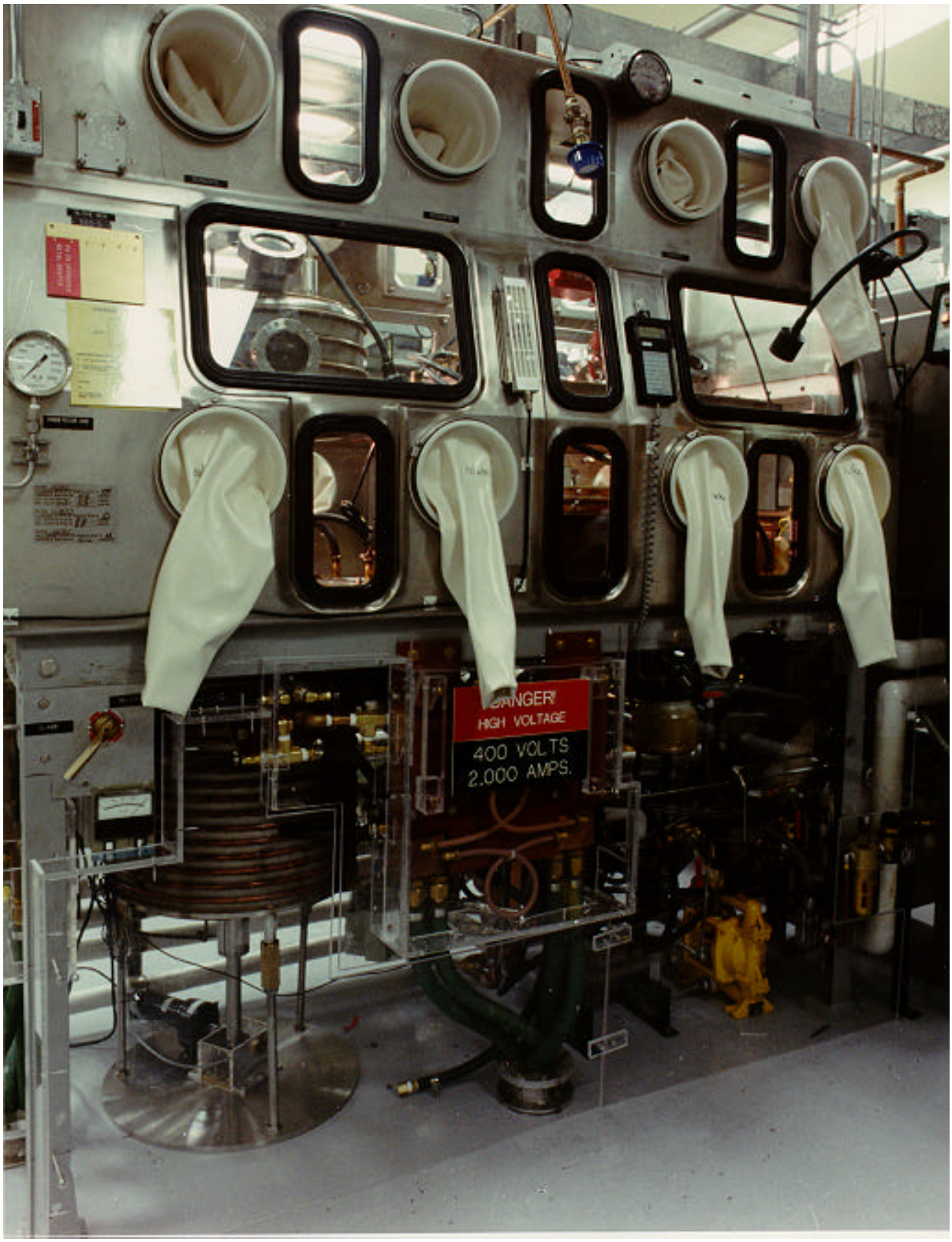

Figure 25b. Back-side of zone refining glovebox.

Figure 25b shows the back side of the glovebox. The induction power leads for the zone refiner are below the glovebox in the center. On the left side, also below the glovebox, is the cryo-pump temperature gauge. This temperature is important because the cryo-pump does not work if the temperature is above 20 K. In Figure 25b, the zone refining apparatus view port in the vacuum chamber lid appears on the right. To the left of this glovebox window is the Handheld Remote Controller Computer (HRCC). Left of the HRCC is the plutonium hand-monitor probe used to check one's self for plutonium contamination each time one removes his or her hands from the gloves. The main body of the distillation vacuum chamber with the induction and water feed-through can be seen on the right side of the illustration below the glovebox floor. The top of the raised distillation lid with view ports can be seen through the rectangular window (Note: the distillation vacuum chamber lid has been rotated 180 degrees from its position when the lid is closed).

5.3. Distillation Runs

First, practice runs were made using 15 ml of copper, and it was found that the vertical crucible worked well at a power setting of 15 kW. But after the process was used with cut rod pieces of the low-purity alloy (15 ml), the process did not work as well. At 15 kW, the copper would heat up to approximately 1200 C and form a molten ball that floated half in and half out of the crucible. But to get the plutonium sample to 1200 C required 40 kW and the plutonium did not form a floating molten ball like the copper did. A temperature of 1200 C is required because the main impurity element of interest is americium and as discussed in Section 4.4.3, 1200 C should be a good operating temperature for the distillation apparatus (Figure 15). The difference between the way copper and plutonium behaved in the

distillation apparatus was mainly due the large difference in density between copper and plutonium. Because of the high power setting needed for plutonium, the amount of cooling to the crucible and induction leads had to be doubled.

After making a number of practice distillation runs, a procedure was determined for the plutonium impurity distillation part of the experiment. This was accomplished by an infrared pyrometer and visual observation of the levitated molten metal.

5.3.1. Low-Impurity Alloy

Two runs were made using the following procedure (Figure 22a):

- The rod pieces were loaded into the vertical crucible (15 ml).
- The vacuum chamber lid was put in place and closed; the valve to the zone refiner was closed.
- The vacuum chamber was evacuated and back-filled three times with high-purity argon.
- The roughing vacuum valve to vacuum chamber was opened for 1 h, and then closed.
- If the thermocouple gauge read less than 5×10^{-3} torr and the cryo-pump temperature read less than 20 K, the cryo-pump valve was opened.
- Cooling water to the apparatus was turned on.
- The RGA was turned on using the computer.
- The first run was started once the vacuum was less than 1×10^{-6} torr as read by the RGA.
- One person turned the power knob slowly until the power (gauge on power supply) reached 40 kW while a second person who was using an infrared pyrometer observed the temperature of the molten plutonium metal.
- Once the power supply gauge read 40 kW, the clock was started for the 2-h run.

- During the run, the RGA was used to monitor total system pressure and partial pressure of any impurities leaving the molten plutonium.
- After the run time was completed, the power to the coil was turned off slowly.
- The vacuum chamber was opened, and the half-sphere of plutonium metal was removed and sent to the sample-handling glovebox
- A 1-g sample was cut from the half-sphere sample using a diamond trim saw. The sample was cut from the center of the sample as shown in Figure 26.
- The second run was made using the same procedure.

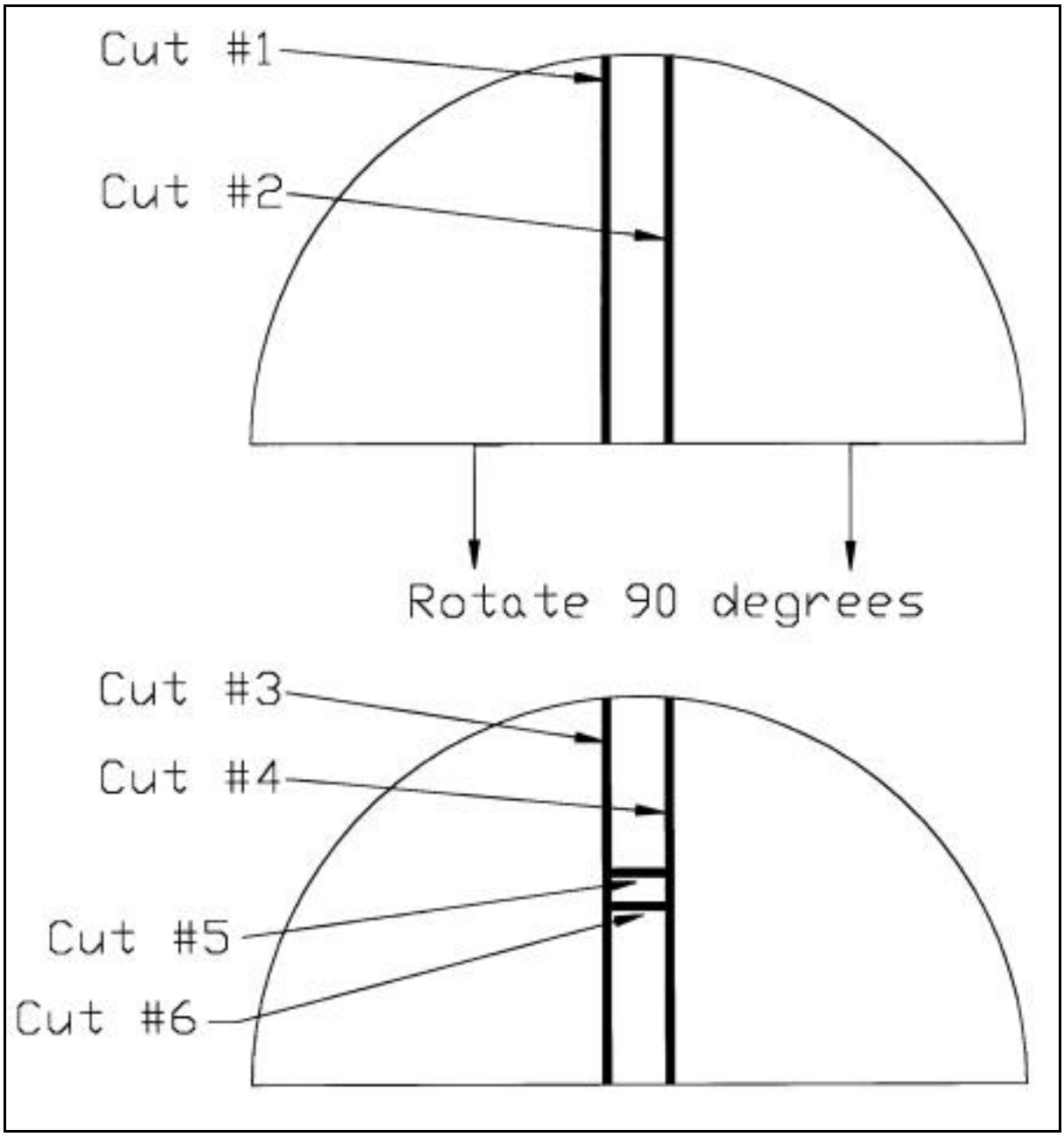

Figure 26. Six cuts used to obtain a chemical analysis sample from the plutonium metal product of the distillation apparatus.

5.3.2. High-Impurity Alloy

These two runs were performed the same as the low-impurity alloy runs (Figure 22b). After completion of each run, a metal shim had to be used to remove plutonium product from the crucible because of the slight volume increase on solidification. The shim was placed between the crucible segments and then used to push the product out of the crucible.

5.4. Zone Refining Runs

First, practice runs were made using rods of the low-impurity alloy (cut to a length of 5.5 in using the diamond trim saw) to determine a starting experimental procedure for making zone refining runs. The goal was to keep the molten zone the desired size and temperature using a single power setting. Unfortunately, it was determined that the power setting would have to be adjusted throughout each run and that the molten zone would have to be observed every five minutes with and without the infrared pyrometer.

5.4.1. Low-Impurity Alloy

Ten runs (five different variable combinations) were made using the following general procedure (Figure 22a):

- The rod was loaded into the apparatus and aligned so that the back of the coil was positioned at the back of the rod (tail-end).
- The vacuum chamber lid was put in place and closed.
- The vacuum chamber was evacuated and back-filled three times with high-purity argon.
- The roughing vacuum valve to the vacuum chamber was opened for 1 h, and then closed.
- Once the vacuum chamber pressure was less than 5×10^{-3} torr and the cryo-pump temperature was less than 20 K, the cryo-pump valve was opened.

- The desired speed (Figure 22a) and the distance the boat would travel was set using the HRCC.
- Cooling water to the apparatus was turned on.
- The power supply was set at 10 kW.
- Once the molten zone reached a temperature of 650 C as measured by the infrared pyrometer, the encoder motor was started (which was the beginning of each pass).
- The molten zone was observed every five minutes and the power supply setting adjusted to keep the molten zone small and the temperature of the molten zone around 675 C.
- After the first pass was complete (the molten zone reached the tail-end of the rod), the power to the coil was turned off and the rod returned to its original position. Then the process equipment was turned off.
- For rods 3 and 4, the rods were removed after each pass and the oxide layer on the rod was removed using the oxide removal system (Figures 27a and b).
- The remainder of the passes were done the same way as the first pass.
- After the last pass was completed, the rod was removed from the apparatus and sent to the sample-handling glovebox.
- Three, 1-g samples were cut from the rod using a diamond trim saw. The samples were cut from the two ends and rod middle as shown in Figure 28.

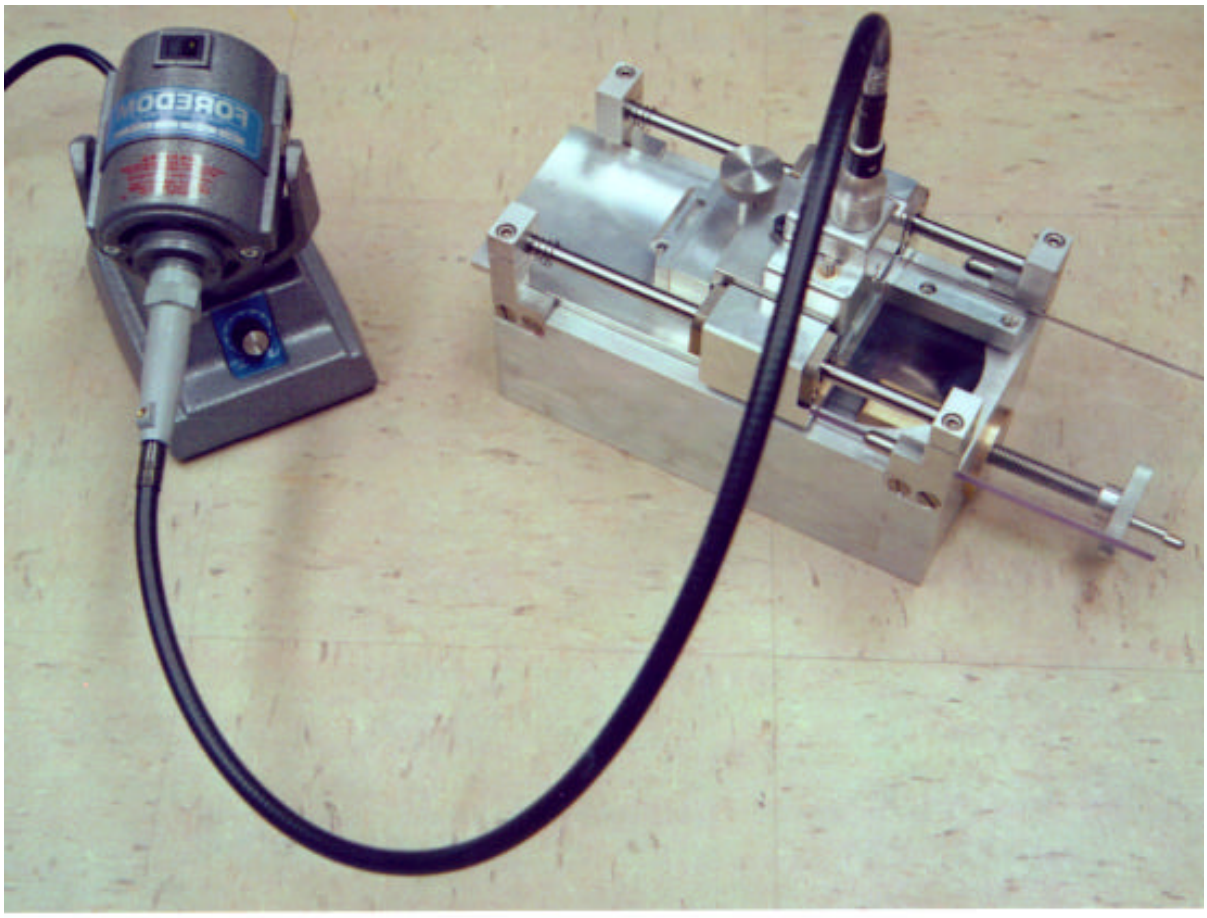

Figure 27a. Oxide removal system.

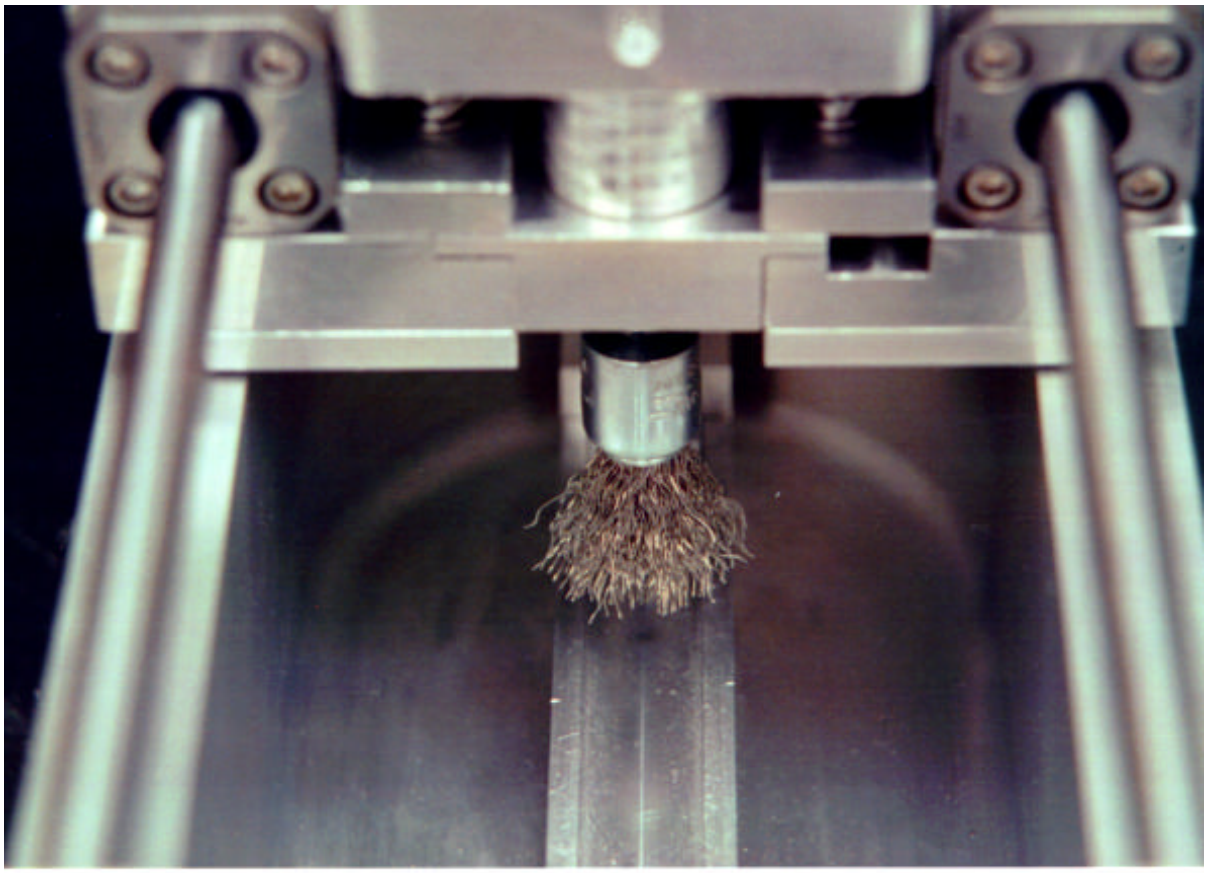

Figure 27b. Oxide removal system wire brush mechanism.

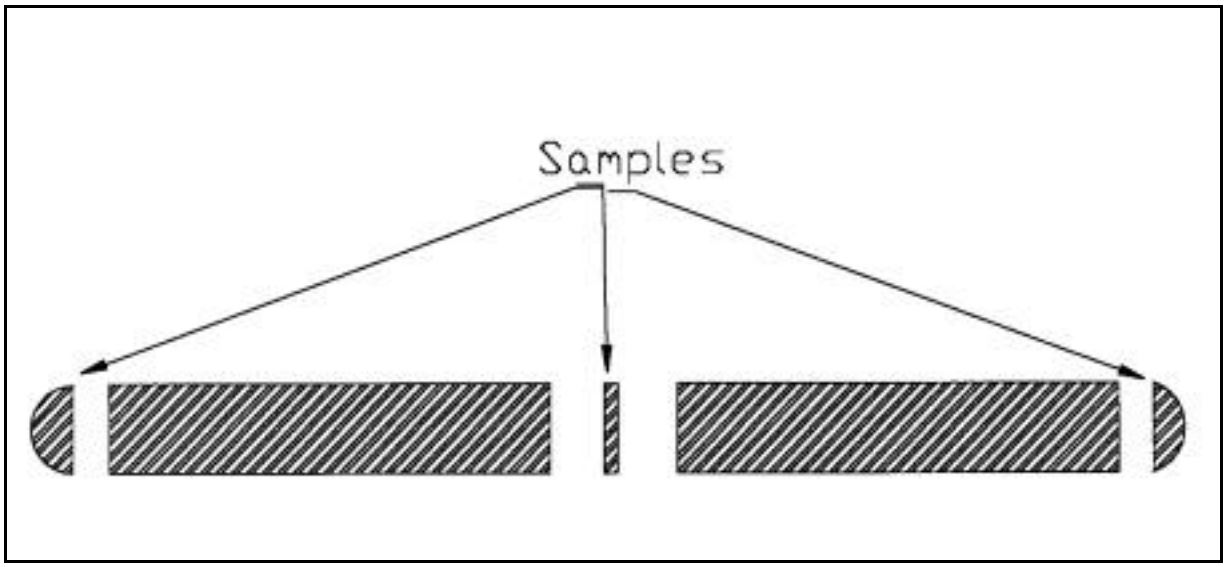

Figure 28. Sampling of zone refined rods for chemical analyses.

5.4.2. High Impurity Alloy

Ten runs (five different variable combinations) were done the same as the low-impurity alloy (including sampling) except for rods 3 and 4 (Figure 22b). Rods 3 and 4 were held under a vacuum of approximately 1 x 10^{-4} torr for 24 h before each pass. The speed settings and the number of required passes for each rod was as shown in Figure 22b.

5.5. Chemical Analysis

Concentrations of gallium and all other impurities in each alloy were determined using x-ray fluorescence. Analyses were performed by the analytical chemistry group at the Los Alamos National Laboratory. Analytical samples were taken as shown in Figure 22a and b.

CHAPTER 6

RESULTS AND DISCUSSIONS

6.1. Analyses of As-Cast Alloys

The results of chemical analyses for the low-impurity as-cast alloy (two samples taken) and the high-impurity as-cast alloys (two samples taken) are shown in Table 2. Most of the added elements in both alloys were close to the targeted levels, except chromium and uranium. One possible explanation was that uranium and chromium were partly held up in the crucible slag during the casting process. The table also shows the estimated distribution coefficient for each impurity element. Figure 29 is a illustration of one of the as-cast _-in diameter rods cast from the high-impurity alloy.

TABLE 2: CHEMICAL ANALYSES OF AS-CAST ALLOYS
Concentration in ppm by weight (precision ± 10%)

Element and (K)	Low-impurity Alloy sample 1	Low-impurity Alloy sample 2	High-impurity Alloy, Sample 1	High-impurity Alloy, Sample 2
Ga (1.4)	-	-	9,800	9,900
Al (1.4)	-	-	1,140	1,100
Am (19)	1,080	1,130	2,820	2,880
Co (0.2)	405	440	1,090	1,100
Cu (0.3)	515	405	1,110	1,100
Cr (0.2)	280	340	540	500
Fe (0.2)	480	485	1,100	1,100
Ni (0.3)	460	478	1,140	1,100
Np (0.8)	-	-	959	965
U (0.6)	-	-	285	210
Mn (0.2)	350	380	4	4
V (0.3)	425	583	7	3

Figure 29. As-cast _-in diameter rod of high-impurity alloy.

6.2. Zone Refining Observations

The most important observation was that every time plutonium metal had to be removed from the Crystalox® horizontal cold boat at either the end of a pass or a run, it was just a matter of reaching in and picking up the plutonium metal rod. Before these experiments, there had never been a documented case where plutonium metal could just be removed from a container (no sticking) after going through any kind of a melting operation. This observation is a strong indication that the secondary purpose of this experiment was achieved; that is, the containment of molten plutonium for long periods with no crucible interaction.

After the first few passes on the first plutonium rod, it was noticed that the G-10 surrounding the induction coil was turning brown in color on one side. The G-10 is a fiberglass substance that acts as an electrical insulator to protect the induction coil from

shorting-out due to any conducting material touching more than one turn in the coil. This color change was determined to be caused by the flux-field concentrator heating up in the induction field and then burning the G-10. After discussions with Fluxtrol®, it was determined that the type of concentrator ceramic used in the zone refining coil may have been wrong for the frequency of the zone refining power supply. A new coil was built at Fluxtrol® with a different flux-field concentrator ceramic and put in the zone refining apparatus. This action only slightly improved the problem. The coil was then rebuilt in the glovebox with less flux-field concentrator on the side of the coil that was burning and new G-10. This last coil worked well enough to continue the experiment, but because of the heating problem Fluxtrol® started design work on developing a new coil design for the zone refining apparatus. Another problem with the induction coil was that the top of the plutonium rod about one inch ahead of the coil was being heated. It was determined that the power lead to the coil was inducing the rod. This was only a minor problem for standard zone refining of plutonium, but would be a significant problem for the solid-state plutonium zone refining used to produce large plutonium crystals. After discussions with Fluxtrol®, a plan was developed for a new coil that would solve both coil problems. This coil was then fabricated at Fluxtrol® for future experiments with the zone refining apparatus.

Figure 30 is a illustration of rod 1 (high-impurity alloy) after completion of the run (six molten zone passes). From the illustration, there is clear evidence of the outgassing of plutonium impurities that occurred as the molten zone traveled along the rod. The amount of outgassing was always the greatest at the head-end of the rod. This was because the further

along the rod, the longer the heat-up time for the plutonium, giving more time for the impurities to outgas. Evidence of this outgassing was observed during each pass as slow bubbling in the molten zone. It was possible to see the impurities condensing on the cold surface of the crucible during each pass. However, the only gases the SRS residual gas analyzer detected that were not already detected in the background were hydrogen and helium. Given the long path to the SRS, this result was not surprising.

Figure 30. Rod 1 (high-impurity alloy) after completion of zone refining run.

6.3. Results of Chemical Analyses on Zone refined Rods

Table 3 shows the results of chemical analysis of the zone refined plutonium rods of both alloys. For each zone refined rod, three samples were taken, one each from the head-end, tail-end, and middle of the rod. The concentration of each metal sample was determined using x-ray fluorescence. Not all the impurity elements that were added to make up the two

alloys are in the table because a funding cut for this experiment limited the amount of analysis that could be done. The only elements that were tracked in all runs were chromium, iron, cobalt, nickel, and copper because these elements were added to both alloys and this allowed for a single analysis setup, allowing the analytical cost to remain in budget.

Table 3 shows how the concentration of the different impurities changed with location along the zone refined rod for all the variable combinations. From this table, it was clear that the impurity elements chromium, iron, cobalt, nickel, neptunium, and copper moved in the same direction as the molten zone, while the elements gallium, americium, and aluminum moved in the opposite direction. This fact agrees with the binary phase diagram for each impurity element.

A comparison of Table 2 to Table 3 indicates that there was an impurity loss due to vaporization (outgassing of plutonium impurities) during the zone refining process. This can be clearly seen by comparing the as-cast analyses for both alloys (Table 2) to any of the middle values shown in Table 3. As shown in Figures 14a and b, the middle value of the zone refined rod is a good approximation of the average composition and is the same as the initial composition if there were no impurity loss through vaporization.

TABLE 3: RESULTS OF CHEMICAL ANALYSES OF ZONE REFINED RODS
Concentration in ppm by weight (precision ± 10%)

Low-impurity Alloy, Speed 0.75 in/h, and 6 Passes						
	Rod 1			Rod 2		
Element	Head-End	Middle	Tail-End	Head-End	Middle	Tail-End
Cr	180	322	474	191	289	452
Fe	299	358	597	311	350	586
Co	296	387	475	284	377	501
Ni	184	254	396	207	268	437
Cu	266	321	382	252	317	373
Low-impurity Alloy, Speed 1.5 in/h, 3 Passes, and Brushing Step						
	Rod 3			Rod 4		
Element	Head-End	Middle	Tail-End	Head-End	Middle	Tail-End
Cr	153	382	621	214	402	656
Fe	318	436	614	307	413	623
Co	297	383	498	316	361	517
Ni	214	329	526	200	334	496
Cu	252	324	444	257	319	423
Am	758	668	537	679	621	528
Low-impurity Alloy, Speed 1.5 in/h, and 6 Passes						
	Rod 5			Rod 6		
Element	Head-End	Middle	Tail-End	Head-End	Middle	Tail-End
Cr	192	349	407	188	339	427
Fe	305	351	514	341	386	531
Co	299	364	401	314	373	403
Ni	169	269	283	216	276	304
Cu	248	318	376	227	306	401
Low-impurity Alloy, Speed 1.5 in/h, and 3 Passes						
	Rod 7			Rod 8		
Element	Head-End	Middle	Tail-End	Head-End	Middle	Tail-End
Cr	213	180	306	256	279	344

Fe	274	357	455	316	366	409
Co	310	332	412	298	346	426
Ni	244	274	290	235	308	312
Cu	284	287	369	264	298	385
Low-impurity Alloy, Speed 0.75 in/h, and 3 Passes						
	Rod 9			Rod 10		
Element	Head-End	Middle	Tail-End	Head-End	Middle	Tail-End
Cr	220	293	418	216	298	430
Fe	257	331	476	264	341	489
Co	287	348	452	274	326	449
Ni	220	291	320	243	306	358
Cu	272	293	370	277	289	355

TABLE 3: RESULTS OF CHEMICAL ANALYSES OF ZONE REFINED RODS

High-impurity Alloy, Speed 0.75 in/h, and 6 Passes						
	Rod 1			Rod 2		
Element	Head-End	Middle	Tail-End	Head-End	Middle	Tail-End
Cr	366	384	695	241	270	792
Fe	724	772	1820	664	1,041	2,295
Co	583	650	1,680	833	915	2,315
Ni	672	696	1,790	854	927	1,168
Cu	859	994	1,200	862	1,110	2,115
Ga	9,700	8,600	6,700	14,684	12,020	7,140
Al	1,300	1,000	870	1,425	940	870
Np	255	267	331	310	322	414
Am	1,690	1,270	1,170	1,710	1,240	1,110
High-impurity Alloy, Speed 1.5 in/h, 3 Passes, and Vacuum Step						
	Rod 3			Rod 4		
Element	Head-End	Middle	Tail-End	Head-End	Middle	Tail-End
Cr	408	452	922	369	421	849
Fe	717	748	1,491	699	736	1,391
Co	644	684	1,166	727	756	1,476
Ni	683	703	1,066	732	760	1186
Cu	1,100	1,200	1,600	1,100	1,200	1,500
High-impurity Alloy, Speed 1.5 in/h, and 6 Passes						
	Rod 5			Rod 6		
Element	Head-End	Middle	Tail-End	Head-End	Middle	Tail-End
Cr	432	550	739	418	457	682
Fe	713	760	1,700	740	811	1,300
Co	688	698	1,600	717	725	1,460

Ni	774	791	1,500	810	827	1,200
Cu	1,100	1,100	1,400	1,100	1,100	1,200
Ga	10,600	9,300	9,000	10,000	9,400	8,700

High-impurity Alloy, Speed 1.5 in/h, and 3 Passes						
	Rod 7			Rod 8		
Element	Head-End	Middle	Tail-End	Head-End	Middle	Tail-End
Cr	387	431	577	381	425	545
Fe	746	785	1,141	786	836	1,242
Co	703	743	970	734	784	976
Ni	826	889	1,066	811	789	1,014
Cu	1,100	1,100	1,100	1,100	1,100	1,200

TABLE 3: RESULTS OF CHEMICAL ANALYSES OF ZONE REFINED RODS

High-impurity Alloy, Speed 0.75 in/h, and 3 Passes						
	Rod 9			Rod 10		
Element	Head-End	Middle	Tail-End	Head-End	Middle	Tail-End
Cr	489	529	1,003	467	521	948
Fe	721	782	1,305	707	734	1,343
Co	694	746	1,131	767	789	1,319
Ni	769	801	1,107	809	829	1,238
Cu	1,000	1,100	1,100	1,000	1,100	1,400

6.4. Determination of Variables for Zone Refining

Table 4 gives the calculated value of percent change in composition from the head-end of the zone refined rod to that of the tail-end for the impurity elements. It also gives a total value, which is the sum of the values determined for the elements chromium, iron, cobalt, and nickel only. This calculated total is a gross indication of how well each variable arrangement produced impurity segregation and is defined as the zone refining yield.

Figures 31a and b are plots that show the effect of each zone refining parameter examined in this study. From Figure 31a, it is clear that decreasing the zone refining speed and increasing the number of passes increases the zone refining yield, which agrees with zone refining theory (Sections 2.3 and 2.4). Figure 31a also indicates which of the two alloys used had no effect on the zone refining yield. Figure 31b clearly shows that by adding the steps of either wire brushing or a high-vacuum hold increased the zone refining yield. This indicates that the presence of oxygen decreases the zone refining yield, which agrees with the same fact discover during uranium zone refining (Section 4.2).

TABLE 4: RESULTS OF CHEMICAL ANALYSES OF ZONE REFINED RODS

Low-impurity Alloy, Speed 0.75 in/h, and 6 Passes Percent change head-end to tail-end; **Total =943**		
Element	Rod 1	Rod 2
Cr	163	137
Fe	100	88
Co	61	76
Ni	115	111
Cu	44	48
Low-impurity Alloy, Speed 1.5 in/h, 3 Passes, and Brushing Step Percent change head-end to tail-end; **Total =1276**		
Element	Rod 3	Rod 4
Cr	306	207
Fe	93	103
Co	68	64
Ni	146	148
Cu	76	65
Am	-42	-29
Low-impurity Alloy, Speed 1.5 in/h, and 6 Passes Percent change head-end to tail-end; **Total =653**		
Element	Rod 5	Rod 6
Cr	112	127
Fe	67	56

Co	34	28
Ni	59	41
Cu	52	77

Low-impurity Alloy, Speed 1.5 in/h, and 3 Passes
Percent change head-end to tail-end; **Total =377**

Element	Rod 7	Rod 8
Cr	44	34
Fe	66	29
Co	33	43
Ni	19	33
Cu	30	46

Low-impurity Alloy, Speed 0.75 in/h, and 3 Passes
Percent change head-end to tail-end; **Total =638**

Element	Rod 9	Rod 10
Cr	90	99
Fe	85	85
Co	58	64
Ni	46	47
Cu	36	28

TABLE 4: RESULTS OF CHEMICAL ANALYSES OF ZONE REFINED RODS

High-impurity Alloy, Speed 0.75 in/h, and 6 Passes
Percent change head-end to tail-end; **Total =1831**

Element	Rod 1	Rod 2
Cr	90	229
Fe	151	246
Co	188	178
Ni	166	37
Cu	401	145
Ga	-45	-106
Al	-49	-64
Np	30	34
Am	-44	-54

High-impurity Alloy, Speed 1.5 in/h, 3 Passes, and Vacuum Step
Percent change head-end to tail-end; **Total =846**

Element	Rod 3	Rod 4
Cr	126	130
Fe	108	99
Co	81	103
Ni	55	62
Cu	46	36

High-impurity Alloy, Speed 1.5 in/h, and 6 Passes Percent change head-end to tail-end; **Total =764**		
Element	Rod 5	Rod 6
Cr	71	63
Fe	138	76
Co	133	104
Ni	94	48
Cu	27	10
Ga	18	15

High-impurity Alloy, Speed 1.5 in/h, and 3 Passes Percent change head-end to tail-end; **Total =373**		
Element	Rod 7	Rod 8
Cr	49	43
Fe	53	58
Co	38	33
Ni	29	25
Cu	36	9

TABLE 4: RESULTS OF CHEMICAL ANALYSES OF ZONE REFINED RODS

High-impurity Alloy, Speed 0.75 in/h, and 3 Passes Percent change head-end to tail-end; **Total =661**		
Element	Rod 9	Rod 10
Cr	105	103
Fe	81	90
Co	63	72
Ni	44	53
Cu	10	40

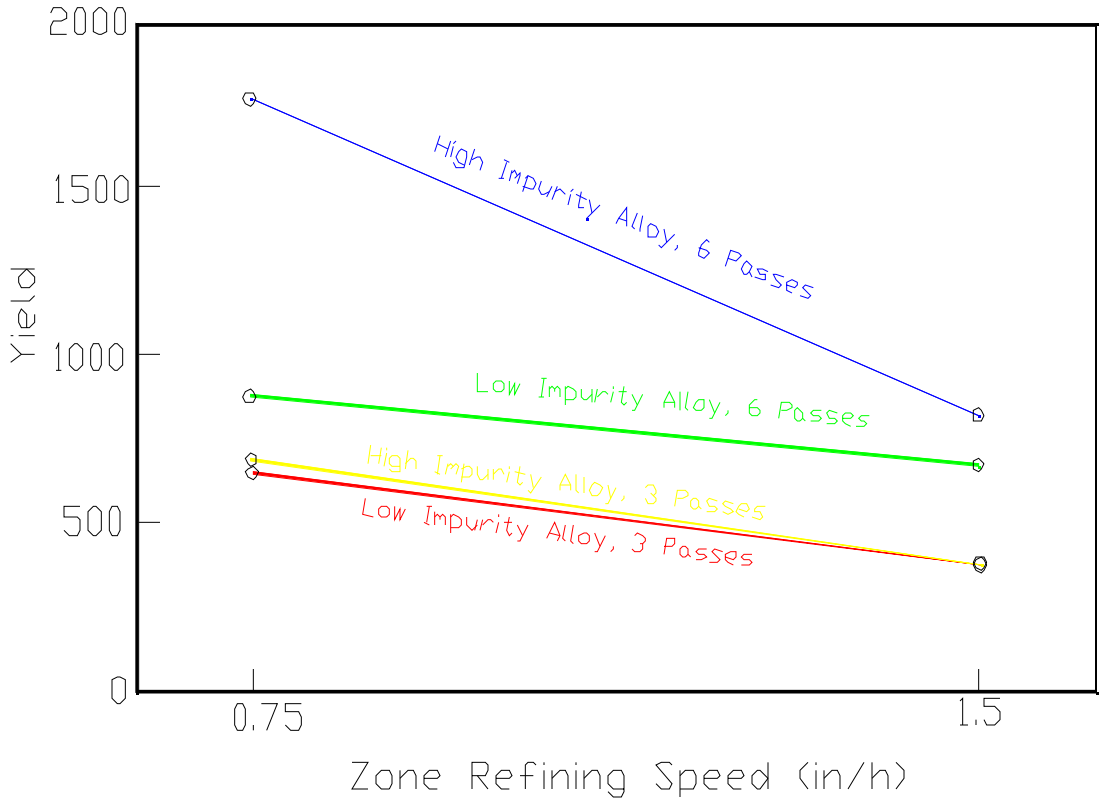

Figure 31a. Zone refining parameters. The change in yield with different speeds, alloys, and numbers of passes.

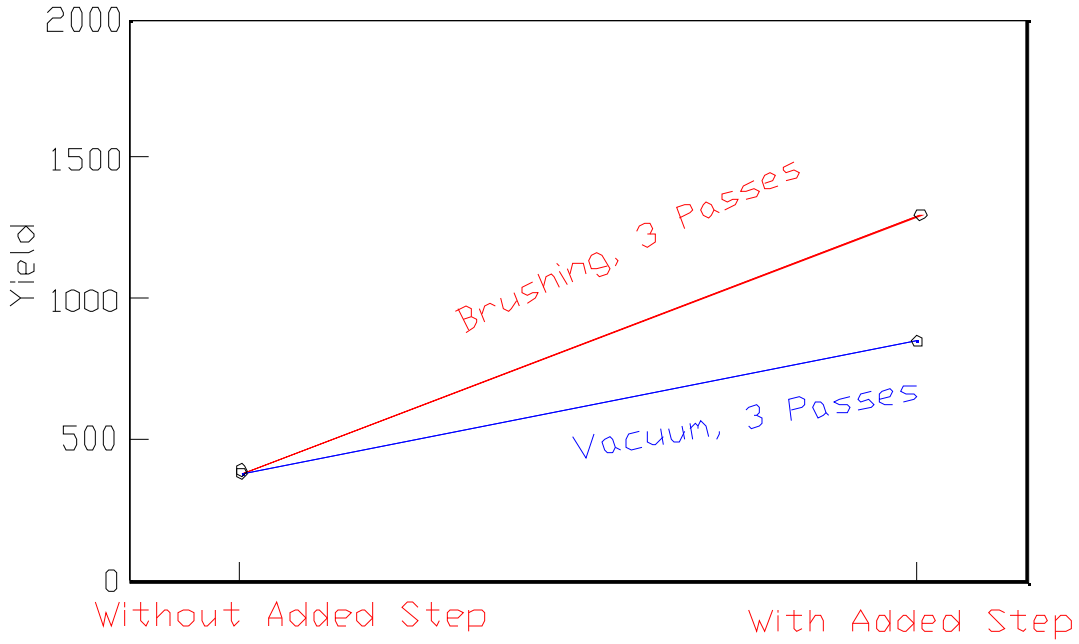

Figure 31b. Zone refining parameters. The change in yield with the added steps of wire brushing and vacuum hold.

The important results (Table 4) for each zone refining variable is shown below:

- **Speed:** The slower the speed the better for both alloys (rods 1 and 2 compared to rods 5 and 6, and rods 7 and 8 compared to rods 9 and 10).
- **Passes:** The more passes the better for both alloys (rods 1 and 2 compared to rods 9 and 10, and rods 7 and 8 compared to rods 5 and 6).
- **Vacuum:** Adding the step of holding the rod under high vacuum before each pass produced a great improvement (high-impurity alloy rods 3 and 4 compared to rods 7 and 8).

- **Brushing:** Wire brushing the rod before each pass was the single greatest improvement (low-impurity alloy rods 3 and 4 compared to rods 7 and 8).

Figures 32a through 321i are plots of the change in composition from nominal for each impurity element after zone refining (high-impurity alloy rods 1 and 2, after six passes at a speed of 0.75 in/h). By comparing these plots to Figures 12 and 14, one can see that in general the results of zone refining of plutonium in this study followed the theory of zone refining. The elements chromium, cobalt, copper, iron, nickel, aluminum, and gallium (Figures 32a, b, c, d, e, g, and i) followed the theory exactly. Figure 32f shows that neptunium had a higher concentration at the tail-end than the head-end as predicted by neptunium's distribution coefficient of 0.8, but all six concentrations taken at the three locations along the rod seemed to be low. The most likely reason for this was that there was a analytical problem with the analysis of neptunium (neptunium analysis is not done frequently). The other possibility was that there was a loss of neptunium through some kind of vaporization mechanism, but this is unlikely (the vapor pressure of neptunium is near that of plutonium). Figure 32h shows that americium had a higher concentration at the head-end than the tail-end as predicted by Am's distribution coefficient of 19, but all six concentrations taken at the three locations along the rod seemed to be low. The most likely reason for this was that Am vaporized off during the zone refining run (the vapor pressure of americium is more than that of plutonium).

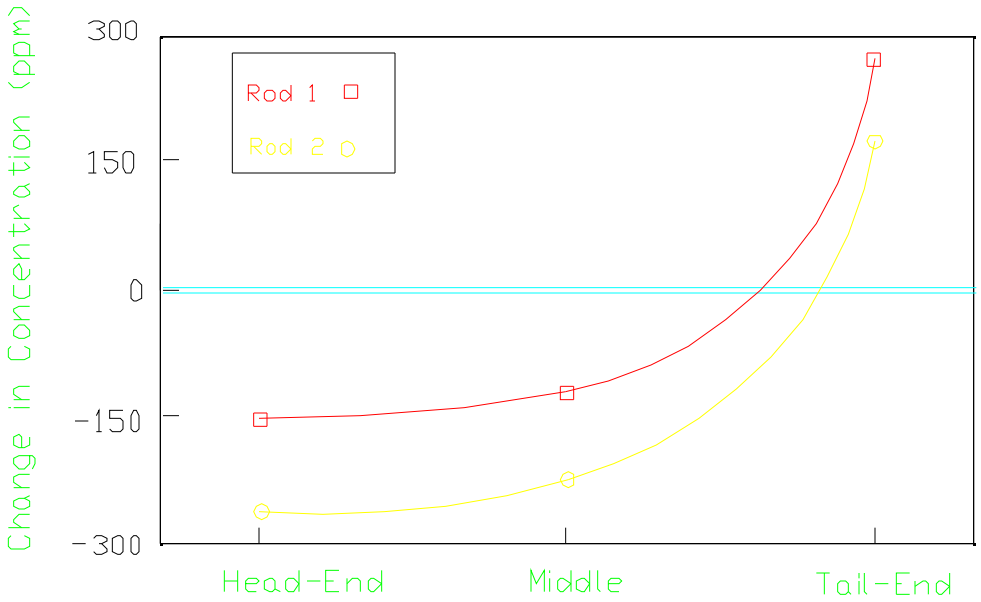

Figure 32a. Change in concentration from nominal (520 ppm) for chromium (K= 0.2) after zone refining (high-impurity rods 1 and 2, After six passes at a speed of 0.75 in/h).

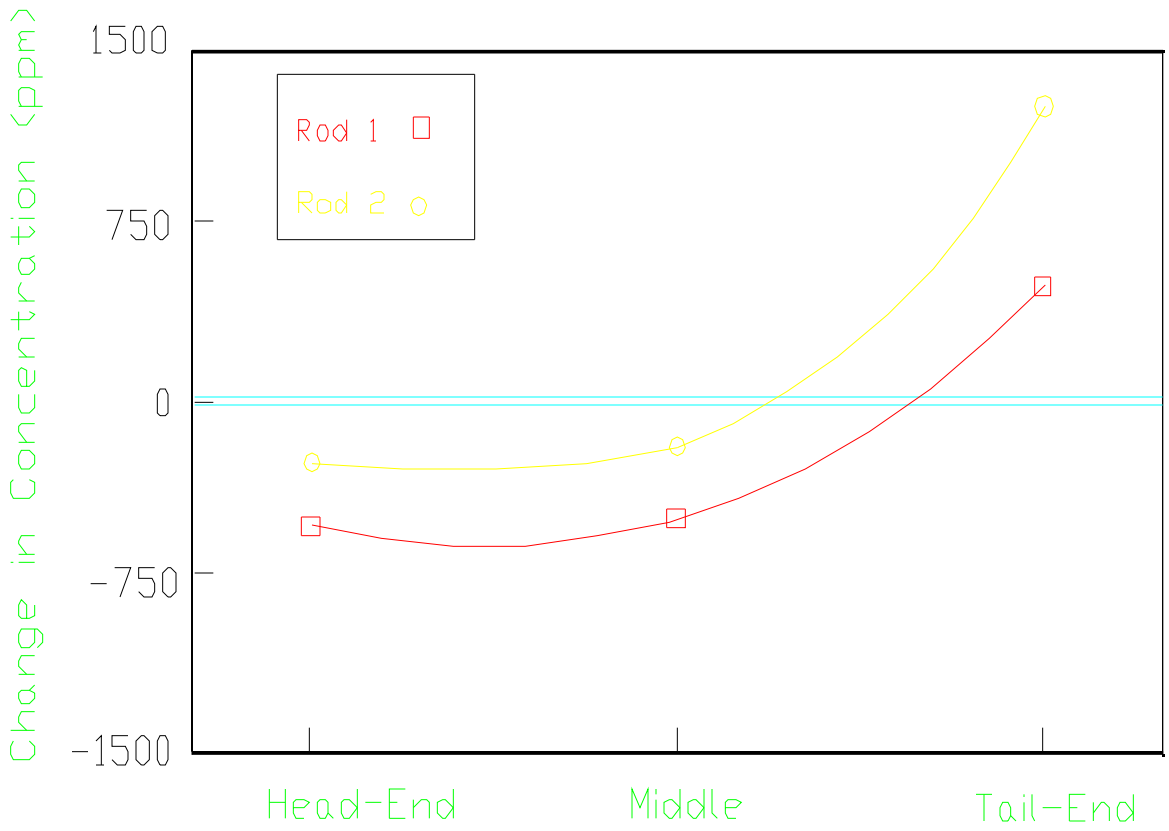

Figure 32b. Change in concentration from nominal (1,095 ppm) for cobalt (K= 0.2) after zone refining (high-impurity rods 1 and 2, after six passes at a speed of 0.75 in/h).

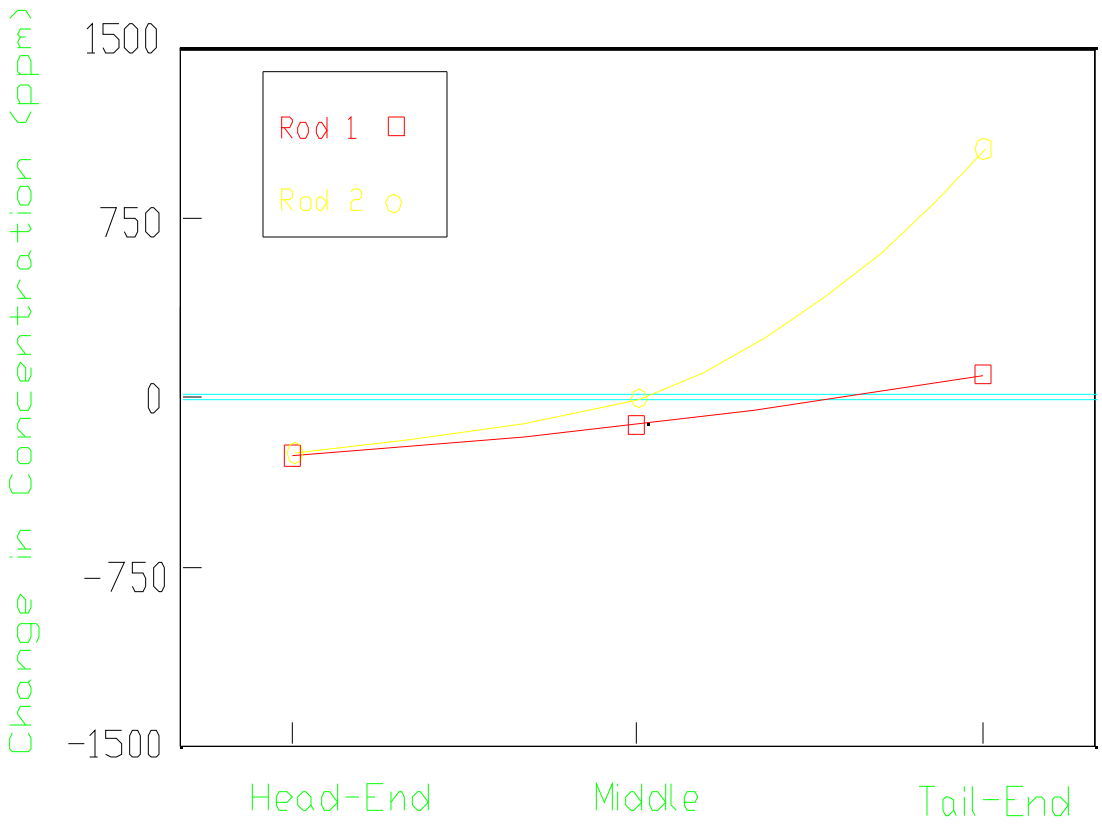

Figure 32c. Change in concentration from nominal (1,105 ppm) for copper (K= 0.3) after zone refining (high-impurity rods 1 and 2, after six passes at a speed of 0.75 in/h).

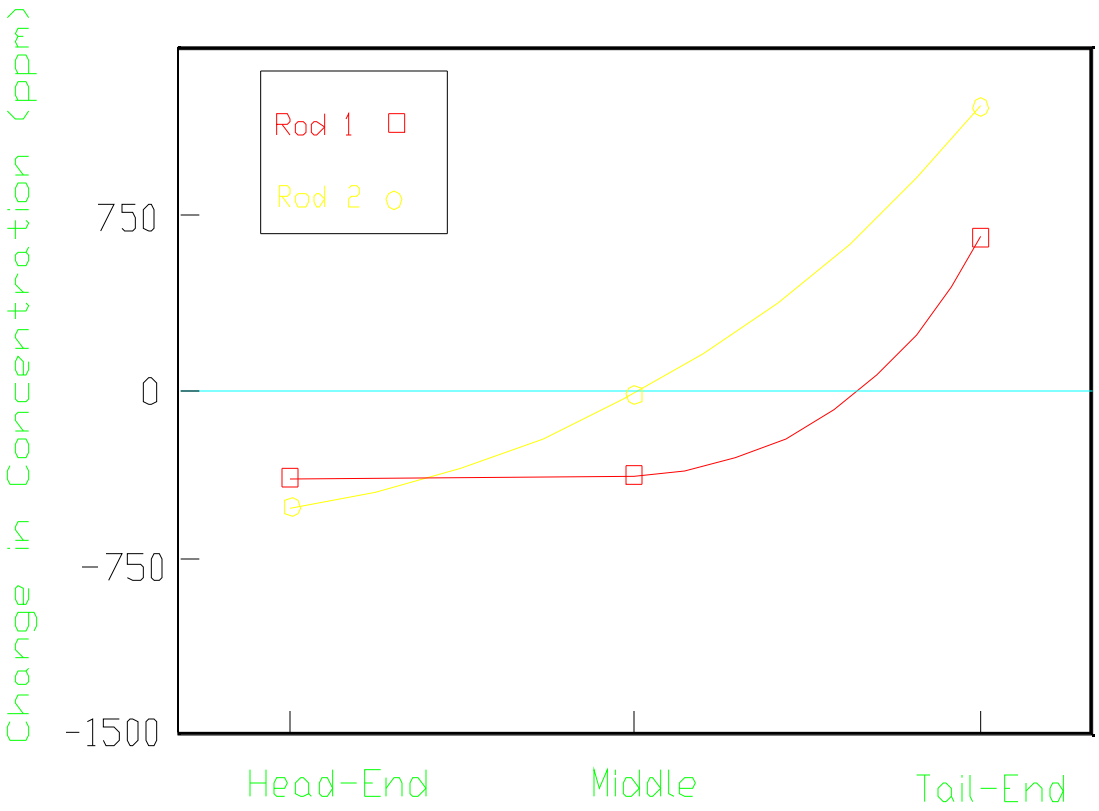

Figure 32d. Change in concentration from nominal (1,100 ppm) for iron (K= 0.2) after zone refining (high-impurity rods 1 and 2, after six passes at a speed of 0.75 in/h).

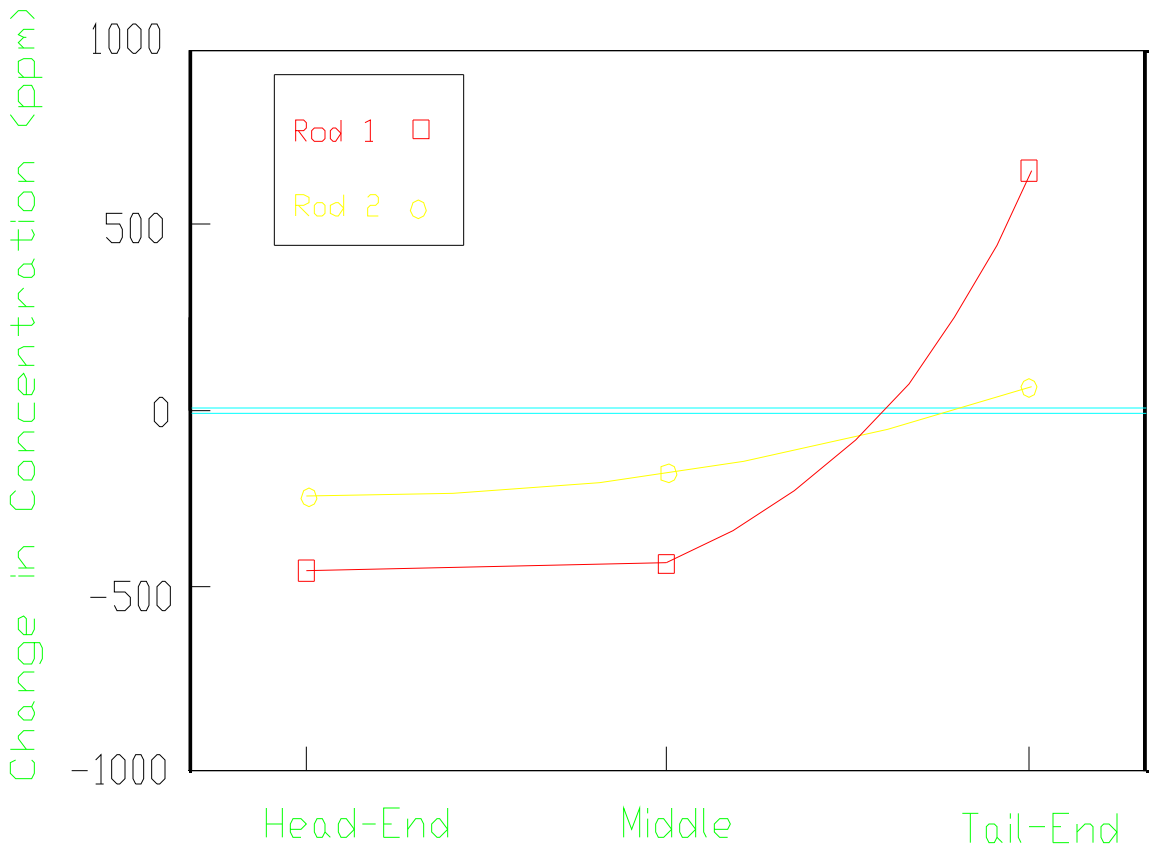

Figure 32e. Change in concentration from nominal (1,120 ppm) for nickel (K= 0.3) after zone refining (high-impurity rods 1 and 2, after six passes at a speed of 0.75 in/h).

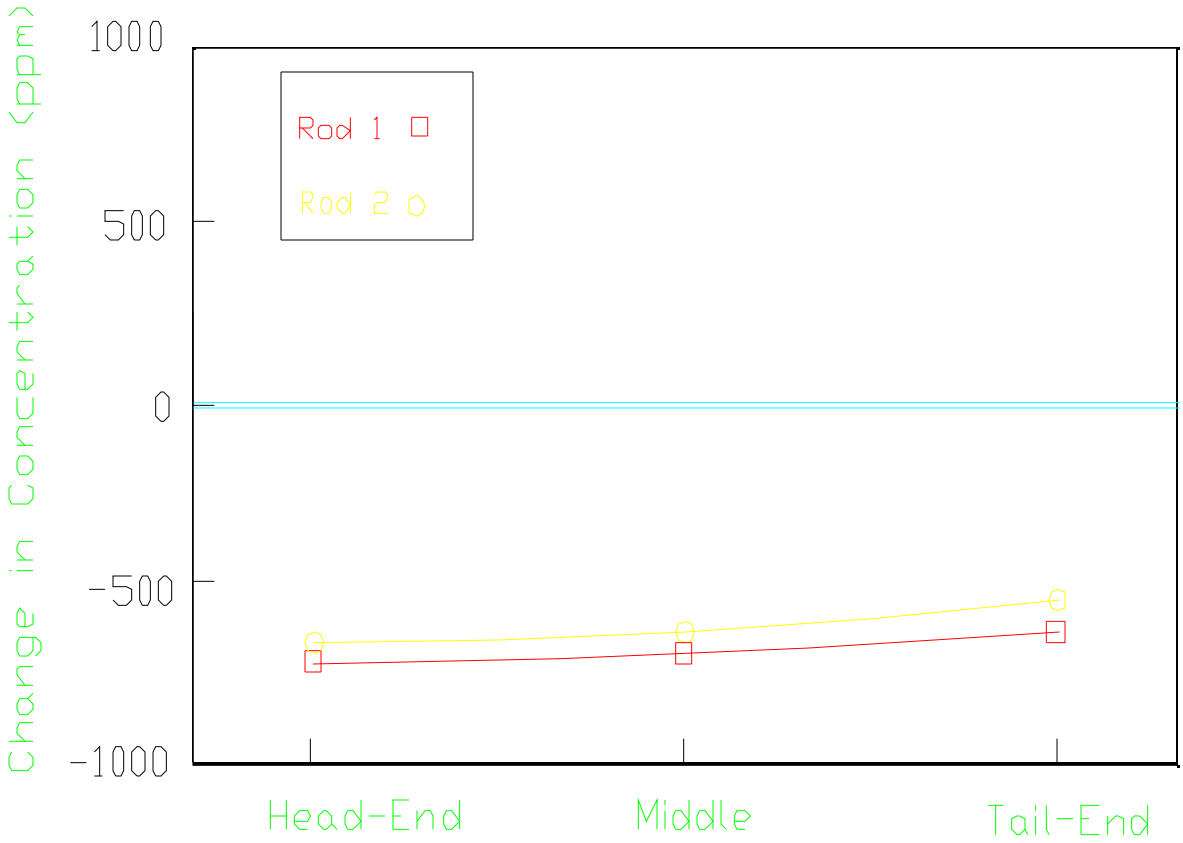

Figure 32f. Change in concentration from nominal (962 ppm) for neptunium (K= 0.8) after zone refining (high-impurity rods 1 and 2, after six passes at a speed of 0.75 in/h).

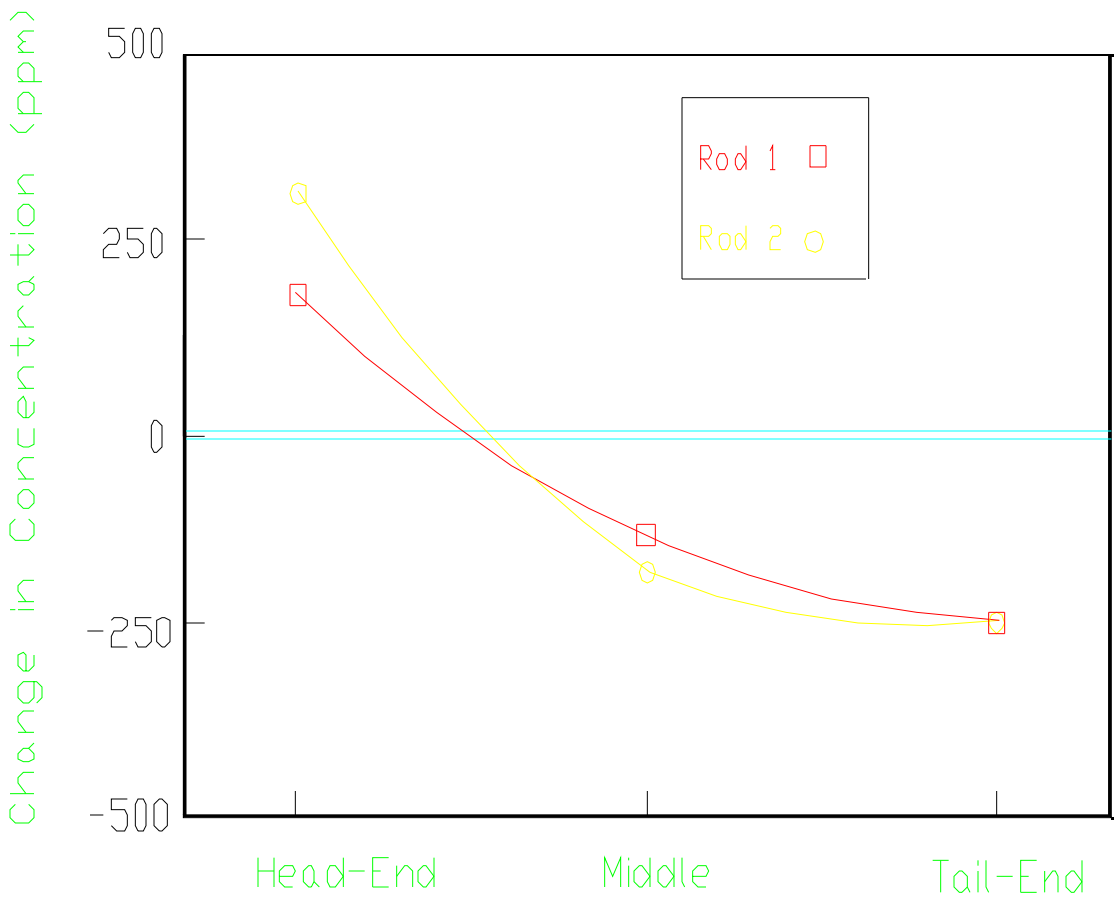

Figure 32g. Change in concentration from nominal (1,120 ppm) for aluminum (K= 1.4) after zone refining (high-impurity rods 1 and 2, after six passes at a speed of 0.75 in/h).

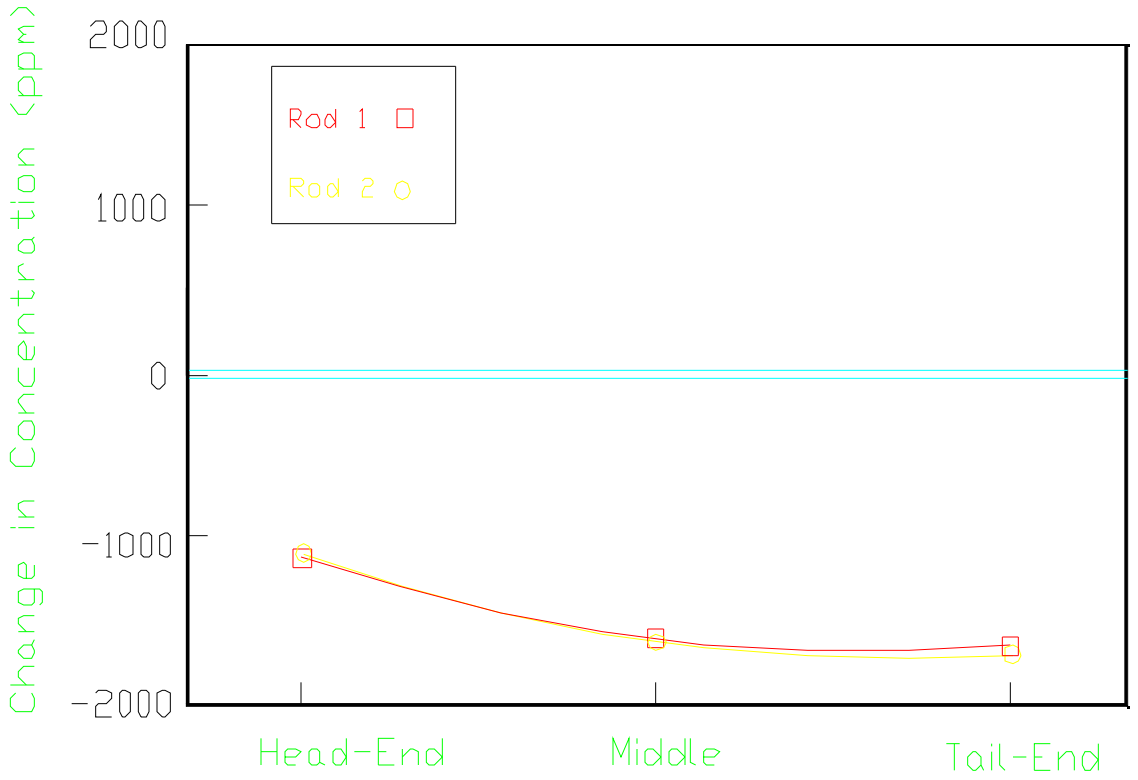

Figure 32h. Change in concentration from nominal (1,120 ppm) for americium (K= 19) after zone refining (high-impurity rods 1 and 2, after six passes

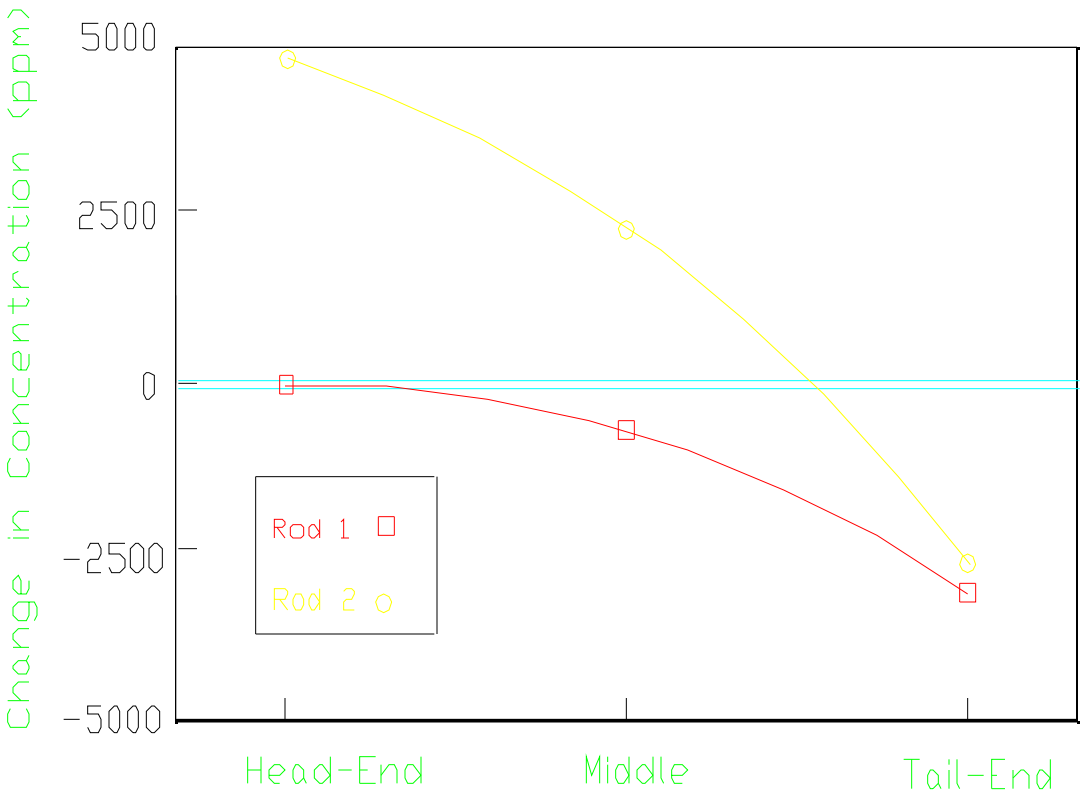

Figure 32i. Change in concentration from nominal (9,850 ppm) for gallium (K= 1.4) after zone refining (high-impurity rods 1 and 2, After six passes at a speed of 0.75 in/h).

6.5. Analysis of Variance of Zone Refining Data

An analysis of variance was performed using a SAS computer program with the data in Table 3 and calculated results in Table 4 for the elements chromium, iron, cobalt, nickel, and copper only. The results are shown in Tables 5 and 6, which give the probability of significance (Pr>F) for the different sources of variation. For example, a (Pr>F) value of 0.05 means that if the null hypothesis of no difference is true, an observed difference this large would occur only 5% of the time. All significant results (Pr>F is 0.05 or less) are shown in bold in these tables. For Table 5, the analysis was a completely random split plot design with a 2^4 factorial arrangement of treatments. The rods were nested within a pass-speed-alloy subclass as the whole plot. Locations within each rod constitute the split plot treatment. The dependent variable was the concentration determined from x-ray fluorescence after the rod had been zone refined. The independent variables in Table 5 were: the number of molten zone passes (three or six) made along the rod during the run (P); the speed (0.75 or 1.5 in/h) at which the molten zone traveled along the rod (S); the plutonium metal alloy (A) used for the zone refining run (either low or high-impurity); and sample location (L) along the zone refined rod (head-end, middle, or tail-end). There were two replications for each variable combination, giving a total of 48 observations per impurity element.

Table 5 clearly shows that there was a significant difference between the concentrations at the three locations along the rods (head-end, middle, and tail-end) for all impurity elements. The table also shows that there was a significant difference between the alloys in all cases. Table 5 does not give much significance to speed or the number of passes.

The table does show an alloy and location interaction, and a number of passes and location interaction.

TABLE 5: STATISTICAL ANALYSES RESULTS (Pr > F) USING A COMPLETELY RANDOM SPLIT PLOT DESIGN WITH A 2^4 FACTORIAL ARRANGEMENT OF TREATMENTS.

	Impurity Element				
Source	**Cr**	**Fe**	**Co**	**Ni**	**Cu**
Passes (P)	0.3192	**0.0073**	0.0524	0.0629	0.5431
Speed (S)	**0.0114**	0.1123	0.1703	0.1574	0.8265
Alloy (A)	**0.0001**	**0.0001**	**0.0001**	**0.0001**	**0.0001**
Location (L)	**0.0001**	**0.0001**	**0.0001**	**0.0001**	**0.0011**
A*S	0.2450	0.1383	0.2612	0.8937	0.8321
A*P	**0.0089**	0.0735	0.0914	**0.0231**	0.5952
A*L	**0.0001**	**0.0001**	**0.0001**	**0.0005**	0.1235
S*P	**0.0001**	0.1296	0.5713	0.6509	0.9240
S*L	**0.0001**	**0.0267**	0.0844	0.3399	0.2328
P*L	**0.0555**	**0.0032**	**0.0033**	0.0566	0.1350
P*S*L	0.1032	0.4959	0.7854	0.9734	0.5596
S*A*L	**0.0028**	0.2085	0.3074	0.9042	0.1587
A*S*P	**0.0013**	0.1836	0.7479	0.8087	0.9813

For Table 6, the dependent variable was percent change in concentration between the head-end and tail-end of the zone refined rod, with the independent variables (P, S, and A) being the same as Table 5. There were two replications for each variable combination, giving a total of 16 observations per impurity element. The reason percent change was used instead

TABLE 6: STATISTICAL ANALYSES RESULTS (Pr > F) USING A 2^3 FACTORIAL MODEL.

	Impurity Element				
Source	Cr	Fe	Co	Ni	Cu
Passes	**0.0179**	**0.0146**	**0.0001**	**0.0274**	0.0613
Speed	**0.0108**	**0.0132**	**0.0001**	0.0875	0.1133
Alloy	0.7209	**0.0305**	**0.0001**	0.8620	0.2601
A*S	0.3940	0.4189	0.0947	0.6630	0.0635
A*P	0.4301	**0.0473**	**0.0001**	0.9279	0.1583
S*P	0.8977	0.3772	**0.0385**	0.4806	0.1044
P*S*A	0.4301	0.3032	0.3712	0.6433	0.0778

of change in concentration was to normalize the results between the two alloys (the high-impurity alloy had concentrations over double the low-impurity alloy).

The first row of Table 6 shows that the number of zone refining passes were significant (copper slightly high). The second row in Table 6 shows that zone refining speed was also significant (nickel and copper high). The third row shows that the segregation produced by zone refining was dependent on which alloy was used for some but not all impurity elements (iron and cobalt were significant, but chromium and nickel were not significant). This disagrees with the result in Table 5, which was one of the reasons for

normalizing the two alloys. Table 6 also shows some interaction between alloy and number of passes as well as speed and number of passes. These interactions can be seen in Figure 31a.

Figures 33a through e show the mean of the percent change between head-end and tail-end for the elements chromium, iron, cobalt, nickel, and copper using the data in Table 4. In each figure, the vertices denote levels of the factors with the mean responses at the vertices. From these figures, one can clearly see the effect of speed, number of passes, and alloy for each of the elements. In most cases, the yield increases with increasing the number of passes and decreasing the zone refining speed. The effect of which alloy is not clear, but these figures indicate that the high-impurity alloy produced larger yields.

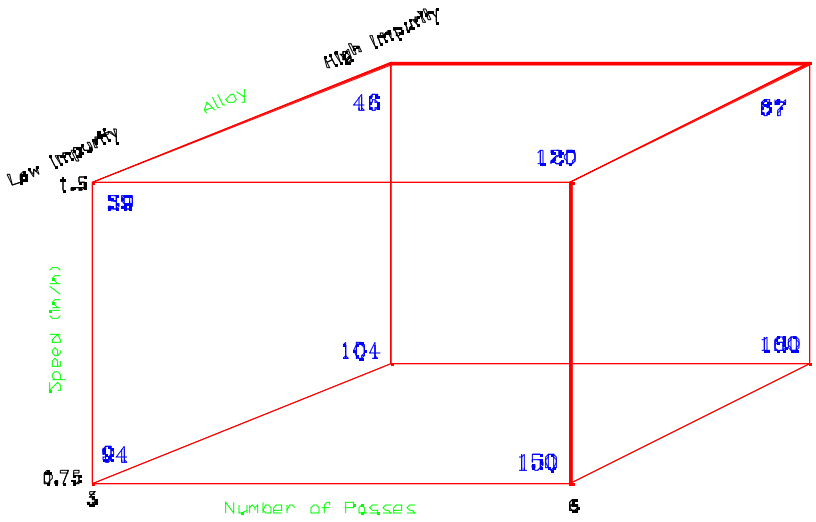

Figure 33a. Percent change (head to tail) for chromium, with the vertices denoting the levels of each factor and the numbers being the mean yield at the vertices.

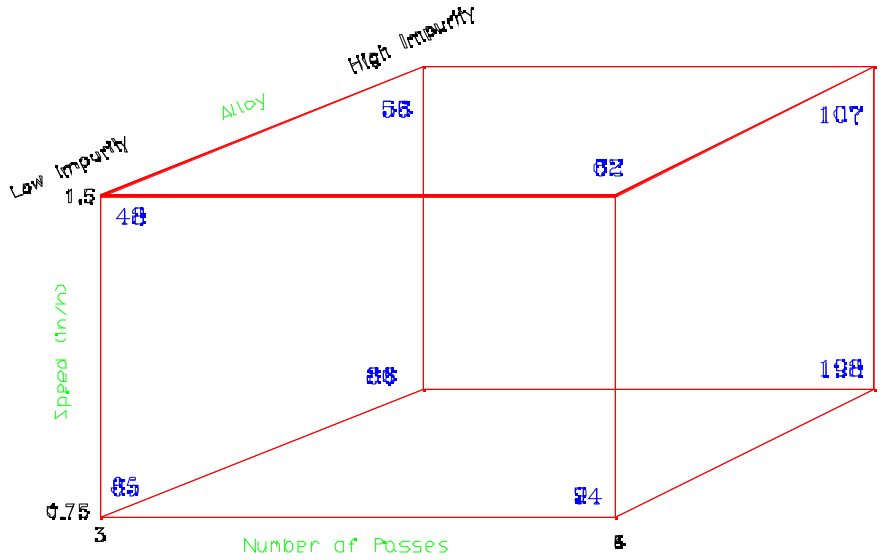

Figure 33b. Percent change (head to tail) for iron, with the vertices denoting the levels of each factor and the numbers being the mean yield at the vertices.

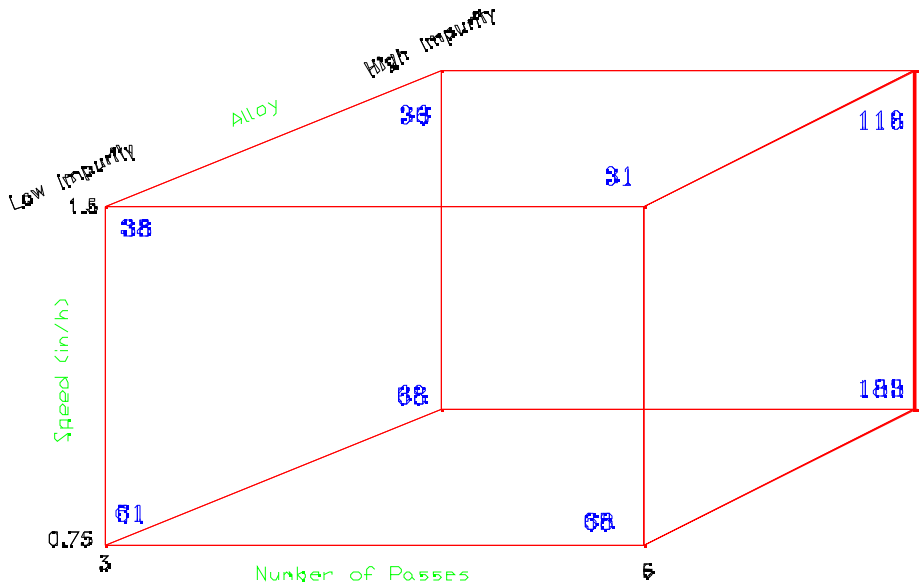

Figure 33c. Percent change (head to tail) for cobalt, with the vertices denoting the levels of each actor and the numbers being the mean yield at the vertices.

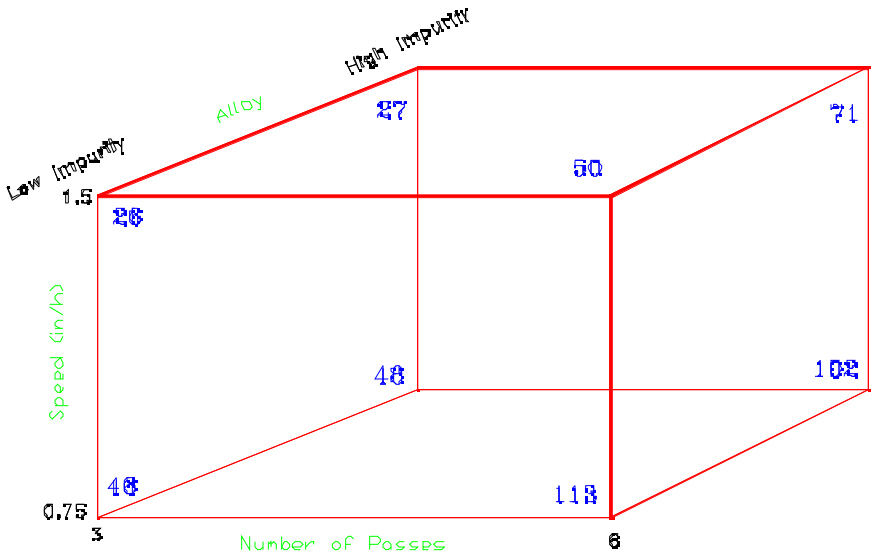

Figure 33d. Percent change (head to tail) for nickel, with the vertices denoting the levels of each factor and the numbers being the mean yield at the vertices.

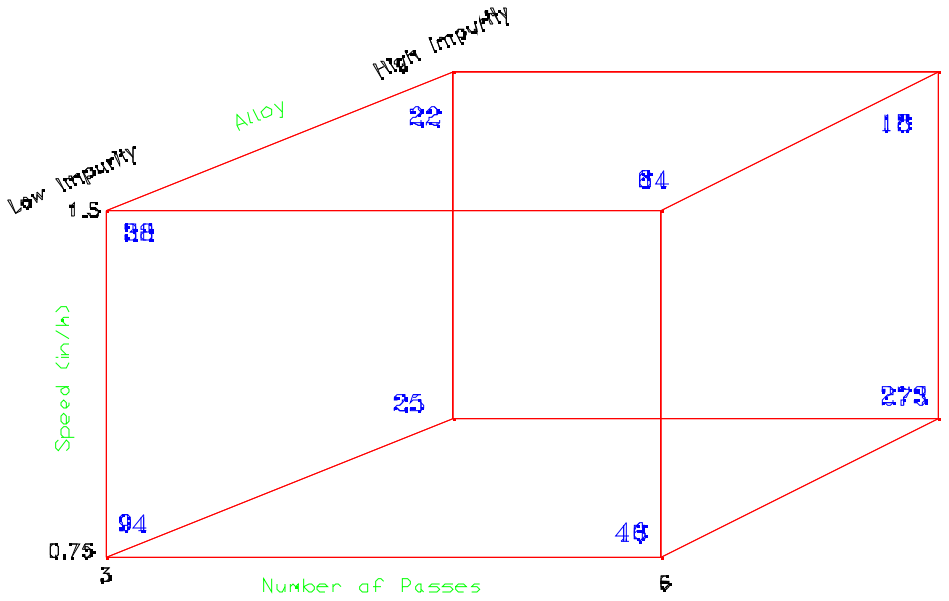

Figure 33e. Percent change (head to tail) for copper, with the vertices denoting the levels of each factor and the numbers being the mean yield at the vertices.

Table 7 shows the statistical regression analysis results of using a 2^3 factorial model of the data in Table 4 for the elements chromium, iron, cobalt, nickel, and copper. The table gives the coefficients of the equation $y = a_0 + a_1 * x_1 + a_2 * x_2 + a_3 * x_3$, where y is the percent change (dependant variable) and x_i are the levels of the three factors. In order to use these factors the following values are given for x_i: set x_1 at 0 for low-impurity alloy and 1 for high-impurity alloy; set x_2 at 0 for a speed of 0.75 in/h and 1 for a speed of 1.5 in/h; and set x_3 at 0 for three passes and 1 for six passes. The first column of numbers in the table are the parameter estimates for each impurity element. In the last column, the Prob > ½T½ is the significance of that factor. If that number is less than 0.05, it contributes significantly to the equation (bold).

From the results shown in Table 7 (the parameter estimates), the alloy variable has the smallest effect on the equations and also has the least significance (Prob > ½T½). Based on the parameter estimates for speed and number of passes, one could conclude that decreasing the speed from 1.5 to 0.75 in/h is the same as increasing the number of passes from three to six.

TABLE 7: STATISTICAL ANALYSES RESULTS (REGRESSION) USING A 2^3 FACTORIAL MODEL.

Chromium

Variable	**Parameter Estimate**	**Standard Error**	**Prob > ½T½**
Intercept	103.75	16.51	
Alloy	-6.625	16.51	0.6953
Speed	-59.13	16.51	**0.0038**
Number of Passes	53.13	16.51	0.0074

Iron

Variable	**Parameter Estimate**	**Standard Error**	**Prob > ½T½**
Intercept	72.50	17.61	
Alloy	39.63	17.61	**0.0439**
Speed	-47.88	17.61	**0.0186**
Number of Passes	46.875	17.61	**0.0207**

Cobalt

Variable	**Parameter Estimate**	**Standard Error**	**Prob > ½T½**
Intercept	44.38	15.47	
Alloy	51.50	15.47	**0.0060**
Speed	-39.25	15.47	**0.0260**

Number of Passes	49.75	15.47	**0.0074**

TABLE 7: STATISTICAL ANALYSES RESULTS (REGRESSION) USING A 2^3 FACTORIAL MODEL.

Nickel

Variable	**Parameter Estimate**	**Standard Error**	**Prob > ½T½**
Intercept	52.38	15.07	
Alloy	3.125	15.07	0.8392
Speed	-33.88	15.07	**0.0441**
Number of Passes	46.88	15.07	**0.0090**

Copper

Variable	**Parameter Estimate**	**Standard Error**	**Prob > ½T½**
Intercept	44.38	44.79	
Alloy	51.50	44.79	0.3935
Speed	-39.25	44.79	0.2186
Number of Passes	49.75	44.79	0.1381

6.6. Impurity Distillation Observations

The most important observation was that every time plutonium metal had to be removed from the Crystalox® vertical cold boat at the end of a run, there was no evidence of crucible interaction. In fact, in the case of the low-purity alloy, it was just a matter of reaching in and picking up the plutonium metal half-sphere. This observation is another strong indication that the secondary purpose of this experiment was proven; that is, containment of molten plutonium for long periods with no crucible interaction. The fact that plutonium could be held at 1200 C for 2 h with no crucible interaction was a surprise to the plutonium community.

The second most important observation was that the molten plutonium did not splatter at all. Splattering of molten plutonium when in a vacuum was one major previous problem with distillation of plutonium impurities (Section 3.6.). When the plutonium in the crucible first went molten, in each case it looked like boiling water (many small bubbles, but no splatter). After about 1/2 h, the bubbling rate slowed down with just the occasional formation of a large bubble, but still no splatter. One could see the levitation and strong

stirring effect due to the induction, which is why there was no splatter. Figure 34 is the view looking through the glovebox window into the distillation apparatus vacuum chamber view port at the plutonium metal (high-impurity alloy) after 1 h at approximately 1200 C (power supply at 40 kW). The illustration shows the levitated molten plutonium in the vertical crucible at approximately 1200 C (measured by a infrared pyrometer). The effect of the levitation force that can be seen in the illustration is that the top surface of the plutonium is spherical instead of flat.

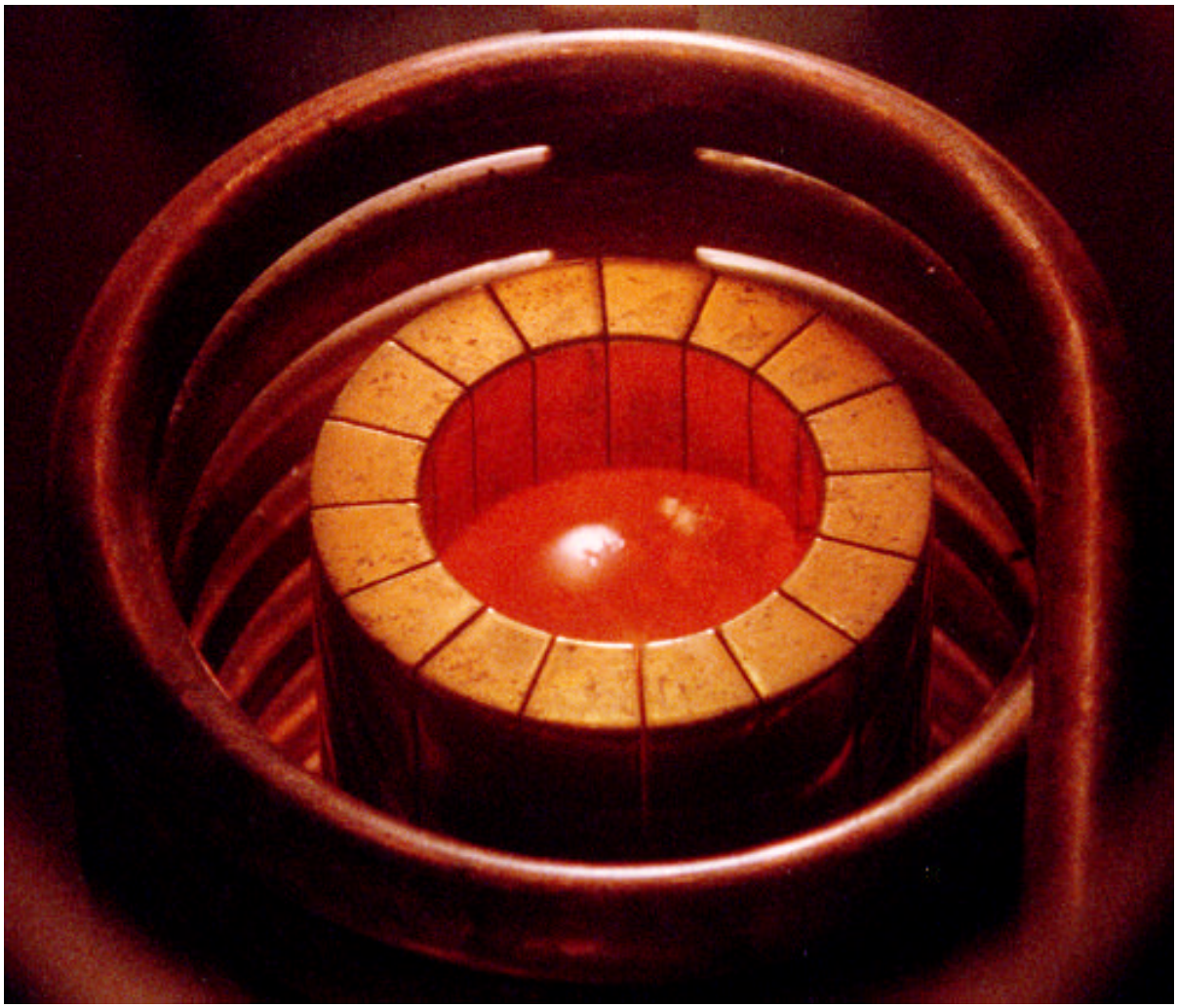

Figure 34. Plutonium metal (high-impurity alloy) in levitation distillation apparatus after 1 h at 1200 C (power supply at 40 kW).

The levitation of plutonium is not as pronounced as it was with copper. In fact, with copper it was hard to keep all the molten copper in the crucible during a run. During a stable run with copper, a complete sphere of molten copper formed and levitated, such that half the sphere was above the top of the vertical crucible. The difference between copper and plutonium is mainly due to the high density (approximately 16.5 g/cc) of liquid plutonium. If there were no levitation force present, the plutonium top surface would be flat and there would be plutonium spatter all over the top of the crucible and induction coil. If this plutonium were held in a standard crucible, it would only take approximately 5 kW to heat the plutonium to 1200 C, but the molten plutonium would receive much less stirring from the induction field and would be more likely to produce plutonium spatter.

Figure 35 is a illustration of what happens when plutonium is melted in a standard magnesium oxide crucible. First, the crucible can only be used once because it must be broken to remove the product (the reason why many molten plutonium processes create large amounts of radioactive ceramic wastes). Second, the plutonium spatters and wets the inside of the crucible (requiring a second process to remove most of the plutonium from the crucible ceramic before it can be discarded). Third, the molten plutonium dissolves magnesium from the crucible, making the plutonium product less pure that the starting charge.

Figure 35. Standard magnesium oxide crucible after melting plutonium metal.

The SRS residual gas analyzer detected hydrogen, helium, and some hydrocarbons during each run. The amounts of hydrogen and helium decreased with run time in all four

runs. With the high-impurity alloy, the SRS unit detected slight traces of gallium. Unfortunately, the SRS residual gas analyzer never detected americium, which would have given an indication of americium removal. Americium is the main element of interest because one objective of this experiment was to prove that running plutonium in the distillation apparatus removed americium. The problem was that there were a number of cold surfaces on which most impurity vapors would condense before they reached the gas analyzer.

Figures 36a and b are illustrations of the plutonium (high-impurity alloy) product formed from using the levitation distillation apparatus. Figure 36a gives a good view of the top surface of the half-sphere and shows the blotches formed on the plutonium surface. These blotches are due to the plutonium impurities forming on the surface of the plutonium during cool down. It was later discovered that these blotches would be intensified if the plutonium cool-down rate were increased. Figure 36b shows the bottom of the half-sphere. From this illustration, one can see the marks produced on solidification by each individual crucible finger and the ceramic piece that sets in the center of the crucible to prevent the pouring of the plutonium inside the crucible.

Figure 36a. Plutonium metal (high-impurity alloy) half-sphere formed from distillation run (top).

Figure 36b. Plutonium metal (high-impurity alloy) half-sphere formed from distillation run (bottom).

One problem discovered while making runs with plutonium was that when the high-impurity alloy was used, it was harder to remove the plutonium from the crucible due to the slight volume increase on solidification (see Figure 2). In an attempt to overcome this problem, a fifth run was made using the high-impurity alloy with a much faster cool down.

The rationale was that the faster the cooling rate, the more coring, the more -phase plutonium formed, the smaller the volume increase on solidification. This task was done by increasing the power from 40 to 50 kW at the end of the run for 5 minutes, then shutting off the power. This added run step did not seem to have much of an effect on the increase in volume upon solidification. However, it did produce some interesting data as shown in Figures 37a and b. The illustration shows that the cooling rate was so great that solidification occurred before the levitated plutonium had time to form a flat surface. From the blowup illustration, it is clear the blotching was worse.

Figure 37a. Plutonium metal (high-impurity alloy) half-sphere formed from distillation run (top) with fast cooling.

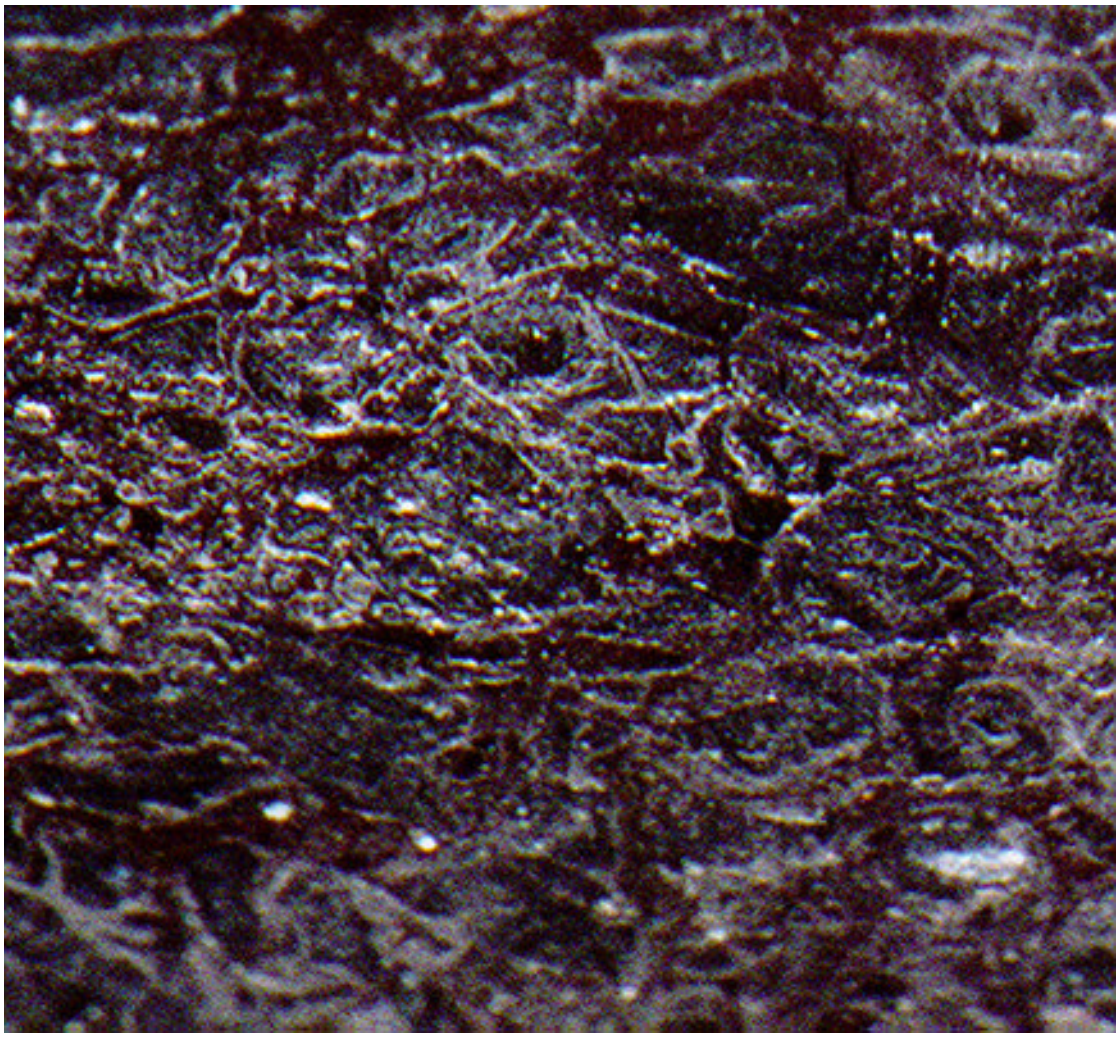

Figure 37b. Blowup (_-in x _-in) of top surface of plutonium metal (high-impurity alloy) half-sphere formed from distillation run.

6.7. Results of Chemical Analysis on Impurity Distillation Samples

The results of chemical analyses of the impurity distillation samples are shown in Table 8. As predicted, the americium concentration decreased due to distillation of americium. This proved one of the main objectives of this experiment, that americium could be removed from plutonium metal using levitation distillation. But in the case of uranium,

it's concentration also decreased, which is the opposite of what the theory states: the vapor pressure of uranium is less than that of plutonium, and thus uranium cannot vaporize out of plutonium. However, the fact that the concentration of uranium decreased during a vacuum process (zone refining) was noted by Blau (5).

TABLE 8: CHEMICAL ANALYSES OF DISTILLATION SAMPLES
Concentration in ppm by weight (precision ± 10%)

	As-Cast		After Distillation (2h)	
Alloy	Am	U	Am	U
High-impurity Alloy	2850	248	1560	143
High-impurity Alloy	2850	248	1490	137
Low-impurity Alloy	1105		481	
Low-impurity Alloy	1105		439	

Vapor Pressure at 1200 C (torr)	Pu	Am	U
	7.6×10^{-5}	2.3×10^{-1}	1.0×10^{-7}

After the third high-impurity alloy half-sphere was formed with the high cooling rate, a sample were taken near the surface for gallium and nickel. The concentration of both impurities was found to be higher than the as-cast concentrations (gallium went from 9,850 ppm to 11,951 and nickel went from 1,120 to 1,668 ppm). This indicates that the levitation distillation apparatus caused the plutonium impurities to migrate to the surface of the formed

plutonium product. Because of this result, a number of other samples were taken, but before the analysis was done the Chemistry and Metallurgy building (the only place at Los Alamos National Laboratory for chemical analysis of plutonium impurities) was shut down for safety reasons and the soonest it will be opened will be some time in 1998.

Based on observations made during the cutting of samples from the half-sphere plutonium products (no porosity), it will be easy to machine the disks from these half-spheres are needed for the radial-strain-anneal process to produce large plutonium crystals.

6.8. Computer Modeling

Computer modeling was used to model a better zone refining coil and the levitation forces produced from induction in the zone refining apparatus.

6.8.1. Zone Refining Induction Coil

Part of the redesign work to overcome the two problems discovered with the zone refining coil was to do a computer model of the resulting induction coil designed at Fluxtrol®. The computer modeling was done at the Center for Induction Technology and the result is shown in Figure 38. The figure shows that the coil will produce a high concentration of flux lines below the coil that will be ideal for both standard and solid-state zone refining. This is because it will produce a very small concentrated heat zone.

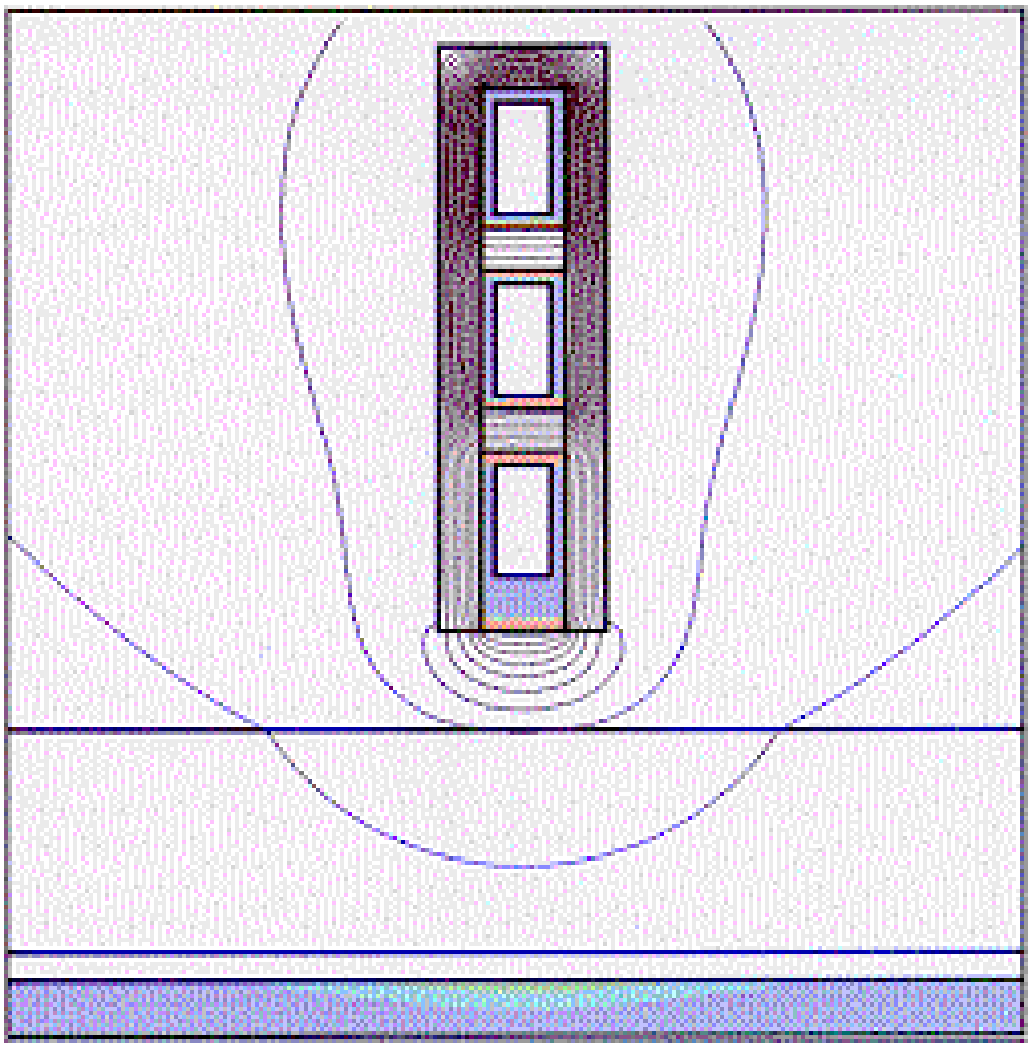

Figure 38. Modeling results of new Fluxtrol® induction coil done at The Center for Induction Technology. The three-turn cylindrical coil (2.5 in dia.) containing flux-field concentrator Fluxtrol A on three sides operated with a frequency of 50 kHz and current of 1000 A. The work piece was the Crystalox® cold horizontal boat containing a _-in dia. rod of plutonium.

Figures 39a and b are illustrations of the new zone refining apparatus that will soon be installed in the levitation glovebox. The view in Figure 39a shows the water-cooled

copper plate on the right side of the induction coil. This copper plate prevents the burning of the G-10 that makes up the outer covering of the coil. Figure 39b shows how the power leads for the coil enter and return. From this design change, the problem of preheating the plutonium rod ahead of the coil is completely fixed.

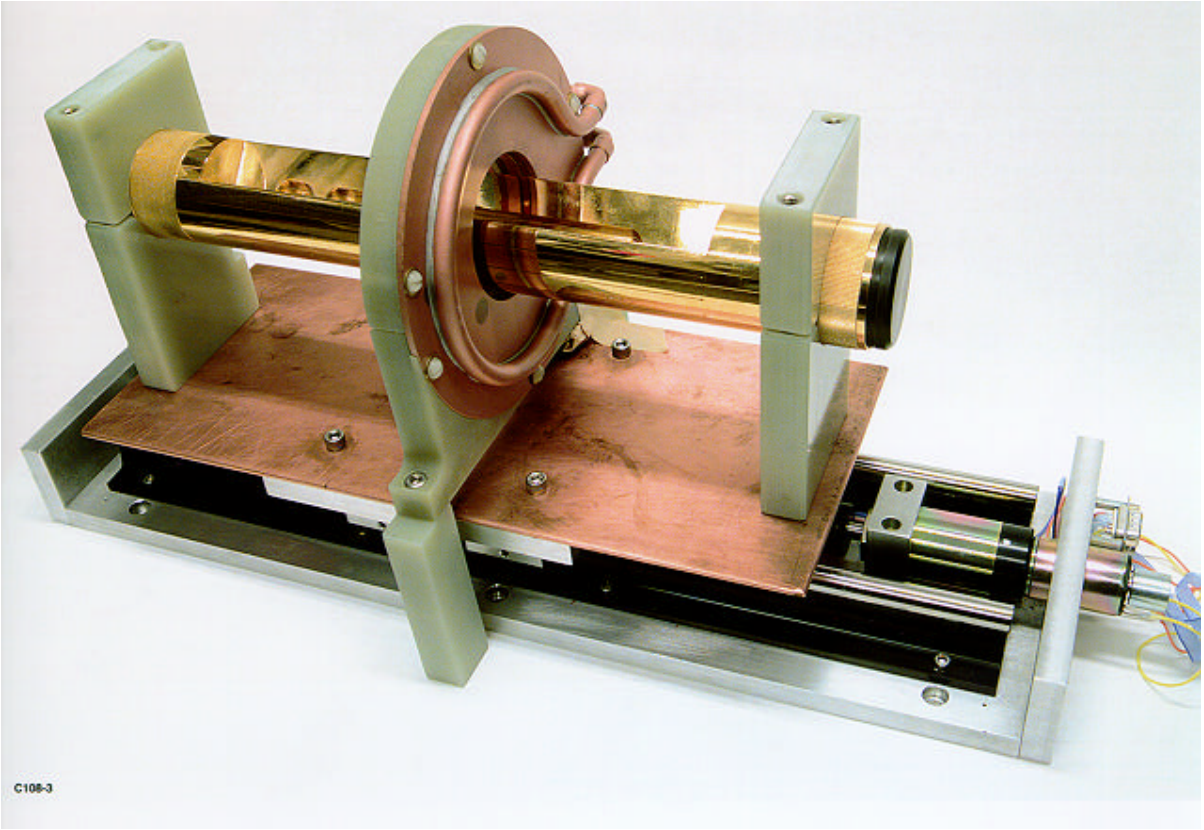

Figure 39a. New zone refining apparatus (side view).

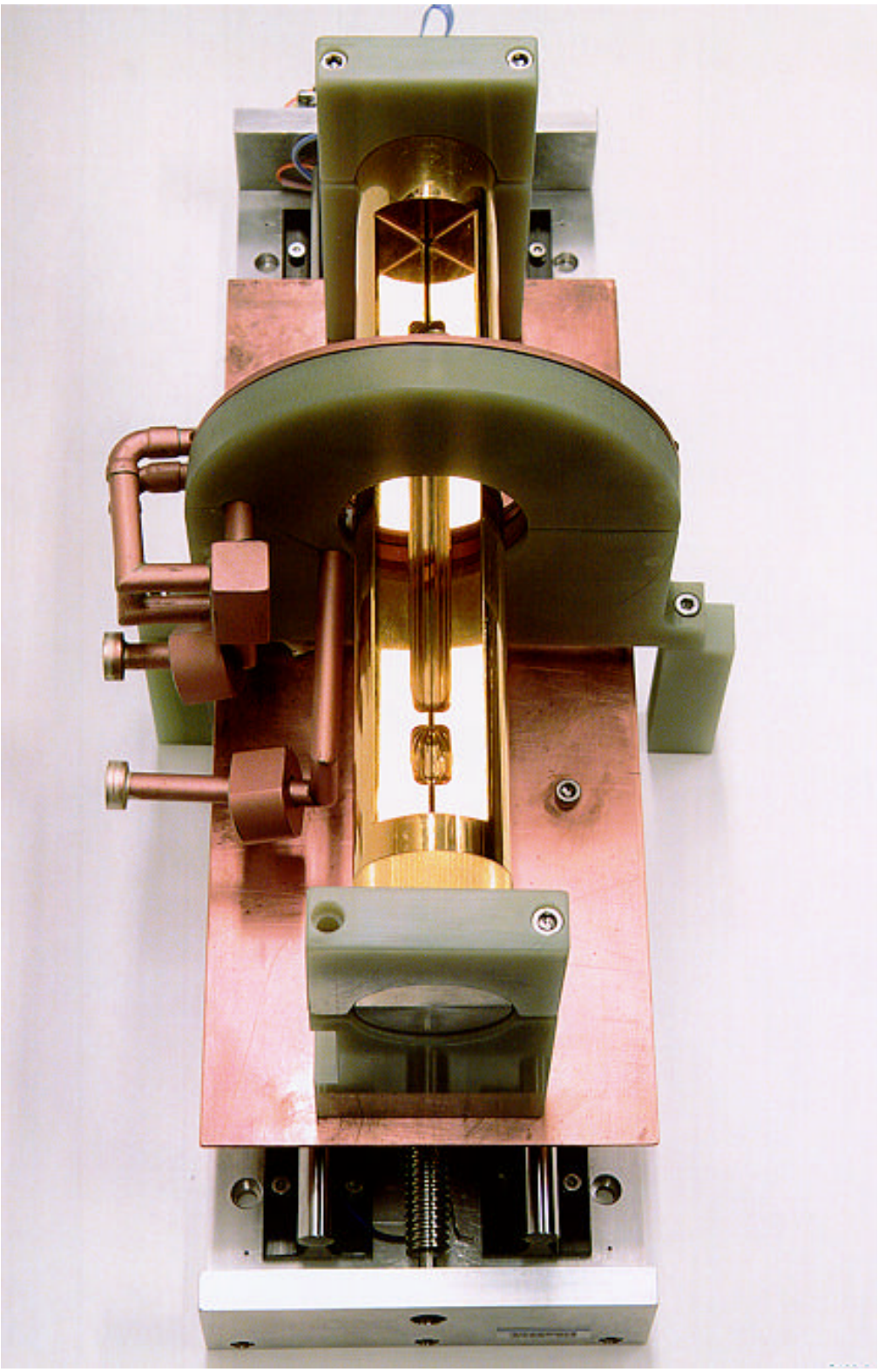

Figure 39b. New zone refining apparatus (top view).

6.8.2. Zone Refining Crucible

The finite element analysis for partial differential equations computer program PDEase2® was used to model the levitation force between the horizontal Crystalox® crucible (zone refiner) and the plutonium rod. This was done by taking a cross section through the center of the horizontal crucible and plutonium rod contained within the crucible and then making the inside edge of each crucible finger a separate region. The inside edge of each finger is where most of the eddy currents are formed in the crucible due to induction. The plutonium rod is made into two regions for the same reason (the rod edge will has most of the eddy currents, with the core having the remainder). The program that was written to run on PDEase2® to do this modeling is in the Appendix.

The results of this modeling are shown in Figures 40a and b. Figure 40a shows the direction of the magnetic fields. This direction is perpendicular to the eddy currents that are produced in the plutonium and crucible. Figure 40b shows the levitation forces (direction and magnitude) that are produced in the crucible and plutonium. This figure shows that most of the levitation force comes from the crucible.

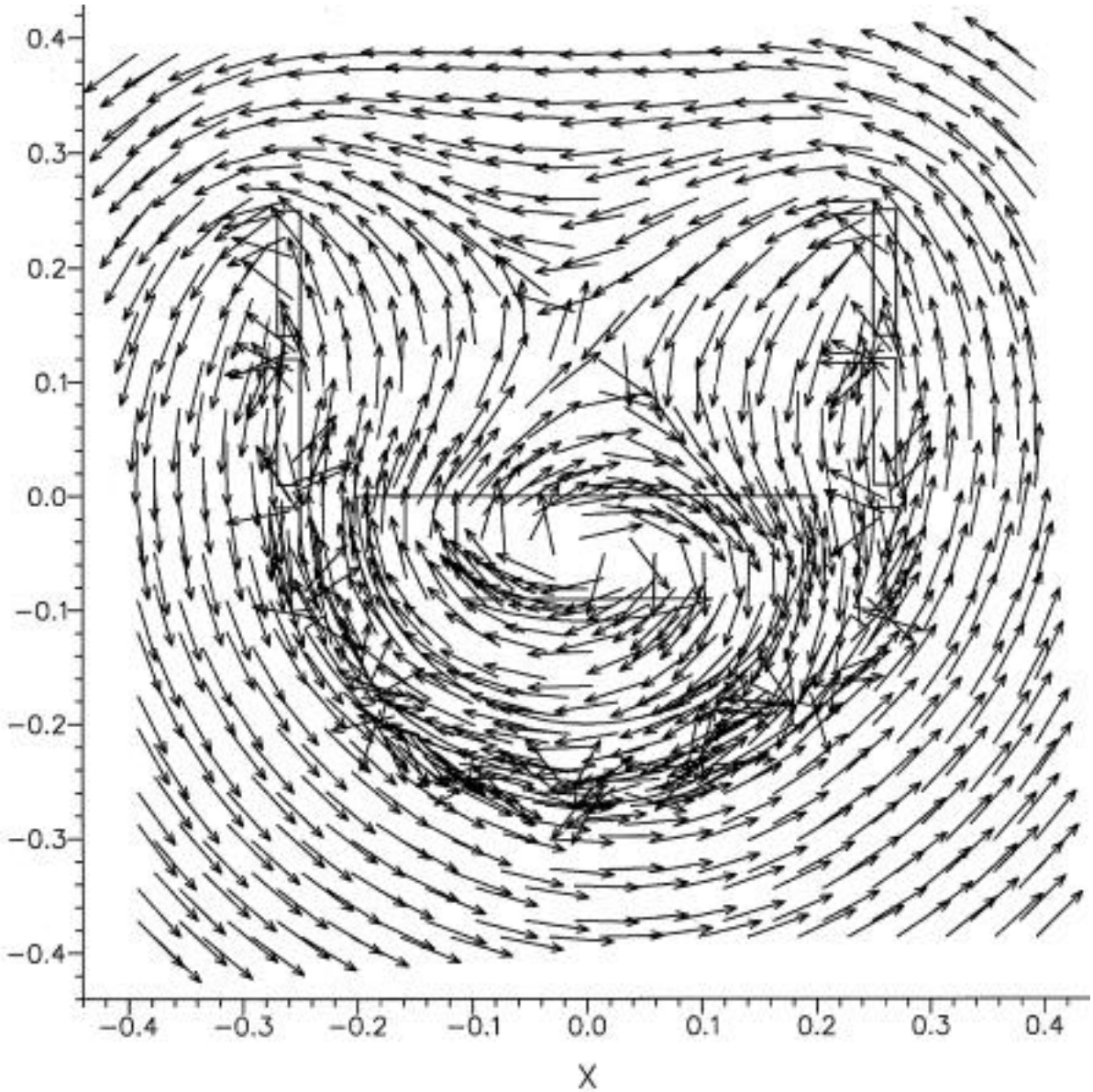

Figure 40a. A cross section of the magnetic flux density (Tesla) produced in the horizontal crucible and molten plutonium contained in the crucible. The axis are distance in inches starting with the center of the crucible cavity being 0,0.

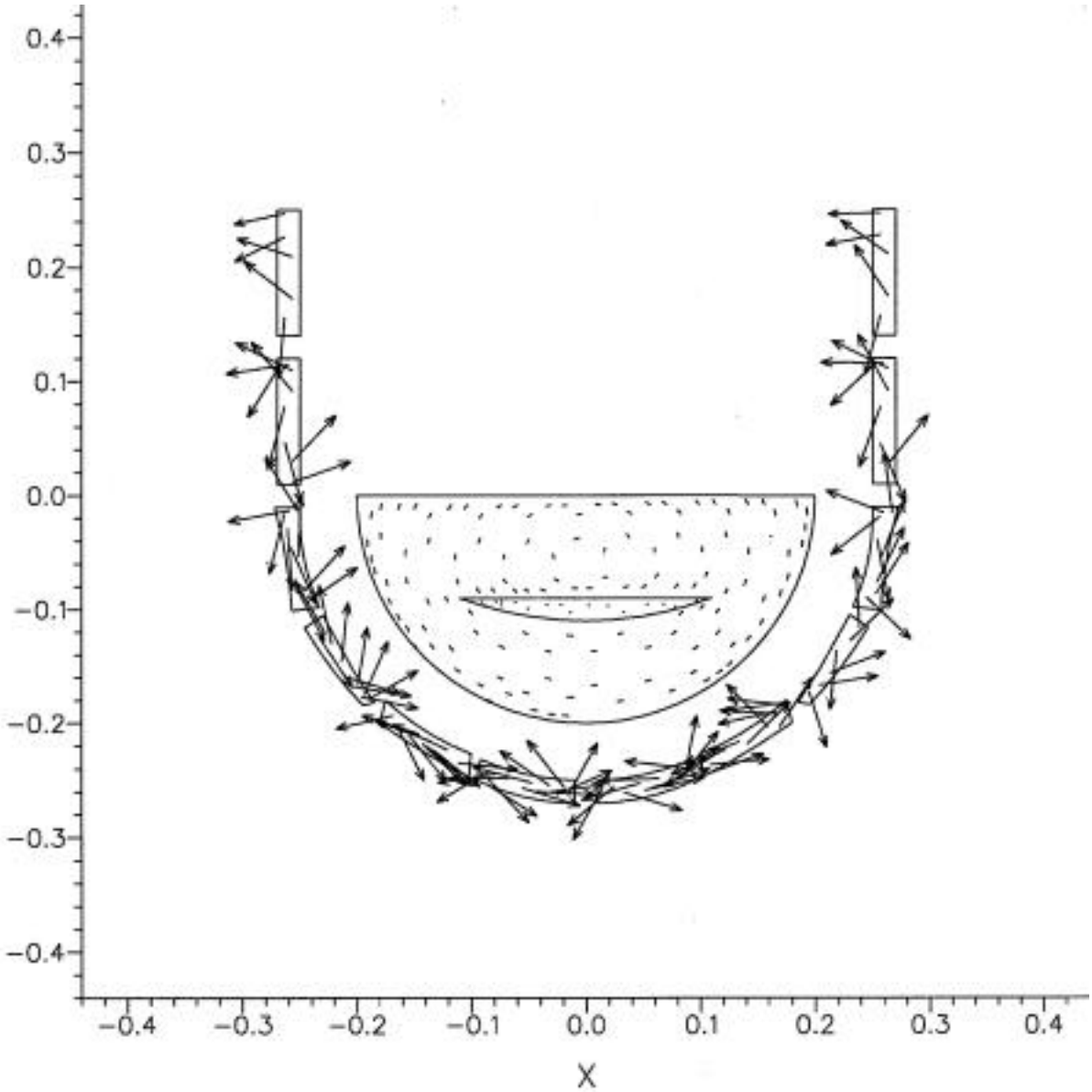

Figure 40b. A cross section of the electromagnetic forces (Newtons) produced in the horizontal crucible and molten plutonium contained in the crucible. The axis are distance in inches starting with the center of the crucible cavity being 0,0.

6.9. Zone Refining Parameters to Produce First Pure Plutonium

Based on the results of this experiment, the parameters for producing the first high-purity plutonium are discussed below:

- Oxygen: The results have clearly shown that the absence of oxygen greatly improves zone refining results. To reduce the amount of oxygen, the following actions will be taken: The levitation glovebox atmosphere will be changed from normal air (20% oxygen) to flush inert with argon (produces a glovebox atmosphere of less than 1% oxygen). Before the start of each pass, titanium turnings will be loaded in the front cavity of the crucible (Figure 39b) and then heated by the induction coil just before the molten zone pass is started. Heating the titanium turnings causes the turnings to be a getter for any oxygen that is still present in the zone refining vacuum chamber. The added steps of wire brushing the rods between passes and holding the rod under high vacuum for at least 10 h before the start of a pass will also reduce the amount of oxygen present in the system during the zone refining process.
- Speed: The results show that the slower the speed the better, and given the fact that the plutonium facility operates on a 10 h day, a speed of 0.5 in/h will be used (rods are 5.5 in long).
- Passes: The results show the more passes the better, but we cannot do an infinite number of passes and will settle on 10 passes.
- Equipment: The whole zone refining apparatus will be replaced with a more robust system (Figure 39) For example, the new translation table has double the load capacity of the one used in this experiment.

CHAPTER 7

SUMMARY AND CONCLUDING REMARKS

This study showed that it is possible to produce the first high-purity plutonium using a levitation zone refining process. Two plutonium alloys were produced with high-enough concentrations of impurities for easy tracking to examine the effect of the different zone refining variables. It was determined that the presence of oxygen had a negative effect on zone refining of plutonium. For example, wire brushing the plutonium rods to remove the oxide layer (between passes) produced the single biggest positive effect. It was determined that decreasing the travel speed of the molten zone along the rod had a positive zone refining effect. It was also determined that increasing the number of passes had a positive zone refining effect. According to zone refining theory, increasing the number of passes and decreasing the travel speed of the molten zone should have a positive effect. In all cases, all plutonium impurity elements tracked; that is, they moved in accord with anticipated element movement based on the distribution coefficient determined from the binary phase diagram of each element with plutonium. Cobalt, copper, chromium, iron, nickel, and neptunium moved in the direction of zone travel. Aluminum, americium, and gallium moved in the opposite direction.

Based on the parameter estimates for speed and number of passes, it was concluded that decreasing the speed from 1.5 to 0.75 in/h had about the same effect as increasing the number of passes from three to six.

Based on the results of this study, a process for producing the first pure plutonium was determined. This new process will be used once the new equipment has been put in

place. Producing high-purity plutonium will be the first step in the Plutonium Single Crystal project at Los Alamos National Laboratory. This new zone refining apparatus will also be used for one of the two methods for trying to produce plutonium crystals by solid-state zone refining very slowly (0.1 in/h) in the δ-phase field.

This study showed that it is possible to remove americium from plutonium using a levitation distillation process. The concentration of americium was determined to drop by approximately 50% after 2 h when distillation runs were made with the distillation apparatus using the two impurity alloys.

This study proved for the first time that it was possible to truly contain molten plutonium (no crucible interaction) for long periods of time. The Crystalox® horizontal cold boat contained molten plutonium for over 300 h at temperatures around 700 C, and the Crystalox® vertical crucible contained molten plutonium for over 10 h at temperatures around 1200 C with no evidence of any plutonium-crucible interaction in either case. This fact may lead to changes in many current processes that produce large amounts of radioactive crucible waste because they have molten plutonium steps.

This study also showed that the levitation forces produced by the zone refining apparatus could be modeled using a computer program.

It was further proven that the Crystalox® vertical crucible could be used to cast δ-phase plutonium parts needed for the current plutonium crystal growing project at Los Alamos National Laboratory. For this project, the Crystalox® vertical crucible will be used to alloy the first pure plutonium with 1 w/o gallium and then cast the δ-phase plutonium into

a half-sphere product that will be machined into the starting sample for one of the proposed methods for producing crystals.

Based on the results of this experiment, it was recently decided that the distillation apparatus would be used to produced the plutonium metal standards needed for the pit rebuild program at Los Alamos National Laboratory. This is because the plutonium standards must be of higher purity than the plutonium metal that will be used to cast plutonium shells for the production of pits (the nuclear trigger in a hydrogen bomb). This will be accomplished by running double electrorefined plutonium metal in the distillation apparatus and then removing the half-sphere surface layer and crushing the plutonium product into the plutonium standards (0.5 to 1.5 g each).

REFERENCES

1. Plutonium Handbook, A Guide to the Technology, O. J. Wick, Ed., Gordon and Breach, New York, NY, 1967.

2 R. E. Tate and R. W. Anderson, Plutonium and its Alloys, "Some Experiments in Zone Refining Plutonium," Inter Science Publishers, New York, 1959, pp231-242.

3. T. B. Massalski, chief ed., H. Okamoto, P. R. Subramanian, and L. Kacprzak, ed. Binary Alloy Phase Diagrams, ASM International, 1990.

4. W. G. Pfann, Zone Melting, Robert E. Krieger Publishing Company, Huntington, NY, 1978.

5. M. S. Blau, Zone Refining of Plutonium Metal, LA-UR-94-2627, Los Alamos National Laboratory, Los Alamos NM, 1994.

6. Transactions of the Electrochemical Society, Vol. 87, W. J. Kroll, "Melting and Evaporating in a Vacuum," 1946, pp571-587, Columbia University, New York, NY.

7. J. G. Reavis, Plutonium Purification by Distillation, LA-UR-85-562, Los Alamos National Laboratory, Los Alamos NM, 1985.

8. J. D. Verhoeven, Fundamentals of Physical Metallurgy, John Wiley & Sons, New York, NY, 1975.

9. D. A. Porter and K. E. Easterling, Phase Transformations in Metals and Alloys, Van Nostrand Reinhold (UK) Co. Ltd., 1981.

10. J. A. Burton, R. C. Prim, and W. P. Slichter, "The Distribution of Solute in Crystals Grown from the Melt," Journal of Chem. Phys., 21, pp1987-1996, 1953.

11. N. W. Lord, "Analysis of Molten-Zone Refining" Journal of Metals, AIME, 200,1954, pp1531-1533.

12. E. J. Vaughan, Zone Refining and Allied Techniques, George Newnes Limited, London, 1960.

13. R. F. Bunshah, Vacuum Metallurgy, Reinhold Publishing Corp., New York, 1958.

14. J. L. Bieber, J. M. Schreyer, and E. L. Williams, Purification of Uranium by Zone-Refining Techniques, Y-1564, Oak Ridge National Laboratory, Oak Ridge, TN, 1967.

15. K. Suzuki, T. Shikama, and A. Ochiai, "Purification of Uranium Metal," Physical Properties of Actinde and Rare Earth Compounds, JJAP Series 8 (1993), pp15-19.

16. V. G. Kas'yanov and P. E. Gajvoronskii, "Crucibleless Zone Melting of Uranium," Radiokhimiya, Vol. 23:1, 1981, pp 135-138.

17. J. D. Olivas and F. W. Schonfeld, A Survey of Metallurgical Research on Several Actinides, LA-UR-93-3628, Los Alamos National Laboratory, Los Alamos, NM, 1993.

18. J. W. Berry, J. B. Knighton, and C. A. Nannie, Vacuum Distillation of Americium Metal, Rocky Flats Plant Report RFP-3211, Denver, CO, January 1982.

19. R. L. Sandvig, Separation of Zinc from Plutonium by Vacuum Melting, Rocky Flats Plant Report CRD-80-073, Denver, CO, January 1980.

20. S. L. Semiatin and D. E. Stutz, Induction Heat Treatment of Steel, American Society for Metals, Metals Park, OH, Carnes Publication Services, Inc., 1986.

21. C. A. Tudbury, Basics of Induction Heating, Vol. 1, Forging Industries Association, Cleveland, OH, 1960.

22. H. F. Sterling, R. W. Warren, Metallurgica, 67, 301, "High-Temperature Melting without Contamination in Cold Crucibles," pp 2-8, 1963.

23. H. F. Sterling, "Towards a Perfect Crucible," reprinted from Discovery 1965, Professional and Industrial Publishing Company, England.

24. Crystalox LTD., 1 Limborough Rd., Wantage, England.

25. R. Madera, Correspondence with Fluxtrol Manufacturing, Inc., on plutonium zone refining, 21/94.

26. D. Kristofova, L. Kuchar, and B. Wozniakova, "Effective Distribution Coefficients of Admixtures in Plutonium," SB VER PR VYS Banske Ostrave Rada Hutn, Vol. 26, 1980.

27. T. B. Barker, Quality by Experimental Design, Marcel Dekker, Rochester, NY, 1985.

28. L. Ott, An Introduction to Statistical Methods and Data Analysis, 3rd. Ed., PWS-Kent, 1988.

29. PDEase2®, Finite Element Analysis for Partial Differential Equations, SPDE, Inc. Fremont, CA, 1995.

APPENDIX

The program that was written to run on PDEase2® (29) to model the magnetic flux density and force in the levitation zone refiner is shown below:

```
select
errlim=5e-9    contours=10   paint=off
variables
  Az
definitions
      mu=1.0         J      I
   r0=0.1      dr0=1.50*r0     r1=1.0
   rad=sqrt(x**2+y**2)
   Bxx=dy(Az)   Byy=-dx(Az)
   Babs=sqrt(Bxx**2+Byy**2)
   F=sqrt((I*Az*Bxx/Babs)**2+(I*Az*Byy/Babs)**2)
   equations
   dx((1/mu)*dx(Az))+dy((1/mu)*dy(Az))+J=0
boundaries
      region 1       J=0     I=0
   start(-1,1)    value(Az)=0
   line to (1,1) to (1,-1) to (-1,-1) to finish
      region 2       J=-3.0  I=-1.5
   start(-.2,0)
   arc to (0,-.2) to (.2,0) line to finish
      region 3       J=1.0  I=0.5
   start(-.11,-.09)
   arc to (0,-.11) to (.11,-.09) line to finish
      region 4       J=24     I=12
   start(.25,.25)
   line to (.25,.14) to (.27,.14) to (.27,.25) to finish
```

```
    region 5      J=24    I=12
  start(.25,.12)
  line to (.25,.01) to (.27,.01) to (.27,.12) to finish
    region 6      J=24  I=12
  start(.25,-.01)
  arc to (.243,-.07) to (.233,-.098) line to (.257,-.101)
  arc to (.260,-.07) to (.272,-.01) line to finish
    region 7      J=24  I=12
  start(.23,-.105)
  arc to (.204,-.152) to (.185,-.182) line to (.195,-.184)
  arc to (.222,-.152) to (.246,-.116) line to finish
    region 8      J=24  I=12
  start(.175,-.18)
  arc to (.15,-.2) to (.1,-.227) line to (.102,-.247)
  arc to (.15,-.22) to (.18,-.2) line to finish
    region 9      J=24  I=12
  start(.092,-.232)
  arc to (.07,-.24) to (.01,-.25) line to (.01,-.27)
  arc to (.07,-.26) to (.095,-.25) line to finish
    region 10     J=24    I=12
  start(-.25,.25)
  line to (-.25,.14) to (-.27,.14) to (-.27,.25) to finish
    region 11     J=24    I=12
  start(-.25,.12)
  line to (-.25,.01) to (-.27,.01) to (-.27,.12) to finish
    region 12     J=24  I=12
  start(-.25,-.01)
  arc to (-.243,-.07) to (-.233,-.098) line to (-.257,-.101)
  arc to (-.26,-.07) to (-.272,-.01) line to finish
    region 13     J=24  I=12
  start(-.23,-.105)
  arc to (-.204,-.152) to (-.185,-.182) line to (-.195,-.184)
  arc to (-.222,-.152) to (-.246,-.116) line to finish
    region 14     J=24  I=12
  start(-.175,-.18)
  arc to (-.15,-.2) to (-.1,-.227) line to (-.102,-.247)
  arc to (-.15,-.22) to (-.18,-.2) line to finish
    region 15     J=24  I=12
  start(-.092,-.232)
  arc to (-.07,-.24) to (-.01,-.25) line to (-.01,-.27)
  arc to (-.07,-.26) to (-.095,-.25) line to finish
monitors
    contour(Az)
plots
```

```
    contour(Az) as 'Vector potertial Az'
    contour(Az) zoom (-.4,-.4,.8,.8)
    contour(Babs)
    contour(Babs) zoom (-.4,-.4,.8,.8)
    contour(F)
    contour(F) zoom (-.4,-.4,.8,.8)
    contour(Babs) zoom (-.24,-.24,.48,.48)
    vector(Bxx/Babs,Byy/Babs) as 'Flux density B'
vector(I*Az*Bxx/Babs,I*Az*Byy/Babs) as 'Force (N)'
    vector(I*Az*Bxx/Babs,I*Az*Byy/Babs) zoom(-.4,-.4,.8,.8)
    vector(I*Az*Bxx/Babs,I*Az*Byy/Babs) zoom(-.3,-.3,.8,.8)
end
```